

Title of thesis

**Haptic Feedback Device for Needle Insertion**

I, **IMRAN FAZAL** , hereby allow my thesis to be placed at the Information Resource Center (IRC) of Universiti Teknologi PETRONAS (UTP) with the following conditions:

1. The thesis becomes the property of UTP.
2. The IRC of UTP may make copies of the thesis for academic purposes only.
3. This thesis is classified as

Confidential

Non-confidential

If this thesis is confidential, please state the reason:

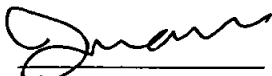
\_\_\_\_\_

The contents of the thesis will remain confidential for \_\_\_\_\_ years.

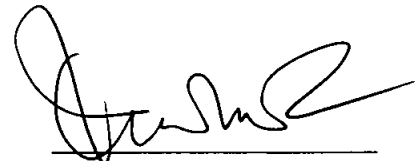
Remarks on disclosure:

\_\_\_\_\_

Endorsed by



Signature of Author



Signature of Supervisor

Permanent : House No 179-180,  
address 25120, Professor Colony,  
Agriculture University Peshawar,  
Peshawar, N.W.F.P, Pakistan.

Date : April 25, 2008

Name of Supervisor  
AP Dr Mohd Noh Karsiti

Date : April 25, 2008

## UNIVERSITI TEKNOLOGI PETRONAS

## Approval by Supervisor

The undersigned certify that they have read, and recommend to the Postgraduate Studies

Programme for acceptance, a thesis entitled

**Haptic Feedback Device for Needle Insertion**

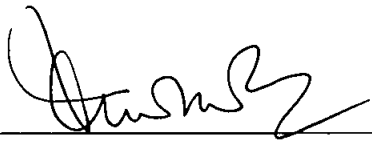
submitted by

**Imran Fazal**

for the fulfillment of the requirements for the degree of

**Masters of Science in Electrical and Electronic Engineering**

Date: April 25, 2008

Signature :   
Main Supervisor : Assoc. Prof. Dr. Mohd Noh Karsiti  
Date : April 25, 2008  
Co-Supervisor 1 : \_\_\_\_\_  
Co-Supervisor 2 : \_\_\_\_\_

UNIVERSITI TEKNOLOGI PETRONAS

**Haptic Feedback Device for Needle Insertion**

By

Imran Fazal

A THESIS

SUBMITTED TO THE POSTGRADUATE STUDIES PROGRAMME

AS A REQUIREMENT FOR THE

DEGREE OF MASTERS OF SCIENCE IN ELECTRICAL AND ELECTRONIC

ENGINEERING

Electrical and Electronic Engineering


BANDAR SERI ISKANDAR,

PERAK

March 2008

**DECLARATION**

I hereby declare that the thesis is based on my original work except for quotations and citations which have been duly acknowledged. I also declare that it has not been previously or concurrently submitted for any other degree at UTP or other institutions.

Signature : \_\_\_\_\_

Name : Imran Fazal

Date : April 25, 2008

## ACKNOWLEDGEMENTS

First and foremost, all praise and grace goes to Allah, without whose guidance, no effort can attain success.

I am indebted to my supervisor, Assoc. Prof. Dr. Mohd Noh Karsiti, for his guidance, inspiring discussions and support throughout this research. Without his never-ending patience, this thesis would probably not exist today. His useful suggestions and feedback have been the greatest help in the completion of this research.

I am thankful to Assoc. Prof. Dr. Herman Agustiawan, Mr. Salman Ahmed and Mr. Saiful Azrin for their enlightening discussions, comments and help at several critical points in my research work. I am thankful to Dr.Sadia, Dr. Noreen Fazal, Dr.Ramzan Hussain for their guidance in the medical and surgical field.

I am grateful to the staff of the Post Graduate Office. I am also deeply grateful to my fellow postgraduate and undergraduate students. They have been constant sources of encouragement and friendships during the course of this research.

Finally, but most importantly, I want to thank my parents and family from the core of my heart. They have been a source of love, support, advice and feedback for me.

## ABSTRACT

Tele-surgery is one of the emerging fields which combine engineering and medical sciences. Application of tele-surgery can be found in remote communities, war-zones and disaster-stricken areas. One of the most complex and tedious issue in tele-surgery is needle insertion. The surgeon relies on haptic feedback during needle insertion. The force exerted on needle during insertion is measured and reproduced at surgeon's end is known as haptic feedback. The realistic force reproduction requires haptic feedback device which should be dynamically identical to needle. The haptic feedback device enables the surgeon to sense the needle insertion remotely.

The basic objective of this thesis is to design a device used for needle insertions in soft tissue. The force information from needle insertions is measured by a sensor. The force feedback produced by the device can be used in robot-assisted needle insertion. A device is designed for reality-based data that results in more accurate representation of a needle insertion haptic feedback scenario.

The device is modeled dynamically and it is clear from the model that the reactive force is reproduced by the friction forces which is controlled by the motors. The system is sensitive to mass of rollers, mass of the stick and friction between the stick and rollers.

The needle insertion force is modeled in three parts; force due to capsule stiffness, friction, and cutting. The force due to capsule stiffness is modeled terms of three components namely diameter of needle, elasticity of tissue and deformation of tissue. The data from model is compared with real time force data. The haptic feedback device input and output forces are compared and the highest correlation factor is 82%. The sensitivity analysis of the device is performed. The capsule stiffness force for 0.9 millimeter diameter needle is 0.98 Newton, the stiffness force for 0.8 millimeter is 0.91 Newton and stiffness force for 0.6 millimeter diameter is 0.41 Newton. The capsule stiffness force for 0.6 millimeter needle is not

following the capsule stiffness model. The insertion force data was collected on chicken skin and meat.

The device designed in this work is having one degree of freedom; it only produces force feedback for vertical needle insertion. This design is not able to produce the force feedback for angular needle insertion.

Graphical User Interface is designed for the visual haptic feedback. The data acquisition is done with the help of a PC sound card. Future work should include the design of a multi-degree of freedom haptic feedback device and to advance the GUI for audio feedback that may be extended to accommodate the design of a simulator.

## TABLE OF CONTENTS

<b>STATUS OF THESIS</b> .....	<b>I</b>
<b>APPROVAL PAGE</b> .....	<b>II</b>
<b>TITLE PAGE</b> .....	<b>III</b>
<b>DECLARATION</b> .....	<b>IV</b>
<b>ACKNOWLEDGEMENT</b> .....	<b>V</b>
<b>ABSTRACT</b> .....	<b>VI</b>
<b>TABLE OF CONTENTS</b> .....	<b>VIII</b>
<b>LIST OF TABLES</b> .....	<b>X</b>
<b>LIST OF FIGURES</b> .....	<b>XI</b>
<b>LIST OF ABBREVIATIONS</b> .....	<b>XII</b>
<b>CHAPTER 1: INTRODUCTION</b> .....	<b>1</b>
1.1 Haptic Feedback.....	1
1.2 Application of Haptic Feedback.....	2
1.3 Background.....	4
1.4 Problem Statement.....	5
1.5 Objective and Scope.....	5
1.6 Thesis Organization.....	6
<b>CHAPTER 2: LITERATURE REVIEW</b> .....	<b>7</b>
2.1 Introduction.....	7
2.2 Haptic Feedback Devices.....	7
2.3 Haptic Feedback in Medicine.....	10
2.4 Haptic Feedback Devices used in Needle Insertion.....	13
2.5 Needle Insertion Force Models.....	15
2.6 Summary.....	16



## **CHAPTER 3: DESIGN OF HAPTIC FEEDBACK SYSTEM .....17**

3.1	Introduction.....	17
3.2	Needle Insertion Force Modeling .....	17
3.2.1	Di Maio Model (Finite Element Method Model) .....	17
3.2.2	Christine Simone Model (Non-linear Model).....	19
3.2.3	Ottensmeyer Model (Linear Model) .....	21
3.3	Dynamic Model of System .....	22
3.4	Sensitivity Analysis .....	26
3.5	Haptic Feedback System Design .....	32
3.5.1	Needle Insertion Module.....	33
3.5.2	Interface Module.....	38
3.5.3	Haptic Feedback Device Module.....	40
3.5.4	Graphical User Interface .....	44
3.6	Summary .....	46

## **CHAPTER 4: HAPTIC FEEDBACK DEVICE RESULTS .....47**

4.1	Introduction.....	47
4.2	Needle Insertion Force Simulation .....	47
4.3	Experimental Results .....	48
4.3.1	Sensor Calibration Results.....	48
4.3.2	Needle Piercing Force.....	50
4.3.3	Experimental Results of Needle Insertion .....	51
4.3.4	Haptic Rendering .....	53
4.3.5	Graphical User Interface .....	56
4.3.6	Sensitivity Analysis Results.....	58
4.4	Discussion .....	58
4.5	Summary .....	62

**CHAPTER 5: CONCLUSIONS AND SUGGESTIONS FOR FUTURE WORK.....63**

5.1	Haptic Feedback Device Accuracy .....	63
5.2	Suggestions for Future Extensions and Developments.....	64

**REFERENCES.....65****APPENDICES .....70**

Appendix-A:	Data Sheets of Electronic Components .....	71
Appendix-B:	Needle Insertion Force by XR440 Pocket Data Logger .....	97
Appendix-C:	Mechanical Drawing of Haptic Feedback Device Components .....	104
Appendix-D:	M-file of Graphical User Interface .....	112

**LIST OF TABLES**

Table 3.1:	Needle Color Coding Parameter .....	34
Table 4.1:	Indentation Force for Different Needle Diameters .....	50
Table 4.2:	Sensor Calibration Readings.....	52
Table 4.3:	Experimental Reactive Force on Needle During Piercing of Skin .....	54
Table 4.4:	Correlation Factor .....	58
Table 4.5:	Sensitivity Analysis Results.....	60
Table 4.6:	Experimental and Model Needle Insertion Forces.....	63

## LIST OF FIGURES

Figure 1.1:	Haptic feedback system .....	4
Figure 2.1:	3D-Haptic Feedback Device .....	7
Figure 2.2:	NASA's Robonauts.....	8
Figure 2.3:	Nintendo 64 Controller's Rumble Pack. ....	9
Figure 2.4a:	Casper .....	10
Figure 2.4b:	Robodoc .....	10
Figure 2.5a:	Pathfinder.....	11
Figure 2.5b:	Neuromate.....	11
Figure 2.6:	Zeus Surgery Console .....	12
Figure 2.7:	daVinci Surgery Console.....	12
Figure 3.1:	Positions of Needle During Insertion.....	21
Figure 3.2:	Parameter of Indentation Force.....	23
Figure 3.3:	Dynamic Model of Haptic Feedback Device with Two Rollers.....	24
Figure 3.4:	Dynamic Model of Haptic Feedback Device with Four Rollers.....	26
Figure 3.5:	Translational Mechanical Diagram.....	27
Figure 3.6:	Free Body Diagram of Haptic Feedback Device .....	28
Figure 3.7:	Block Diagram of Experimental Setup .....	33
Figure 3.8:	Beveled and Diamond Shaped Needle.....	34
Figure 3.9:	Needle Holder Made of Teflon .....	35
Figure 3.10:	Force Sensor.....	36
Figure 3.11:	Internal Wheat Stone Bridge of Force Sensor .....	37
Figure 3.12:	Interface Circuit Diagram .....	38
Figure 3.13:	Working Block Diagram of Interface Circuitry.....	39
Figure 3.14:	Designed Haptic Feedback Device .....	41
Figure 3.15:	Roller Isometric View.....	42
Figure 3.16:	Block Diagram of GUI.....	44
Figure 3.17:	Pictorial View of GUI Environment.....	45
Figure 4.1:	Relation of Indentation Force to Needle Diameter .....	48
Figure 4.2:	Force vs Output Voltage of Sensor .....	52

Figure 4.3:	Force vs Time from Pocket Logger XR440.....	53
Figure 4.4:	Experimental Piercing Force According to Diameter of Needle .....	55
Figure 4.5:	Needle Reactive Force vs Time .....	56
Figure 4.6:	Reactive Force Reproductive Circuit.....	56
Figure 4.7:	Input Force Signal of Haptic Feedback .....	57
Figure 4.8:	Output Force of Haptic Feedback Device.....	57
Figure 4.9:	Correlation of Haptic Feedback Device.....	58
Figure 4.10:	Graphical User Interface of Haptic Feedback Device with Needle Insertion..	59
Figure 4.11:	Graphical User Interface of Haptic Feedback Device with Error.....	60
Figure 4.12:	Comparison of Experimental and Simulation Results .....	61
Figure 4.13:	Skin Layered Structure Diagram .....	62

### LIST OF ABBREVIATIONS

UAV	Unmanned Ariel Vehicle
FEM	Finite Element Method
MOSFET	Metal Oxide Silicon Field Effect Transistor
BJT	Bipolar Junction Transistor
OPAMP	Operational Amplifier
PMDCM	Permanent Magnet Direct Current Motor
MIS	Minimal Invasive Surgery
GUI	Graphical User Interface
DAQ	Data Acquisition Card
DOF	Degree of Freedom

**NOTE: THE DIAGRAM TAKEN FROM CITATIONS IS REPRINTED WITH PERMISSION.**

## **CHAPTER 1**

### **INTRODUCTION**

A new technology emerging in the field of surgery is tele-surgery [1]. In this new technology, surgeons perform surgery over the patient from a distant place remotely. This technology saves the traveling time of the surgeons. In this type of surgery, robots are used to perform the surgery [2]. The robot at the patient's end is known as slave, controlled by the master at surgeon's end. The console by which the surgeon controls the slave is known as the master. The surgeon gives a command to the master. The command is communicated to the slave electronically by the use of Internet and the slave performs the requested actions accordingly. However, there are some limitations to telesurgery. The most drastic is the lack of information about the kinesthetics of the environment of the slave to the master. The same kinesthetic environment needs to be re-produced at the master. This is achieved with the help of a haptic feedback device.

#### **1.1 Haptic Feedback**

The term haptic comes from the Greek which means pertaining to the sense of touch. Haptic technology refers to the technology which interfaces the user via the sense of touch by applying forces, vibrations and motions to the user. This mechanical stimulation is used to create haptic information [3].

One of the earliest forms of haptic device is used in lighter aircraft without servo systems. As the aircraft approaches a stall, the aerodynamic buffeting is felt in the pilot's controls via a system of mass and spring. This is a useful warning to the pilot of a dangerous flight condition. This control shake is not felt when servo control systems are used in the aircraft. To replace this missing clue, the angle of attack is measured, and when it approaches the critical stall point a "stick shaker" (an unbalanced rotating mass) is engaged, simulating the effects of a simpler control system. This is known as haptic feedback or force feedback device [4].

## 1.2 Application of Haptic Feedback

Haptic feedback is applied in numerous fields. Tele-operators are remote controlled robotic tools. When contact forces are reproduced to the operator, it is called haptic tele-operation. In haptic tele-operations, the force applied on the robotic tool is sensed. Data is generated by the sensor accordingly and transferred to the device which produces the opposing force to the user applied force.

The first electrically-actuated teleoperators were built in the 1950's to remotely handle radioactive substances [5]. Since then, the use of "force feedback" has become more widespread in all kinds of teleoperators.

Haptic feedback plays a key role in stations where visual feedback environment is limited. Unmanned aerial vehicle is one of such cases [6]. The UAV uses haptic feedback to inform the operator about obstacles to avoid collision. In this kind of research, the UAV is surrounded by proximity sensors measuring the proximity of the obstacles. When the obstacle passes by the proximity limit, a force feedback is produced according to the distance between the UAV and the obstacle. The same design criteria is used to design omni-directional wheel chair. The wheel chair has the same mechanism to measure the proximity of the obstacle [7]. It gives an audio feedback to the wheel chair user. The strength of the audio signal is proportional to the distance of the obstacle.

Minimal invasive surgery is one type of tele-surgery. In minimal invasive surgery, the surgeon controls the manipulation from a remote place. In this type of surgery, small incisions are made in the body of the patient. In other words, the surgery is performed inside the body of the patient. An instrument equipped with a gripper and a camera is inserted in the body of the patient. Minimal invasive surgeries have advantages over open surgeries. The recovery time is less compared to open surgery. The minimal invasive surgery can be performed manually or autonomously. In both cases, the surgeon needs a force feedback from the instrument in the body of the patient.

The lack of force feedback can cause tissue damage and life-threatening surgical mistakes. These mistakes can make the surgery more painful and hectic. In the case of complicated surgery such as cardiac surgery, force feedback is more favorable for a successful surgery as it decreases the complication of the surgery by canceling the beats of the heart.

In tele-surgery, needle insertion is one complicated task for the surgeon, especially in soft tissue. Percutaneous therapy mostly involves the tubular delivery of devices such as needles, trocars, bone drills and screws tightening etc. To achieve the desired depth or location, intra-operative imaging devices are normally used. Haptic feedback devices are also used for the location and depth accuracy. During surgery, use of imaging devices such as CT, MRI, ultrasound, and fluoroscopy can make the surgery more complicated and requires more workspace. The imaging devices have the shortcoming that the operator has to refer to them at all times and is thus more laborious. More importantly, these devices do not provide kinesthetic information to the operator.

The kinesthetic information of the environment can be made known to the operator by haptic feedback. The operator can then sense the force applied on the tissues. Accuracy of the depth and location of the insertion can be achieved if the operator knows how much force is required for the layer that is in the path of the needle.

Minimal invasive surgery is the surgery in which a small incision is made in the body of the patient. In this surgery, the vision of the operator is limited due to small workspace. Therefore, haptic feedback can play a key role by enabling the operator to apply and control the force precisely. Therefore, the force feedback of the needle is essential to avoid any trauma, which may cause surgery complications and longer recovery of the patient.

As mentioned earlier, the surgeon performs robotic surgery remotely. The needle insertion is a complicated task in robotic surgery and the surgeon needs the kinesthetic information about the needle. The surgeon has to avoid slip-over of the needle over soft

tissue and thus force feedback will help him. To avoid slip-over, the surgeon changes the direction of his applied force. The surgeon needs to be sure that the needle is inserted; he must thus have force feedback of the piercing needle. To avoid over-insertion of the needle due to soft tissue, haptic feedback is used to pull the needle back to compensate for the overshoot. Hence, needle insertion in robotic surgery and minimal invasive surgery can be performed easily with the help of haptic feedback device.

### 1.3 Background

In haptic feedback, the sensor system senses the force. The sensor data is given to the safety monitoring system, which ensures the safety limits. At the surgeon's end, the actuators reproduce the force at the patient's end. The force applied at the surgeon's end is also sensed for comparison with that at the patient's end. A tactile sensor is used to sense the stiffness of the patient's tissues. The tactile feedback is reproduced on the screen and visual feedback to the surgeon is given by the laparoscope. Consequently, the surgeon can observe the internal action along with sensing the forces and stiffness of the tissues.

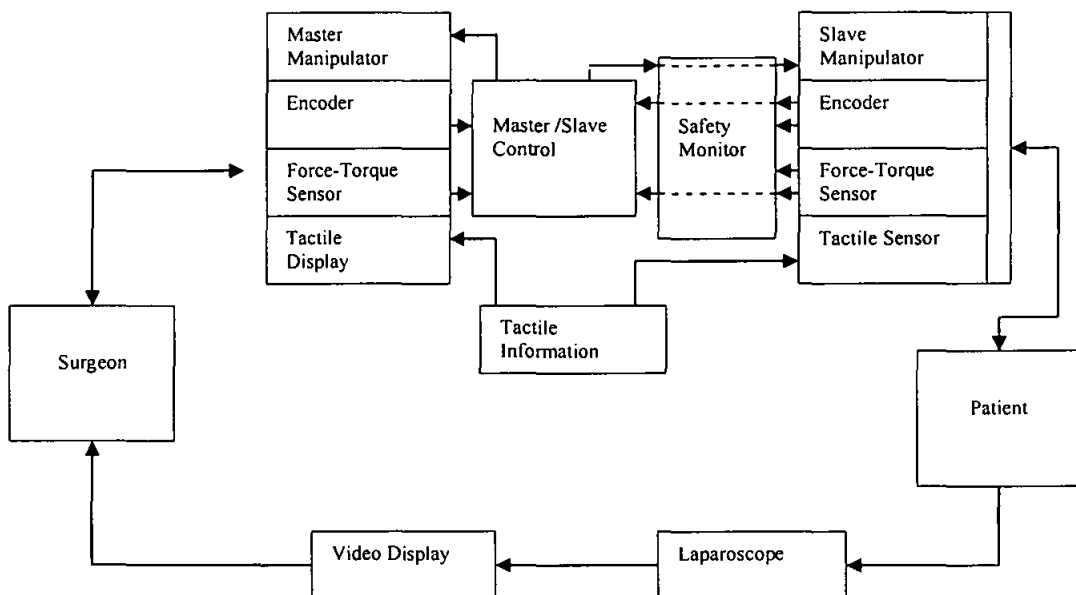


Figure 1.1: Haptic feedback system



The current study is based on a needle insertion haptic feedback model. The needle insertion forces model is based on the total forces acting on the needle during insertion. This model considers the force as a function of depth of the needle. Secondly, needle indentation model is based on the piercing force of the needle. The indentation model considers properties of the tissue.

#### **1.4 Problem statement**

The needle insertion is one of the most complicated tasks during tele-surgery. The lack of needle insertion force feedback makes this task more hectic than open surgery. Therefore, a haptic feedback device is needed to be designed, which enables the surgeon to sense the force exerted on needle during insertion. The device should require less workspace and reproduce output force identical to actual force sensed by the force sensor. The device should be dynamically identical to the needle. Furthermore, the device should enable the surgeon to sense the piercing of the tissue.

#### **1.5 Objectives and Scope**

This study is focuses on the design of the haptic feedback system for needle insertion. A prototype of the haptic feedback device is designed and analyzed. A dynamic model of the device is presented. The device is mathematically modelled. A graphical user interface (GUI) prototype is designed for visual haptic feedback. The real-time needle insertion experiment is performed on chicken skin. Visual haptic feedback for the experiment is reproduced on GUI.

Different needle insertion models are studied and simulated and comparison of results between experiment and model is made. Interface circuitry is designed for haptic feedback device and needle insertion sensor system. Data logging is performed and applied with the help of Pocket data logger XR440 and data acquisition is achieved using

MATLAB. The Graphical user interface is designed in GUI MATLAB. The dynamics of the haptic feedback device is studied and the device is modeled dynamically. Haptic feedback reproduction is correlated with input signal of the device and correlation profile is found. This work can be used as a foundation for the future work on haptic feedback device.

## **1.6 Thesis Organization**

This thesis is structured as follows. Chapter 2 presents literature review of the haptic feedback device. Chapter 3 presents the mechanical setup and experimental setup for needle insertion and haptic feedback of the needle insertion. Chapter 4 presents the needle insertion force model identification and results of the haptic feedback device. Chapter 5 presents conclusion of the thesis and future work.

## CHAPTER 2

### LITERATURE REVIEW

#### 2.1 Introduction

The haptic feedback is playing important in the fields where hand-eye coordination is not good. Haptic feedback devices are used for reproduction of haptic feedback. In this chapter section 2.2 discusses haptic feedback devices. The section 2.3 discusses the telesurgery systems used for surgery. The section 2.4 discusses the importance of haptic feedback in needle insertion. The section 2.5 discusses the needle insertion models presented by the researchers.

#### 2.2 Haptic Feedback Devices

Haptics is gaining widespread acceptance as a key part of virtual reality systems, adding the sense of touch to previously visual-only solutions such as 'The Wedge' and more recently in laptop-based VR solutions such as the '3D-Mobile Immersive Workstation' [14], as shown in Figure 2.1. Most of these solutions use stylus-based haptic rendering, where the user interfaces the virtual world via a tool or stylus, giving a form of interaction that is computationally realistic in today's hardware.

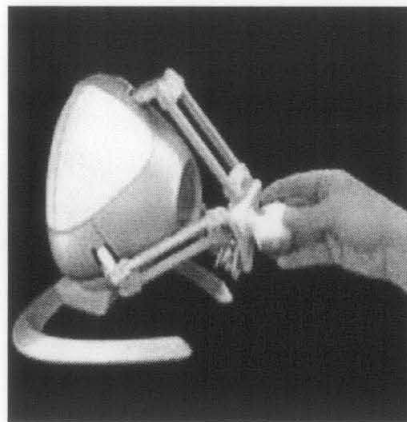


Figure 2.1 3D-Haptic feedback device.

Shadow Dexterous Robot Hand (SDRH) uses the sense of touch, pressure, and position to reproduce the human grip in all its strength, delicacy and complexity. The SDRH was developed by Richard Greenhill and his team of engineers in Islington, London, as part of The Shadow Project (now known as the Shadow Robot Company), an ongoing research and development program whose goal is to complete the first convincing humanoid. An early prototype can be seen in NASA's collection of humanoid robots, or robonauts shown in Figure 2.2 [15]. The Dexterous Hand has haptic sensors embedded in every joint and in every finger pad which relay information to a central computer for processing and analysis. Carnegie Mellon University in Pennsylvania and Bielefeld University in Germany have found the Dexterous Hand as an invaluable tool in progressing our understanding of haptic awareness and are currently involved in research with wide-ranging implications [16].

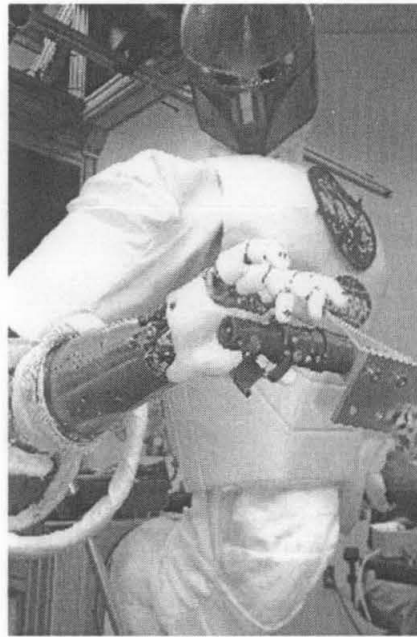


Figure 2.2 NASA's robonauts.

Haptic feedback devices are also used in computer games in the form of controllers such as joysticks or steering wheels. Pioneers in the field of software games developed Nintendo 64 Controller's Rumble Pack (Figure 2.3). This device is capable of producing vibration in selected situations which are firing some weapon or receiving damage. The

steering wheel is designed to provide the feel of acceleration or slipping over during turning of the vehicle [17].

Haptic feedback also has a significant role in fields where the hand-eye coordination is important. It helps the operator to not rely only on visual information but also enables the operator to use the sense of touch and grasping. It is one of the challenging issues in the field of medical sciences. Effectiveness of haptic feedback depends upon the accuracy of force reproduction.



Figure 2.3 Nintendo 64 controller's rumble pack.

Haptic feedback devices are classified into two categories: grounded and ungrounded haptic feedback. Grounded devices are those devices which are positioned on the operator's body or hand. An example of grounded devices is Haptic Glove. The operator's body acts as a base for the device. Grounded devices are placed on the operator's arm at several intermediate locations. Therefore, these devices provide more realistic interaction. Grounded haptic devices are designed to connect on the arm of the operator [18] [19] [20]. Some devices are placed on the operator's hand [21] [22] [23] [24].

Ungrounded devices are those which are placed on the desk or wall. The operator only interacts with the end of the master arm. These devices are non-portable. These devices support their weight and prevent the master from sliding or toppling. Examples of ungrounded devices are joysticks [25] [26]. Some of the ungrounded devices are string-based [27] [28]. Haptic feedback in these devices is proportional to the tension in the strings, with which an operator interacts.

### **2.3 Haptic Feedback in Medicine**

Minimally invasive surgery (MIS) has improved patient surgical outcomes by enabling open surgical procedures to be completed through small incisions. While MIS has led to reductions in post-operative pain and surgical complications, its applications are restricted due to limited haptic feedback. Researchers are trying to reduce this limitation. This problem is solved by different approaches but the main objective is the same: to reproduce the force at the operator's end with help of a haptic feedback device.

During the 1990s, several robotic systems for surgery left research institutes and entered dedicated medical centers for evaluation purposes or even daily practice. The first application area is represented by the systems Caspar™(Figure 2.4a) from Universal Robotic systems Ortho GmbH [29] and Robodoc™ from Integrated Surgical Systems [30] (Figure 2.4b). Integrated Surgical Systems provides also the system NeuroMate™ (Figure 2.5a) which, together with PathFinder from Armstrong Healthcare Ltd. [31] (Figure 2.5b), represent robotic neurosurgery.

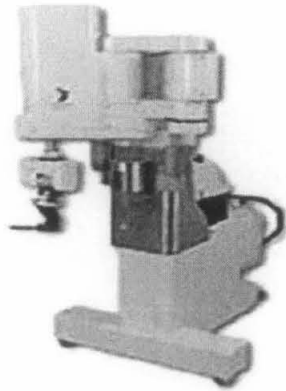


Figure 2.4a Casper

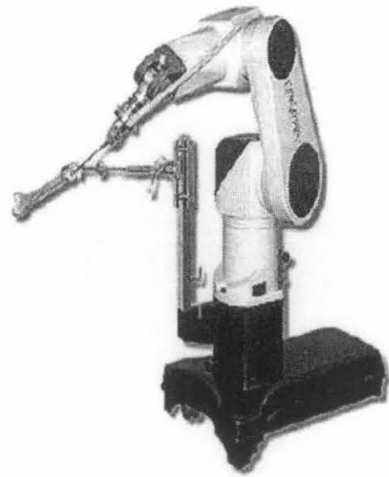


Figure 2.4b Robodoc



Figure 2.5a Pathfinder

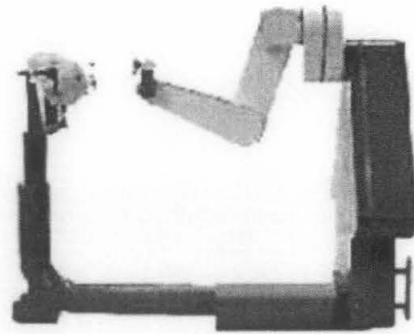


Figure 2.5b Neuromate

Two of the robotic surgery consoles available commercially are Zeus<sup>TM</sup> and daVinci<sup>TM</sup>. Zeus<sup>TM</sup> and daVinci<sup>TM</sup> are more technically mature and commonly used in operation rooms. These two provide scaling of motion, tremor filtering, optical magnification with 3D visual feedback. Zeus<sup>TM</sup> system has three robots fixed on a table. The daVinci<sup>TM</sup> is a little bit slimmer than Zeus<sup>TM</sup>, providing space for surgery assistants. The surgeon at the daVinci<sup>TM</sup> console is immersed at the master. The Zeus<sup>TM</sup> master is open, providing direct view of slave and patient to the surgeon. Figure 2.6 shows Zeus<sup>TM</sup> [32] [33] while Figure 2.7 shows daVinci<sup>TM</sup> [34]. Both these consoles provide partial haptic feedback to

the surgeon. Generally, haptic feedback is still in the research stage. Hence, the surgeon has to rely on visual feedback. [35]

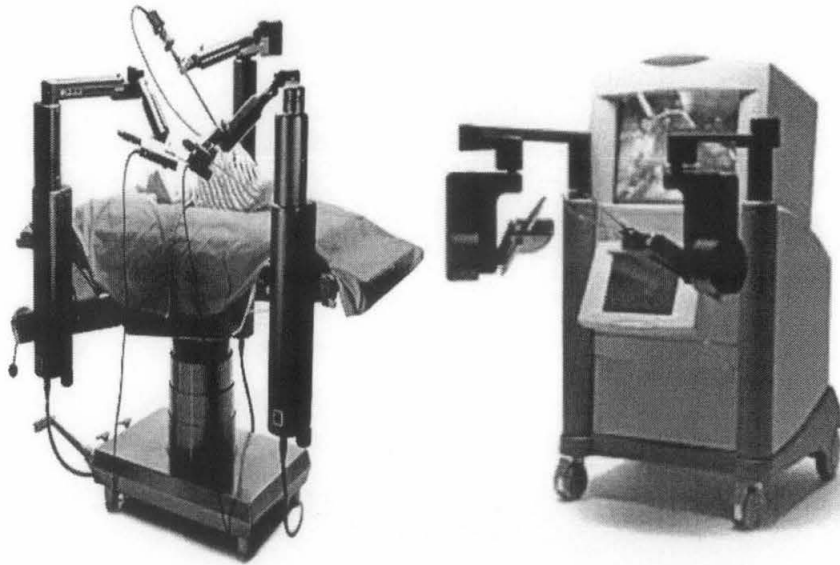


Figure 2.6 Zeus surgery and console.

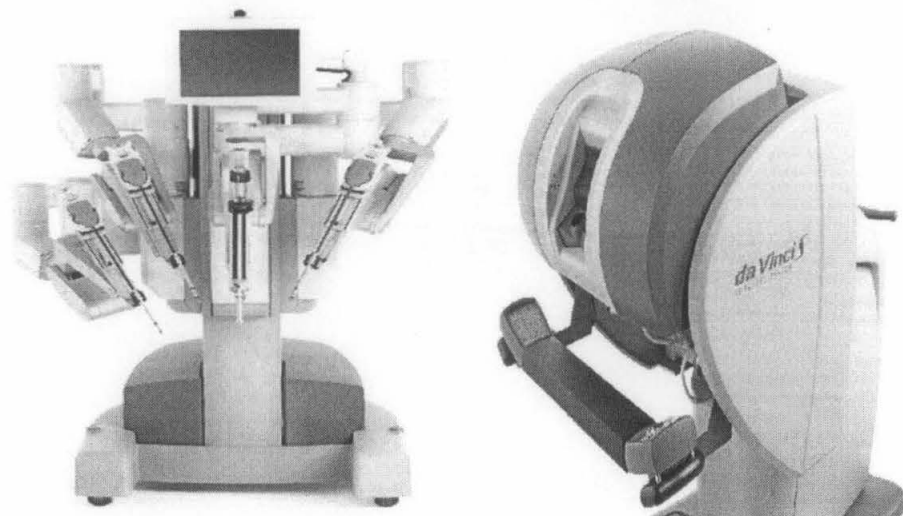


Figure 2.7 daVinci surgery console.



## 2.4 Haptic Feedback Devices Used in Needle Insertion

Needle insertion is one of the complex tasks in tele-surgery. Researches today have keen interest in needle insertion haptic feedback. Needle insertion purely depends on force feedback. Most of the researchers design a haptic simulator for the procedure. Most of the researchers focused on training the surgeons for haptic feedback [8].

The 4-DOF haptic feedback device is designed for hysteroscopy simulation [36]. The hysteroscopy device is mounted on a rod, which is running through a tube. The tube is acting as a foundation for rollers and actuators. The rollers are controlling the dynamics the rod. One roller is controlling transverse motion, the second roller controls rotation of the rod. The rollers are mechanically coupled to separate motors, while the motors are controlled by haptic interface circuitry.

Needle insertion assumes a key role in Brachytherapy, which is one type of therapy for cancerous tissue and is gaining popularity among surgeons. In this therapy, radioactive seeds are implanted in the cancerous tissue to prevent or reduce damage to healthy tissues. The seed implantation is achieved with the help of a needle or a catheter. The efficiency of this therapy depends upon accurate seed implantation [37]. A brachytherapy simulator has been designed in the research described in [38]. The simulator is virtual-reality based and provides only visual feedback and partial force feedback.

Instead of training the surgeons, some of the researchers focus on realistic force feedback. An autonomous blood sampling robot from the forearm was designed in [11]. The robot senses the stiffness of the forearm. The area that has higher stiffness is considered as the vein. This system is not capable to distinguish stiffness due to factors like illness or skin disease. Furthermore, the system cannot handle slip-over of the inserted needle on the vein. Thus, this system is not capable of effectively providing force feedback to the operator.

In another research, needle insertion is sensed by change in impedance at the needle's tip [12]. Electrodes are installed at the tip of the needle. Impedance between these electrodes drops due to conduction in internal fluids. The change in impedance is used for haptic feedback.

Thus, an efficient design of haptic feedback device and development of haptic needle insertion force simulation model are required. Different researchers have presented different models for different environments and tissue mechanical properties. These models are used to extract the needle insertion force. Every model has some assumptions and some limitations. The models whose assumptions are favorable for the system are discussed in the forthcoming section.

## 2.5 Needle Insertion Force Models

This section focuses on the needle insertion force modeling. Di Maio research in [9] [39] is based on force estimation along the shaft of needle during needle insertion. The model is based on the finite elements method. The force is estimated with the help of tissue deformation.

A non-linear model is presented by Christine Simone in [8]. Forces in this model are classified into three components and every component is treated differently. These are force due to stiffness of the tissue and its capsule, force due to the cutting of the tissue and force due to friction between needle and tissue.

Ottensmeyer focused on modeling and measuring mechanical properties of the living tissues [10]. This model is based on the needle and tissue parameters. The model is also known as elasticity model as it focuses on the elasticity of the tissue.

## **2.6 Summary**

In this chapter, literature review of the haptic feedback device is presented. In the first section, the haptic feedback devices available commercially and classification of the haptic feedback devices is also discussed. In the second section, focused on the haptic feedback in medicines and tele-surgery, some commercially available systems are also part of this section. The third section discusses the different haptic feedback systems and some of the related researchers work. Three needle insertion force estimation models by the researchers were presented.

In the next chapter, the design of the haptic feedback system is presented. The basic idea of the system design is taken from the literature review. Electronic interface circuitry and Graphical user interface.

## **CHAPTER 3**

### **DESIGN OF HAPTIC FEEDBACK SYSTEM**

#### **3.1 Introduction**

This chapter discusses the design of haptic feedback system. In section 3.2, the needle insertion force modeling is discussed followed by dynamic modeling in section 3.3 and sensitivity analysis of the system is presented in section 3.4. Lastly the mechanical design of the system is discussed in section 3.5.

#### **3.2 Needle Insertion Force Modeling**

In this section the needle insertion force modeling is discussed. This section focuses on model study and deriving force from model presented for mechanical properties. Three models are studied and needle insertion force is derived from each model. The models studied are Di Maio model, Christine model and Ottensmeyer model.

##### **3.2.1 Di Maio Model (Finite Element Method Model)**

Tissue deformation is measured by finite element method. The tissue is divided into small elements. The element's area changes with the deformation of the tissue. The change in the area of elements is measured by camera. The tissue deformation is proportional to elasticity of the tissue. The force is estimated from strain energy  $E_{strain}$  is presented in Equation 3.1 [40].

$$E_{strain} = \frac{1}{2} \int_{\epsilon}^T (x) \sigma(x) dx \quad 3.1$$

Where as

$\epsilon$  = Mechanical strain

$\sigma$  = Mechanical stress

$x$  = Displacement

$T$  = Total area of material

$n$  = Number of discrete element

The strain energy  $E_{strain}$  in the material can be written as in Equation 3.2.

$$E_{strain} = \frac{1}{2} \sum_{i=0}^n \epsilon (n) \sigma(n) \quad 3.2$$

The total  $E_{strain}$  takes the form as in Equation 3.3.

$$E_{strain} = \frac{1}{2} \epsilon \sigma \quad 3.3$$

The “ $\epsilon$ ” is given by Hook’s law of elasticity and it is defined in Equation 3.4. Therefore, Equation 3.3 takes the form of Equation 3.5.

$$\epsilon = \frac{\sigma}{E} \quad 3.4$$

Where as

$E$  = Constant of elasticity

$$E_{strain} = \frac{1}{2} \frac{\sigma^2}{E} \quad 3.5$$

The strain energy “ $E_{strain}$ ” is given in terms of linear force and linear deformation in [40]. and in Equation 3.6.

$$E_{strain} = \frac{1}{2} P x_1 \quad 3.6$$

Where as

$P$  = Applied force

$x_1$  = Linear deformation

Comparing Equation 3.5 with Equation 3.6, Equation 3.7 is formed:

$$P = A^2 E x_1 \quad 3.7$$

The “P” in Equation 3.7 gives the force acting on the needle during insertion in material.

Where as

$A$  = Area of cross section of needle.

### 3.2.2 Christine Simone Model (Non-linear Model)

The force due to the stiffness of the tissue capsule acts on the needle before the puncture. When the puncture in the capsule occurs, the stiffness force vanishes and the force acting on the needle drops to a low value. The forces after the puncture are the cutting force and the friction force. The drop in the insertion force is used to sense the needle insertion and to avoid overshoot in needle position. In this model, the cutting force is assumed to be constant. The stiffness force is modeled as a nonlinear function of deformation. The

friction force is modeled by a modified version of Karnopp's model [8]. The cutting force is applied on the needle when the needle is slicing the tissue to move through it. The total force exerted on the needle is a summation of these components. The summation is represented by Equation 3.8. The stiffness force in the model is given as in Equation 3.9.

$$F_{needle} = F_{stiffness} + F_{cutting} + F_{Friction} \quad 3.8$$

$$F_{stiffness} = \begin{cases} 0 & z_{tip} \leq z_0 \\ f_x & z_1 \leq z_{tip} \leq z_2 \\ 0 & z_{tip} \geq z_2 \end{cases} \quad 3.9$$

Where “ $f_x$ ” is instantaneous stiffness force,  $z_{tip}$  is the location of the needle tip. Figure 3.1 shows the distribution of stiffness force during needle insertion. In the figure  $z_1$ ,  $z_2$  and  $z_3$  represent locations of the needle during insertion.

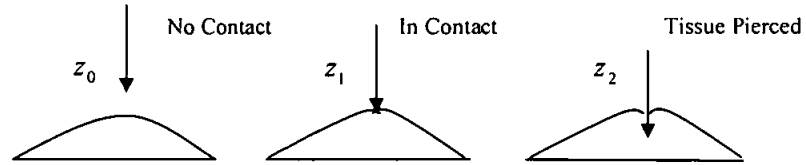


Figure 3.1 Positions of needle during insertion

The stiffness force  $f_x$  is nonlinear and represented by a second-order polynomial in Equation 3.10. The intercept  $a_0$  is assumed zero as the force on needle is zero before needle contact the tissue. The terms  $a_1$  and  $a_2$  are nonlinear stiffness parameters. The parameters are estimated as  $a_1=0.0204 \text{ N/m}$  and  $a_2=0.0008 \text{ N/m}^2$ , for the simulation [41]. Thus, Equation 3.10 takes the form of Equation 3.11.



$$f_x = a_0 + a_1z + a_2z^2 \quad 3.10$$

$$f_x = 0.0204z + 0.0008z^2 \quad 3.11$$

### 3.2.3 Ottensmeyer Model (Linear Model)

The research is focused on modeling Young's modulus of the tissue. The model is presented in Equation 3.12 [10]. There are some assumptions for deriving the model which includes the tissue being isotropic, homogeneous and linear.

$$E = K \frac{3k}{8a} \quad 3.12$$

In the model,  $E$  represents the Young's Modulus of the tissue.  $K$  is the geometric factor which 1 for semi-infinite body and greater than 1 for thin material on a rigid substrate.  $k$  in the model represents stiffness of the tissue and  $a$  represents the radius of indenter.  $K$  is 1 for semi-infinite body. The skin is a semi-infinite body [42] therefore  $K$  is 1 for needle insertion in the skin. Hence, Equation 3.12 takes the form:

$$E = \frac{3k}{8a} \quad 3.13$$

$k$  is stiffness of the tissue and stiffness is the force per deflection.  $k$  can be written as in Equation 3.14, where  $f_z$  is the applied force producing deflection " $\delta$ ".

$$k = \frac{f_z}{\delta} \quad 3.14$$

Substituting the value of  $k$  in Equation 3.13, Equation 3.15 is formed:

$$E = \frac{3f_z}{8a\delta} \quad 3.15$$

Equation 3.16 rearranges Equation 3.15 for the indentation force. Figure 3.2 shows the parameters of the indentation force.

$$f_z = \frac{8a\delta E}{3} \quad 3.16$$

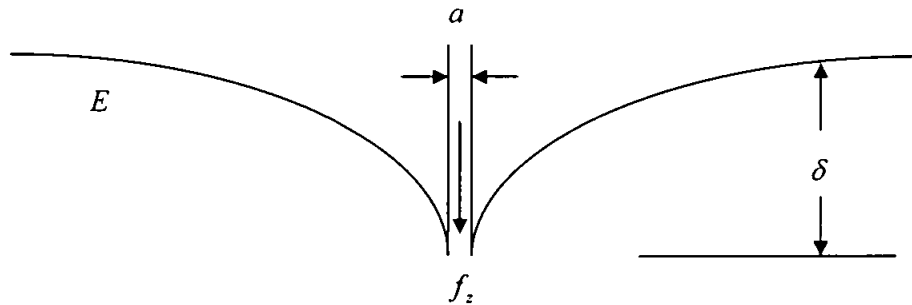


Figure 3.2 Parameter of indentation force

The three models presented in this section are estimating the needle insertion force. Di Maio model is slower and cause delay in the surgeon response. Ottensmeyer estimation is for elasticity of the living tissues by needle insertion from this model needle insertion force is simulated. Christine models the needle insertion is by its components.

### 3.3 Dynamic Model of System

Dynamic modeling is modeling of different parameters changing their behavior with time. In other words, it is modeling of the interdependent parameters. Mostly, it refers to modeling of the forces and torques acting on the system under consideration. This modeling is very important for systems which interact with forces and torques.

Modeling is performed in this research to study the effects of force on system behavior. Forces acting on the system are responsible to produce translational force or vibration force. Modeling is done to study the effect of torque, which is rotation or twisting effect. Friction and damping effects of the system are also studied in the modeling.

The modeling is done by considering one point as reference and the force on the reference point is assumed to be zero. The reference point in the system acts as a sink or ground in the electric circuit. The same reference point is referred to torques as well. The forces and torques are drawn with respect to the reference point. The force vectors coming to the reference point are cancelled out. Forces and torques of the same magnitude yet in the opposite direction cancel each other. Finally, the effect of total forces and torques on the system is clear.

In Figure 3.3, the dynamic model of the system is shown, where two horizontal rollers are under consideration. The horizontal and vertical rollers have the same dynamic model; hence, the horizontal rollers are analyzed and the analysis is then extended to the vertical rollers. The lined point is considered as reference point as it is connected to the foundation of the device.

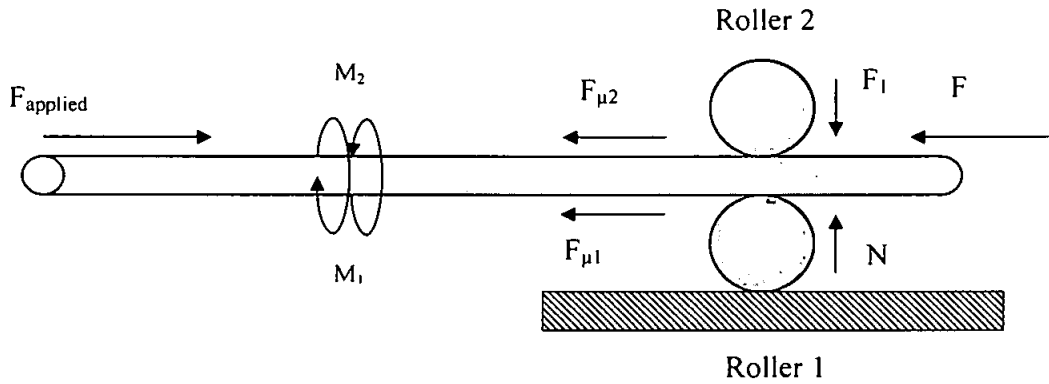


Figure 3.3 Dynamic model of haptic feedback device with two rollers

In Figure 3.3,  $F_{applied}$  is the force applied by the user during needle insertion.  $M_1$  and  $M_2$  are moments of inertia.  $F_{\mu 1}$  and  $F_{\mu 2}$  are friction forces due to roller 1 and roller 2 respectively, acting in opposite direction of the applied force. Force  $F_1$  is the force applied by the horizontal roller connected to the motor. Normal force  $N$  is applied by the roller connected to the reference point; hence, the total force that is opposing the applied force is given in Equation 3.17:

$$F_{applied} = F_{\mu 1} + F_{\mu 2} + F_1 - N \quad 3.17$$

The moments of inertia  $M_1$  and  $M_2$  are equal but in opposite direction. The moments of inertia cancel one another hence; these have no effect on the haptic feedback output stick. Mathematically, it is illustrated as

$$M_1 = M_2 \quad 3.18$$

The roller connected to the foundation is canceling the effects of roller 1 to move the stick downward; therefore, the stick is at equilibrium in the horizontal direction. Figure 3.4 shows the dynamic model of a haptic feedback device with four rollers. The vertical rollers keep the stick at equilibrium in the vertical direction. The total opposing force is shown by Equation 3.19:

$$F_{applied} = F_{\mu h1} + F_{\mu h2} + F_{\mu v1} + F_{\mu v2} - Nh - Nv \quad 3.19$$

In figure  $F_{applied}$  applied force by the user.  $F_{\mu v1}$ ,  $F_{\mu v2}$  are friction forces due to rollers connected vertically.  $F_{\mu h1}$ ,  $F_{\mu h2}$  are friction forces due to rollers connected horizontally.  $F_1$ ,  $F_2$  are opposing forces applied by horizontal and vertical roller connected to motors.  $N$  is normal force to keep the stick at equilibrium. Same force is applied by vertical rollers as well.

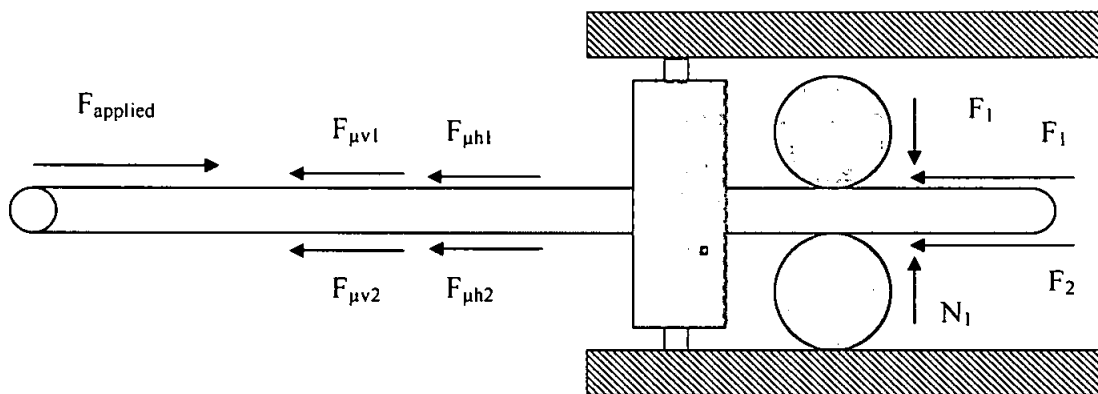


Figure 3.4 Dynamic model of haptic feedback device with four rollers

### 3.4 Sensitivity analysis

Sensitivity of system is defined as the change of response of the system with respect to fractional change of the system parameter. In other words sensitivity is ratio of the fractional change in the function to the fractional change in the parameter as the fractional of the parameter approaches to zero. The sensitivity  $S_{F,P}$  of the function  $F$  is with respect to parameter  $P$  is shown in Equation 3.20 [47].

$$S_{F,P} = \lim_{\Delta P \rightarrow 0} \frac{\Delta F / F}{\Delta P / P} \quad 3.20$$

According to definition of differentiation given in Equation 3.21

$$\lim_{\Delta P \rightarrow 0} \frac{\Delta F}{\Delta P} = \frac{\delta F}{\delta P} \quad 3.21$$

Comparing Equation 3.21 and Equation 3.20 sensitivity takes the form of Equation 3.22

$$S_{F,P} = \frac{P}{F} \frac{\delta F}{\delta P} \quad 3.22$$

Dynamic model of haptic feedback device illustrates the forces that are acting to oppose the applied force and used to reproduce the reactive force. The system parameters are mass of the stick, mass of the roller and friction between rollers and stick. Figure 3.5 shows translational mechanical diagram. Translational mechanical diagram shows the forces and location of forces.

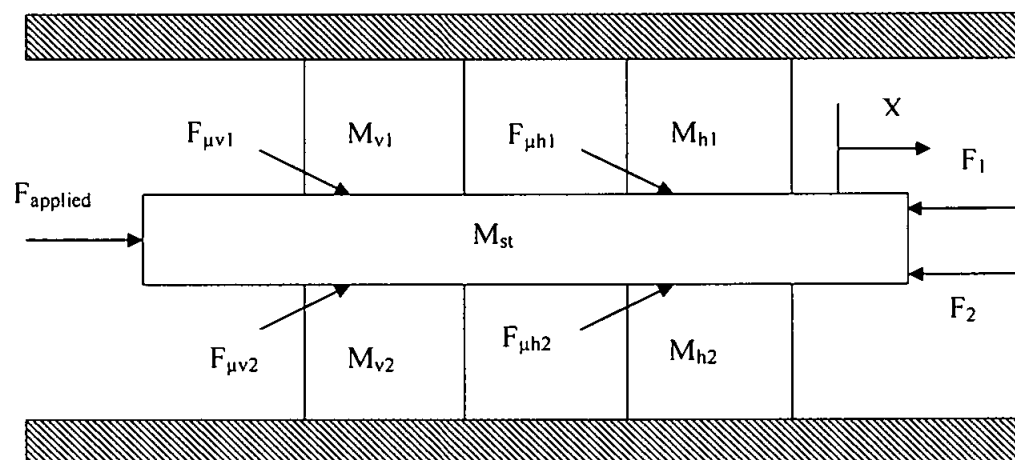


Figure 3.5 Translational mechanical diagram

In Figure 3.5,  $F_{\mu v1}$  and  $F_{\mu v2}$  are friction forces due to rollers connected in vertical position.  $F_{\mu h1}$  and  $F_{\mu h2}$  are friction forces due to rollers connected in horizontal position.  $M_{v1}$  and  $M_{v2}$  are masses of the rollers connected in vertical position.  $M_{h1}$  and  $M_{h2}$  are masses of the rollers connected in horizontal position.  $M_{st}$  is mass of haptic feedback device steel rod moving in between the four rollers, the haptic feedback is produced on it.  $F_{applied}$  is force applied by operator and opposition to this force is produced by these parameters.

Figure 3.6 shows the free body diagram of the stick. The free body diagram shows all the forces acting on the stick. The free body diagram is drawn to examine the forces and in which direction the forces are acting.  $s^2xM_{v1}$ ,  $s^2xM_{v2}$ ,  $s^2xM_{h1}$ ,  $s^2xM_{h2}$  and  $s^2xM_{st}$  are inertial forces of the rollers and stick. Inertial force is that force which is required for a mass to move or to stop it. The inertial force is product of mass and acceleration.  $sxF_{\mu v1}$ ,  $sxF_{\mu v2}$ ,  $sxF_{\mu h1}$  and  $sxF_{\mu h2}$  are friction force between roller and the stick. The friction force is the product of velocity and friction coefficient.  $F_1$  and  $F_2$  are the force applied by one vertical roller connected to motor and one horizontal roller connected to horizontal roller.

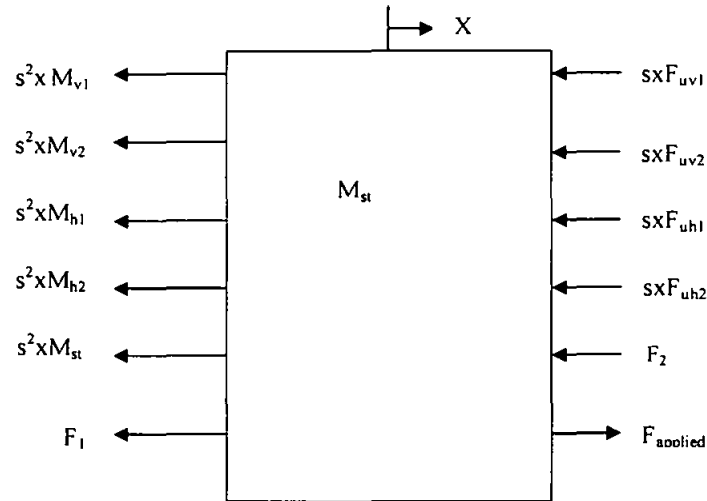


Figure 3.6 Free body diagram of haptic feedback device

The applied force is given in Equation 3.23

$$F_{applied} = F_1 + s^2xM_{v1} + s^2xM_{v2} + s^2xM_{h1} + s^2xM_{h2} + s^2xM_{st} + sxF_{\mu h1} + sxF_{\mu h2} + sxF_{\mu v1} + sxF_{\mu v2} + F_2 \quad 3.23$$

Rearranging the Equation 3.23 by shifting forces to left side Equation 3.24 is formed

$$F_{applied} - F_1 - F_2 = s^2xM_{v1} + s^2xM_{v2} + s^2xM_{h1} + s^2xM_{h2} + s^2xM_{st} + sxF_{\mu h1} + sxF_{\mu h2} + sxF_{\mu v1} + sxF_{\mu v2} \quad 3.24$$

The forces are the same quantities; therefore, it can be replaced by same variable as in Equation 3.25

$$F = F_{applied} - F_1 - F_2 \quad 3.25$$

Putting the Equation 3.25 in Equation 3.24. The Equation 3.8 takes the form of Equation 3.26.

$$F = s^2xM_{v1} + s^2xM_{v2} + s^2xM_{h1} + s^2xM_{h2} + s^2xM_{st} + sxF_{\mu h1} + sxF_{\mu h2} + sxF_{\mu v1} + sxF_{\mu v2} \quad 3.26$$



The rollers are identical; therefore, their masses are same. Hence, masses can be replaced by same variable as in Equation 3.27

$$M_{v1} = M_{v2} = M_{h1} = M_{h2} = M_r \quad 3.27$$

The material between four rollers and stick is rubber; therefore, friction is same for all rollers. Hence, friction force is also replaced by one variable as shown in Equation 3.28

$$F_{v1} = F_{v2} = F_{h1} = F_{h2} = F_r \quad 3.28$$

Hence Equation 3.26 takes the form as in Equation 3.29

$$F = s^2 x 4M_r + s^2 x M_{st} + s x 4F_r \quad 3.29$$

Rearranging the Equation 3.30 for transfer function,

$$F = x(s^2 4M_r + s^2 M_{st} + s 4F_r) \quad 3.30$$

Transfer function is the ratio between output to input as written in Equation 3.31

$$\frac{x}{F} = \frac{1}{s((4M_r + M_{st})s + 4F_r)} \quad 3.31$$

The substitution is made for analysis shown in Equation 3.32

$$M_{hj} = 4M_r + M_{st} \quad 3.32$$

The transfer function of the system is given in Equation 3.33

$$Tf = \frac{1}{s(M_{hf}s + 4F_r)} \quad 3.33$$

Closed loop transfer function is given in Equation 3.34

$$Tf_{cl} = \frac{1}{M_{hf}s^2 + 4F_r s + 1} \quad 3.34$$

The sensitivity formula is applied to closed loop transfer function. Firstly the sensitivity due to roller masses is found in Equation 3.35.

$$S_{Tf_{cl}:M_r} = \frac{M_r}{Tf_{cl}} \left( \frac{\delta Tf_{cl}}{\delta M_r} \right) \quad 3.35$$

Putting the value of closed loop transfer function in Equation 3.35, the sensitivity due masses of the roller is given in Equation 3.36

$$S_{Tf_{cl}:M_r} = \frac{-4s^2 M_r}{(4M_r + M_{st})s^2 + 4F_r s + 1} \quad 3.36$$

Sensitivity due to friction between rollers and stick is found in Equation 3.37

$$S_{Tf_{cl}:F_r} = \frac{-4sF_r}{(4M_r + M_{st})s^2 + 4F_r s + 1} \quad 3.37$$

Similarly, sensitivity due to the mass of the stick is found in Equation 3.38

$$S_{Tf, M_{st}} = \frac{-s^2 M_{st}}{(4M_r + M_{st})s^2 + 4F_r s + 1} \quad 3.38$$

Steady state error sensitivity is to observe the effect of parameters on the steady state error [47]. To find steady state error sensitivity, the steady state error is calculated. Then, the sensitivity formula is applied on the steady state error equation. The system type is one; therefore, velocity constant  $K_v$  is found by formula given in Equation 3.39.

$$K_v = \lim_{s \rightarrow 0} sTf \quad 3.39$$

$$K_v = \lim_{s \rightarrow 0} \frac{s}{s(M_{st}s + 4F_r)} \quad 3.40$$

$$K_v = \frac{1}{4F_r} \quad 3.41$$

The steady state error is reciprocal of velocity constant written in Equation 3.42

$$e(\infty) = \frac{1}{K_v} \quad 3.42$$

Steady state error of the system is given in Equation 3.43

$$e(\infty) = 4F_r \quad 3.43$$

Steady state error sensitivity with respect to  $M_r$  is zero in Equation 3.44. Therefore steady state error is not sensitive to mass of the rollers. The mass of the rollers has no effect on the steady state error of the system.

$$S_{e(\infty)M_r} = \frac{M_r}{e(\infty)} \frac{\delta e(\infty)}{\delta M_r} = 0 \quad 3.44$$

Similarly, steady state error sensitivity due mass of the stick is also zero; therefore, mass of the stick have no effect on the steady state error of the system.

$$S_{e(\infty)M_{st}} = \frac{M_{st}}{e(\infty)} \frac{\delta e(\infty)}{\delta M_{st}} = 0 \quad 3.45$$

The steady state error sensitivity due to friction coefficient is one; therefore, the steady state error is directly proportional to the friction coefficient of rubber and material of the rollers.

$$S_{e(\infty)F_r} = \frac{F_r}{e(\infty)} \frac{\delta e(\infty)}{\delta F_r} = 1 \quad 3.46$$

### 3.5 Haptic Feedback System Design

The force exerted on the needle during needle insertion is the reactive force exerted by the tissues of the skin. The main aim of this research is to measure this force and reproduce it remotely. The force sensor senses the needle insertion force. The sensor provides the output voltage according to the input force. The output of the sensor is given to the data acquisition card and also given to the interface circuitry. Data acquisition card provides input to Matlab graphical user interface. The interface circuitry amplifies the

output from preamplifier and makes it suitable for motors used in haptic feedback mechanism. The block diagram in Figure 3.7 shows the function of the experimental setup. Experimental setup consists of four modules namely; needle insertion module, interface module, haptic feedback module and graphical user interface.

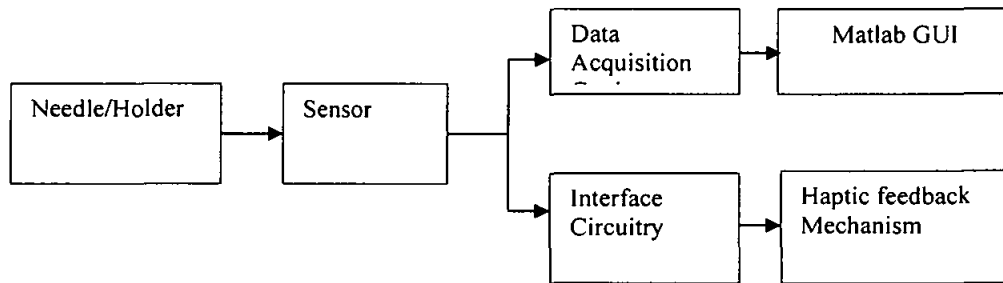


Figure 3.7: Block diagram of experimental setup

### 3.5.1 Needle Insertion Module

The needle insertion module consists of a needle, a needle holder and a sensor. In this module, the needle and sensor are connected by a needle holder. The sensor senses force exerted on the needle. Reactive force exerted on needle depends upon the needle parameters.

Needle shapes and other parameters may change according to the application. Generally, two types of needles are used; namely, the beveled shaped needle and diamond shaped needle. The beveled shaped needle is commonly used for percutaneous therapies whereas the diamond shape is used for tissue biopsy purposes. The beveled shaped needle has no

pre-puncture as compared to diamond shape. The tissue reactive force also depends upon the diameter of the needle and the length of the needle. Figure 3.8 shows the beveled and diamond shaped needle tip. The typical needle parameters are given in Table 3.1 provided by Trumo®. The first column in the Table 3.1 gives the product codes. The second column provides the color code of the hub of the needle. The third column provides the Gauge and diameter of the needles and the last column shows the needle length in milli-meter and in inches [43].



Figure 3.8: Beveled and diamond shaped needle.

Table 3.1: Needle color coding parameter

Product Code	EN/ISO Hub Color Code	Diameter Gauge/mm		Needle Length (mm)
KN-1838SB	Pink	18G	1.20	40
KN-2025R	Yellow	20G	0.9	25
KN-2138RB	Green	21G	0.80	40
KN-2316RB	Blue	23G	0.60	16
KN-2325RB	Blue	23G	0.60	25
KN-2332RB	Blue	23G	0.60	32
KN-2516RB	Orange	25G	0.50	16
KN-2525RB	Orange	25G	0.50	25
KN-2713RB	Grey	27G	0.40	12

The needle holder is shown Figure 3.6. The needle is held by a holder. The needle holder is made of material known as Teflon. This material is used because it is light-weighted

and flexible. The holder holds the needle and the reactive force that is sensed is then transferred to the sensor. The holder can hold needles of different diameter and length. The needles from 18G to 23G have different holder from the needles 25G to 27G due to the differences in length. The sensor is also held by the holder in such a way that force exerted on the needle is sensed by the sensor.

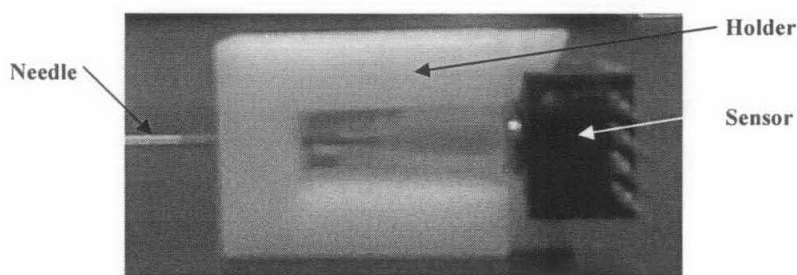


Figure 3.9: Needle holder made of teflon

The Figure 3.10 shows the force sensor. The sensor used in this module is a Piezoresistor. Piezoresistor is a resistor whose value changes when normal force is applied on its crystal. The piezoresistor is internally connected to the balanced Wheatstone Bridge. When the resistance of one terminal changes, it disturbs the equilibrium at deflection nodes. The voltage shows the resistance change that is increasing or decreasing. The sensor output is very low and it is immune to noise [44].

In this setup, the sensor output is in the range of milli-volts. The low noise power supply is used for the biasing the sensor. Referring to Figure 3.10, pin 1 and pin 3 are connected to biasing voltage, whilst pin 2 and pin 4 are the output voltages. Input to the sensor which is the force is given on the load cell. Since the sensor has low resistances, the

terminals are specially insulated to avoid short circuit with one another. The sensor pictorial view is shown in Figure 3.10.

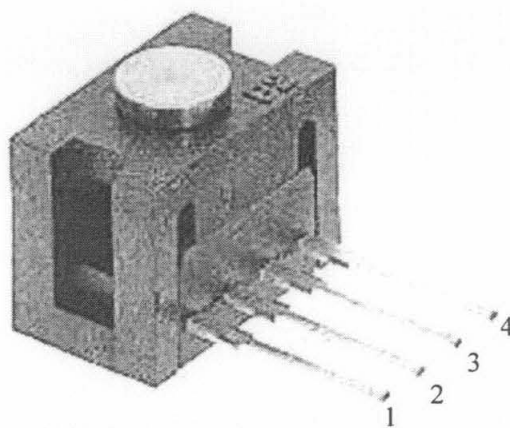


Figure 3.10: Force sensor.

The force sensor is calibrated experimentally. The sensor calibration experiment consists of an electronic weighing machine, different weights, a multimeter and a low noise power source (regular dry-cell battery). The sensor is biased by the battery according to the pin configuration in the data sheet of the sensor: Pin 1 is connected to the positive terminal of the power supply, Pin 3 is connected to the negative terminal of the power supply and pins 2 and 4 are connected to the multimeter. The sensor terminals 2 and 4 have very low voltage change as force is applied on it, therefore the multimeter measures millivolt readings. The sensor is of piezoresistor type: its resistance changes with the force applied on its load cell. The piezoresistor is connected internally with a wheat stone balance bridge. The change in resistance is sensed by the wheat stone bridge. The wheat stone bridge is unbalanced due to the change in resistance, therefore the deflection terminal gives the voltage to balance it. Figure 3.11 shows the internal wheat stone bridge of the sensor [44].



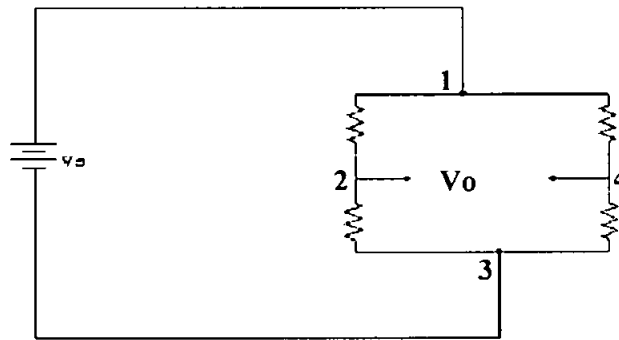


Figure 3.11 Internal wheat stone bridge of force sensor.

The calibration experiment is carried out by placing weights on the weighing machine to measure their weight. The same weight body is placed on the load cell of the sensor. The reading is taken by the multimeter. This experiment is carried out for twenty different weights.

The force from tissues is exerted on the needle. The holder holds needle steadily. The force exerted on needle is sensed by the sensor. The sensor converts the input force into voltage but in the milli-volts range. Therefore, the sensor output has to be pre-amplified. The output from the sensor is given to the Graphical User Interface Module for visual feedback. The output from sensor is also given to the interface circuitry. This circuitry processes the input for haptic feedback module.

### 3.5.2 Interface Module

Interface circuitry is designed to interface the haptic feedback module to the needle insertion module. Furthermore, this circuitry is used for the isolation of the low current module from high current module. The needle insertion module is a low current module, the sensor has very low input and output resistance. The haptic feedback is a high current module as motors are producing opposing force to applied force. Figure 3.12 shows the circuit diagram of interface circuitry.

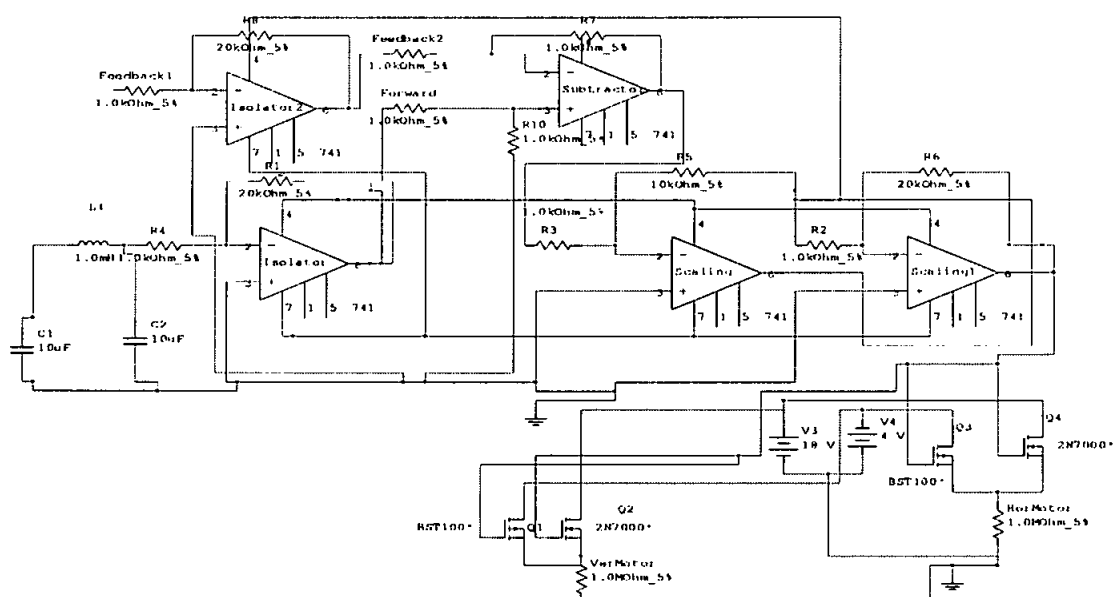


Figure 3.12: Interface circuit diagram

In the interface circuitry, the cascaded scaling amplifiers achieve the amplification. Operational amplifiers are used as scaling amplifiers because of its accurate scaling and very high noise rejection. The summing junction in feedback is also op-amp based. The stall torque of the motor is cancelled by applying reverse voltage. This voltage produces

torque in the direction to oppose the stall torque. The interface circuitry has power MOSFETs to derive motor. There are two MOSFET set for every motor. One is the P-channel MOSFET while the other is the N-channel MOSFET. The P-channel MOSFET is used to drive the motor in clock wise while the N-channel is used to derive motor in anti clock wise.

The output of the sensor is the input of the isolator. The isolator is connected to the set of cascaded scaling amplifier. The output of the scaling is given to the motor drive circuits which are the power MOSFETs. These MOSFETs drive the motor according to the input at gate as MOSFET is voltage controlled resistor. The conduction through source to drain is controlled by gate voltage. The gate voltage is controlled according to sensor output.

Figure 3.13 shows the diagram of the interface circuitry.

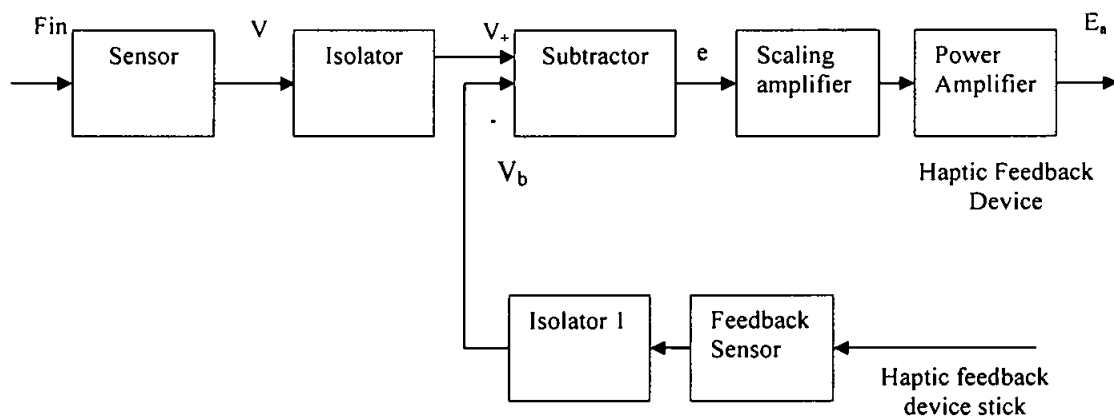


Figure 3.13: Working block diagram of interface circuitry

In the feedback part, the sensor used is the same type of sensor that is used to measure the force from haptic feedback device. The isolator 1 is used to isolate the feedback sensor from over loading. Power amplifier is MOSFET driven circuitry. This is the driving motors of the haptic feedback device. One MOSFET set is for one motor. Therefore, two MOSFETs are driving the horizontal motor and the other two are driving the vertical motor. The MOSFET has many advantages over transistor. This is the reason why the transistor is not used. The MOSFETs are voltage-controlled resistors. The gate voltage controls the voltage between the source and drain whereas the transistor can control the emitter-collector voltage by base current. Therefore, transistor is current controlled device.

### **3.5.3 Haptic Feedback Device Module**

The designed haptic feedback device uses friction as reactive force. The designed haptic feedback device is based upon the theory that when a one body slides on other body, there are some forces acting on the sliding body to oppose its motion. That opposition is known as friction. The friction is of two types. Static friction is offered to the body when it is tending to start motion. Dynamic friction is offered when the body is in motion. The design device is one of the dynamic friction devices.

The concept of this device is taken from the device designed for the hysteroscopy. This device is of 4DOF [36]. The designed device also consists of four rollers. The designed haptic feedback device is shown in Figure 3.14.

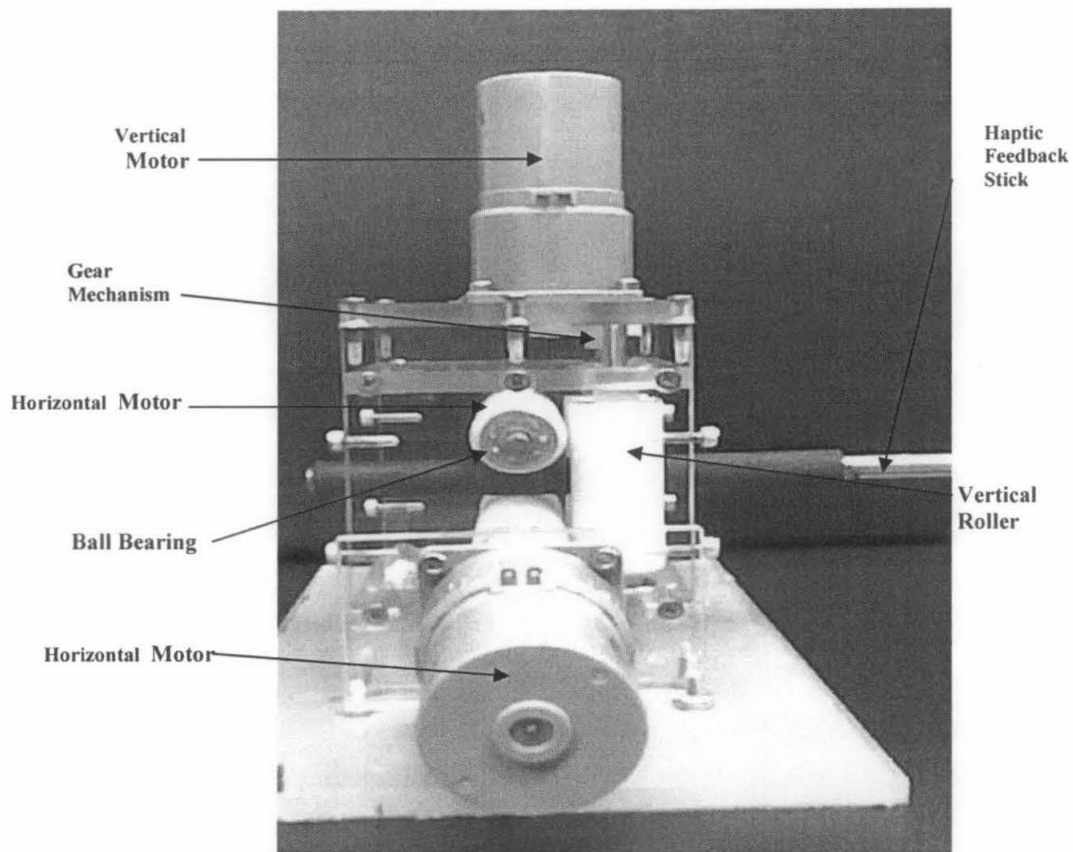


Figure 3.14: Designed haptic feedback device

These rollers are used for the production of dynamic friction. The rollers are made of Teflon material. This material is used because of its rigidity and light weight. This material is commonly used for the production of plastic gears. It has less wear and tear as compared to other materials available. The diameters of the rollers are 5-millimeter. The lengths of these rollers are 20-millimeter. The stainless steel rod is installed in the roller axially. The steel is used as the shaft of the roller. The diameter of this rod is 2.5 millimeters. The two rollers are installed horizontally while two rollers vertically. This arrangement is done to distribute the reactive force uniformly along the output stick and to avoid the undesirable movement of the stick. One vertical and horizontal roller is

connected to the motor by gear mechanism. Gear mechanism is used to avoid slippage at joint between roller and motor. To avoid friction between the rollers and their foundation ball bearings are installed. Therefore, every attachment point of the rollers have ball bearings. Figure 3.15 shows the isometric view of the roller.

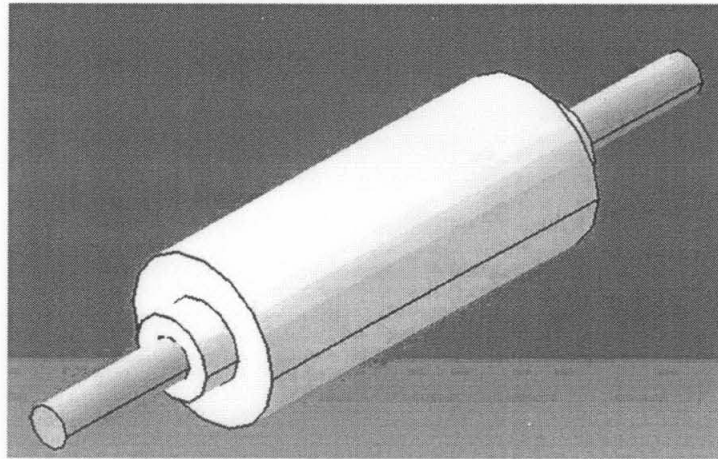


Figure 3.15: Roller isometric view

The rollers are driven by motors to produce the reactive torque. The motors used in this design are permanent magnet DC motor. The torque of these motors is proportional to the applied voltage. The applied voltage is the amplified form of sensor voltage. The motors have stall torque equal to 15 milli Newton meter that can be produced by the 4.2 volts in opposite direction.

The reactive torque can be converted to tangential force by placing a body on the roller. The torque is equal to the product of tangential force to the moment arm. The moment arm is the distance between the axes of rotation and the applied force and vice versa.

Therefore the output stick is placed in between the rollers. The output stick is made of stainless steel. The reactive force produced on the stick is the friction between it and the rollers. The friction force is equal to the torque over the moment arm. The moment arm is the radius of the rollers. The rollers are rotating along its center. The friction between the rollers (Teflon) and steel is very low especially for smooth surfaces. To avoid slippage between the steel stick and rollers, a rubber sleeve is putted on the stick. The friction coefficient of rubber and Teflon is higher than Teflon and steel. The roughness of the surfaces is not applicable because it will produce vibrations in friction force which is the reactive force. The gravitational pull is cancelled out by bending moment analysis. The steel stick length is found, which obeys the bending moment equations. In this analysis, the stick is treated as the beam is connected at one end to support and the other end is free. At the free end, the feedback sensor of the interface circuitry feedback terminal is connected. This connection is manual, which means that the operator will have to hold the sensor at the end in his hand.

The interface circuitry module gives the input to the motors of this haptic feedback module. The inputs of these motors are proportional to the reactive force exerted on needle during needle insertion. The motors produce the reactive torques. The torques are transferred to the rollers with the help of gears and ball bearings. The reactive force produces the reactive tangential force along the circumferences of the rollers. The reactive force is transferred to the stick as a friction force to the applied force. The applied force is acting on another end of the stick. This force is analogous to reactive

force applied on needle by tissues. The applied force is force acting on the needle to be inserted while the reactive force is the force opposing the exerted force.

### 3.5.4 Graphical User Interface Module

This consists of two parts i.e. the data acquisition and user interface. In this module, the sound card of the computer is configured as the data acquisition card. The sound card is used to minimize the processing delay as compared to the other DAQ cards. The trigger is set manually. When the start button in the GUI is pressed, the sound card is triggered and it will start acquiring data. The signal from the force sensor is analog. The sound card of the computer also does the analog to digital conversion as it is done for voice signal. The level of the sound card is -1 to 1 volt. Therefore, the pre-amplifier and filter is used. The sampling rate is 8000 samples per second to achieve a higher level of accuracy. The sound card gives force data to matlab workspace and the figure is updated accordingly. The figure provides a visual haptic feedback. Figure 3.16 shows the block diagram of the GUI setup.

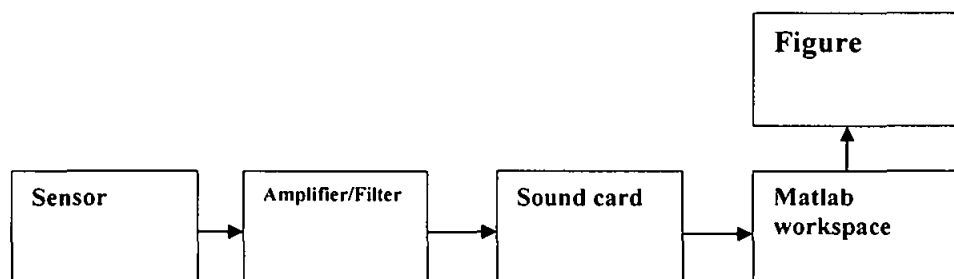


Figure 3.16: Block diagram of GUI.



Figure 3.18 shows the view of graphical user interface environment. The GUI decides the needle status by model force. The parameters are entered into the GUI environment by the user manually. These parameters are elasticity of the tissue in  $K_{pa}$ , diameter of needle in millimeter and the depth of the needle in millimeter. Then the GUI compares the input force and the model force at insistent these two are equal than the GUI shows that needle inserted.

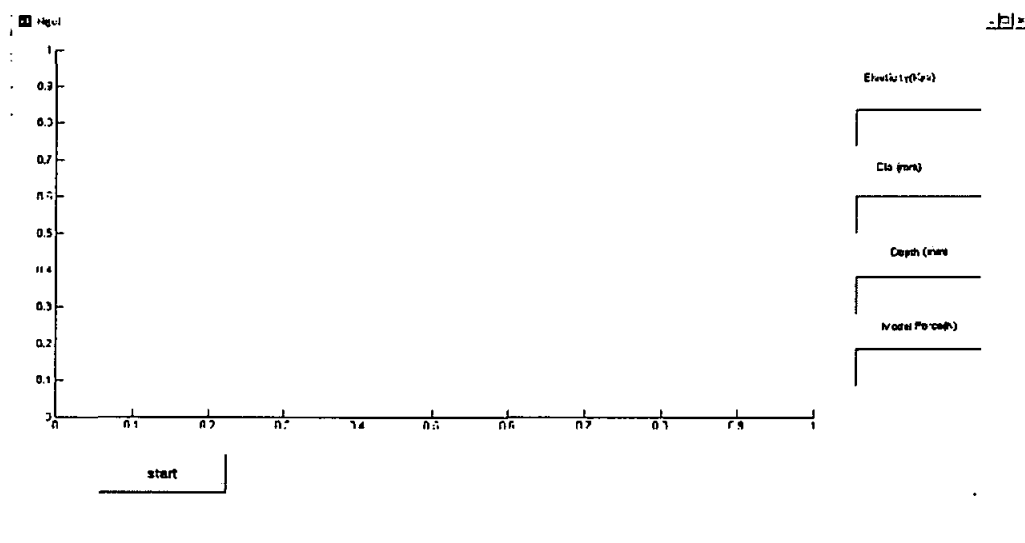


Figure 3.17: Pictorial view of GUI environment.

The operator has option to change the condition of the decision making of GUI for the needle insertion status. The GUI makes decision that needle is inserted when needle force is greater than model force. Also GUI can make decision from the force data acquired by DAQ card. When abrupt drop in the force occur than the GUI status changes to needle is inserted.

### 3.6 Summary

In this chapter the haptic feedback system design is discussed. The first section discusses needle insertion force models. Second section of the chapter discusses the dynamic modeling. The third section discusses the sensitivity analysis of the system. Last section discusses the design of system.

In the next chapter, the simulation and experimental results is discussed. Firstly needle force simulation results are presented followed by experimental results of sensor calibration, needle insertion on chicken skin, haptic rendering, GUI results and sensitivity analysis on the system is discussed. Lastly the comparison between experimental results and model is discussed.

## CHAPTER 4

### HAPTIC FEEDBACK DEVICE RESULTS

#### 4.1 Introduction

In this chapter the results of the system is discussed. Section 4.2 discusses the model simulation results. In section 4.3 discusses the experimental results of Needle piercing force, sensor calibration, haptic rendering, GUI results and sensitivity results. Section 4.4 provides the discussion based on experimental results.

#### 4.2 Needle Insertion Force Simulation

Simulation of the model is carried out by substituting the values of elasticity [13]. The value of the needle diameter is substituted from Table 3.1 which is given by the needle manufacturer, Trumo® [43]. The tissue deformation value is assumed to be 20 millimeters. Table 4.1 shows the values of the parameters and Figure 4.1 shows the simulation results of the model.

Table 4.1: Indentation force for different needle diameters

Diameter(mm)	Deformation(mm)	Elasticity(Kpa)	Force (N)
0.4	20	23	0.490666667
0.45	20	23	0.552
0.5	20	23	0.613333333
0.55	20	23	0.674666667
0.6	20	23	0.736
0.65	20	23	0.797333333
0.7	20	23	0.858666667
0.75	20	23	0.92
0.8	20	23	0.981333333
0.85	20	23	1.042666667
0.9	20	23	1.104
0.95	20	23	1.165333333
1	20	23	1.226666667
1.05	20	23	1.288
1.1	20	23	1.349333333
1.15	20	23	1.410666667

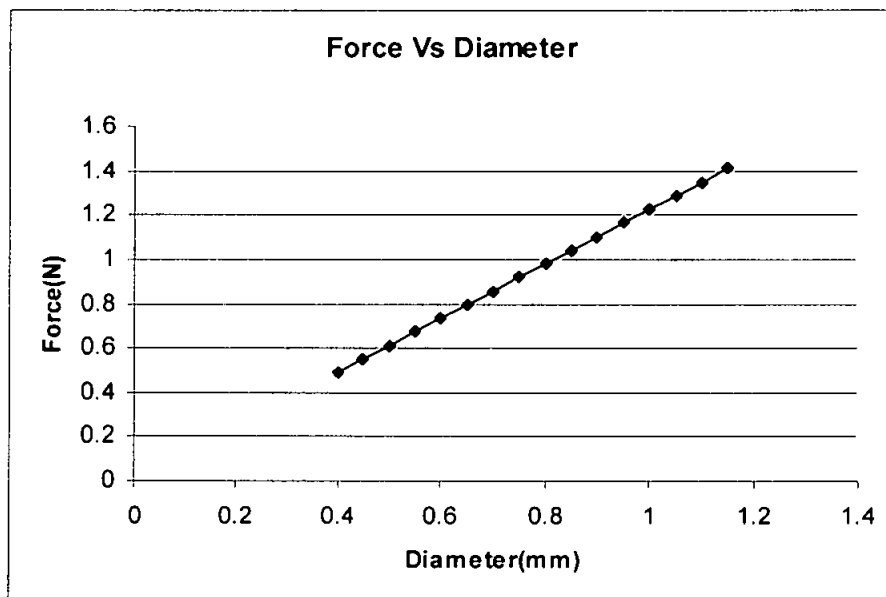


Figure 4.1 Relation of indentation force to needle diameter

Simulation results are showing that needle insertion force is linearly related to diameter of needle. Increase in the diameter of the needle the reactive force will increase as well.

### 4.3 Experimental Results

In this section results of experiments performed on the haptic feedback system is presented. Firstly, the results of sensor calibration are presented, and then this is followed by needle insertion force profile. Needle insertion forces for different diameters, haptic rendering results and GUI results are also presented in this section. Lastly the sensitivity analyses of the system are presented.

#### 4.3.1 Sensor Calibration Results

The finding of sensor calibration experiment is given in Table 4.2. The first column is the value of mass. The mass is converted to weight with the help of gravitational constant. The voltage output of the sensor is given in millivolts in the fifth column. For every reading, the conversion factor from force to volts is found which is given in the seventh.

The average value conversion factor is constant  $0.0285 \pm 0.007$ . The Figure 4.2 shows the relation between input of the sensor and output of the sensor i.e. force and voltage. From Figure 4.2, it is clear that input output is linearly related to each other; therefore, the sensor is linear for the range of the needle insertion force.

Table 4.2: Sensor calibration readings

Mass (g)	Mass (Kg)	Gravitational Constant (g=9.8)	Force(N)	Volts(V)	Volts to gram	Volts to Newton	Average for V to N
0	0	9.8	0	0.0027	0	0	0.0002799
24	0.024	9.8	0.2352	0.005	0.000208333	0.021258503	
32	0.032	9.8	0.3136	0.0073	0.000228125	0.023278061	
40	0.04	9.8	0.392	0.0101	0.0002525	0.025765306	
54	0.054	9.8	0.5292	0.0136	0.000251852	0.025699169	
66	0.066	9.8	0.6468	0.0178	0.000269697	0.027520099	
78	0.078	9.8	0.7644	0.0215	0.000275641	0.028126635	
100	0.1	9.8	0.98	0.02806	0.0002806	0.028632653	
108	0.108	9.8	1.0584	0.0318	0.000294444	0.030045351	
124	0.124	9.8	1.2152	0.039	0.000314516	0.032093483	
134	0.134	9.8	1.3132	0.0395	0.000294776	0.030079196	
150	0.15	9.8	1.47	0.0424	0.000282667	0.028843537	
162	0.162	9.8	1.5876	0.0502	0.000309877	0.031620055	
188	0.188	9.8	1.8424	0.0554	0.000294681	0.030069475	
208	0.208	9.8	2.0384	0.0605	0.000290865	0.029680141	
216	0.216	9.8	2.1168	0.064	0.000296296	0.030234316	
230	0.23	9.8	2.254	0.0677	0.000294348	0.030035492	
242	0.242	9.8	2.3716	0.0718	0.000296694	0.03027492	
258	0.258	9.8	2.5284	0.078	0.000302326	0.030849549	

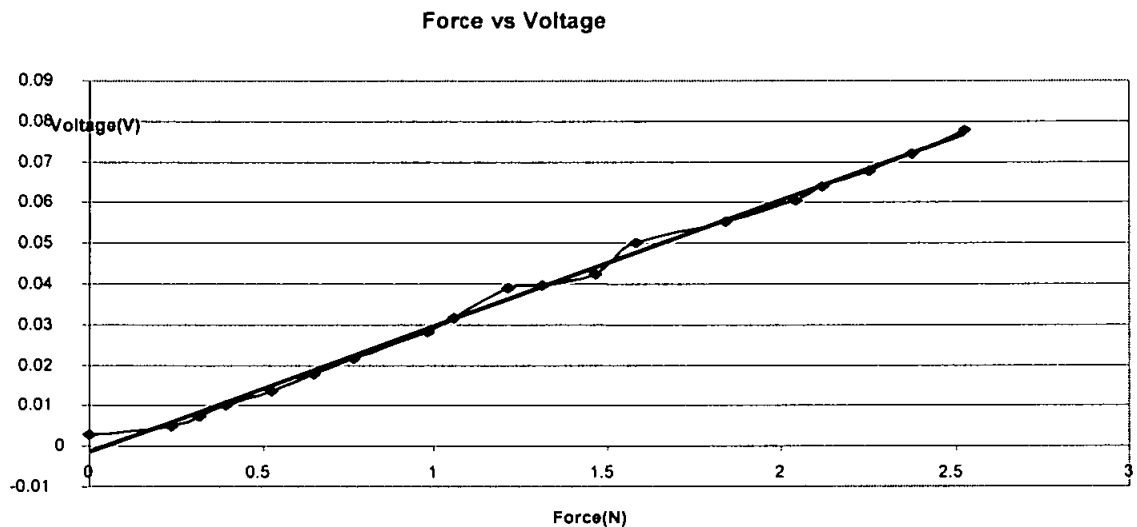


Figure 4.2 Force vs output voltage of sensor

These experimental results show that the sensor is linear for the range of needle insertion force. The range is different for various tissues in literature [8] [13] [41]

#### 4.3.2 Needle Insertion Force

Figure 4.3 shows the experimental results of the needle insertion reactive force acting on the needle. The reactive force starts to increase as the needle contacts the tissue. The reactive force increases up to a certain point and then drops down as shown by the arrow. The point at which reactive force reaches its first maximum that applied force is equal to the stiffness of the tissue capsule. The reactive force falls to a very low value and this may cause overshooting of needle position. This point is very significant for needle insertion haptic rendering. The stiffness force vanishes as the needle pierces through the skin and the reactive force is now the result of friction and cutting forces [41]. Data of needle insertion reactive force is acquired by pocket logger XR440 and is taken on chicken meat with skin. The first spike shown by arrow in the reactive force profile shows that at this instant, the skin of the chicken is pierced and the needle is entered into the tissue.

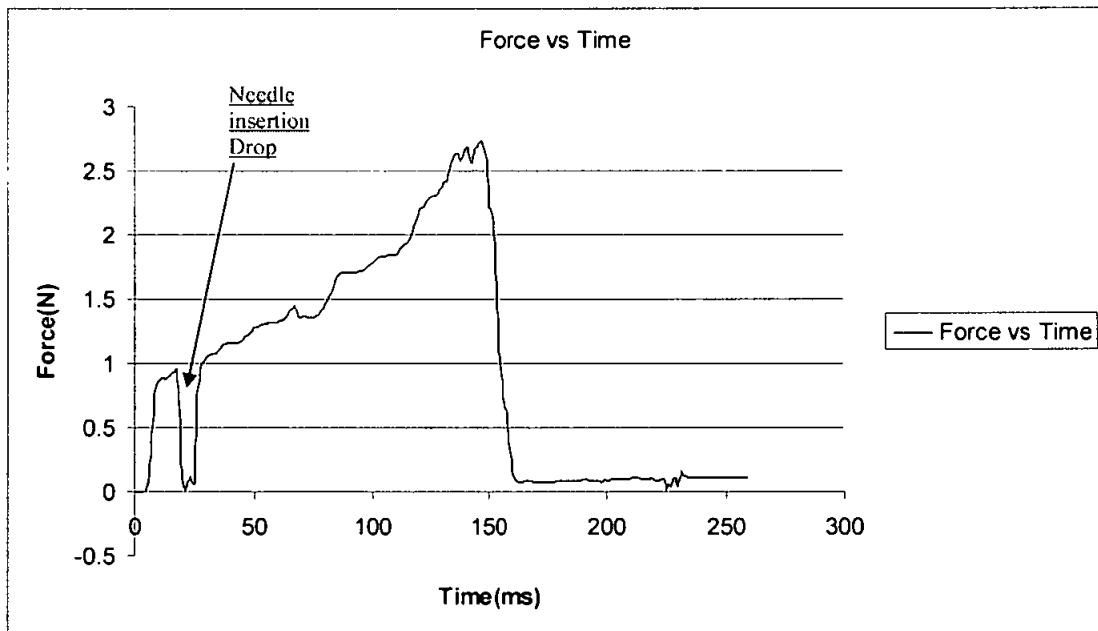


Figure 4.3: Force vs time from pocket logger XR440

### 4.3.3 Experimental Results of Needle Insertion

Readings of the force profile are taken on needles of different diameters. The needle gauges are already shown in Table 3.1 in the previous chapter. These are 20G, 21G and 23G. Table 4.3 shows the needle piercing force according to diameter. Figure 4.4 plots needle piercing force for different diameters of the needle.

Table 4.3: Experimental reactive force on needle during piercing of skin

Gauge	Dia	Voltage	Converting Factor	Force
20	0.9	3.24	0.3	0.972
20	0.9	3.34	0.3	1.002
20	0.9	3.07	0.3	0.921
20	0.9	3.54	0.3	1.062
21	0.8	3.1	0.3	0.93
21	0.8	2.75	0.3	0.825
21	0.8	3.05	0.3	0.915
21	0.8	3.33	0.3	0.999
23	0.6	1.19	0.3	0.357
23	0.6	1.1	0.3	0.33
23	0.6	1.39	0.3	0.417
23	0.6	1.78	0.3	0.534

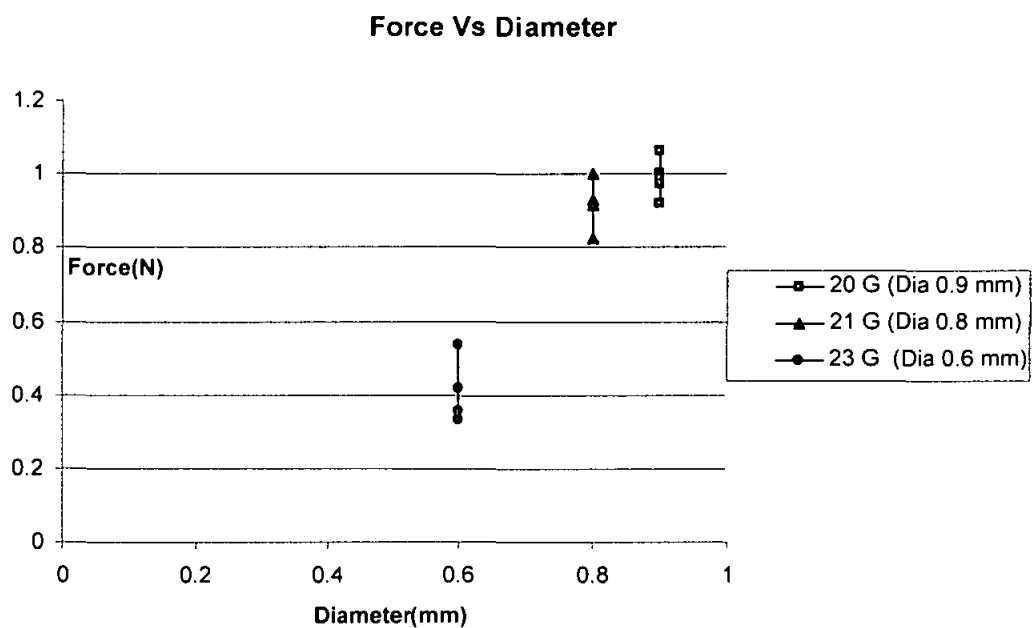


Figure 4.4: Experimental piercing force according to diameter of needle.

The average force needle insertion force for 20 gauge needle is  $0.989 \pm 0.072$  Newton, average needle insertion force for 21 gauge needle is  $0.917 \pm 0.092$  Newton and average needle insertion force for 23 gauge is  $0.41 \pm 0.12$  Newton.



#### 4.3.4 Haptic Rendering Results

To study the correlation of applied force and reproduced force of the haptic feedback device, the needle insertion reactive force is given in Figure 4.5. This is the applied force which is input to the haptic feedback device, while an identical signal generated electronically via the interface circuitry is shown in Figure 4.6.

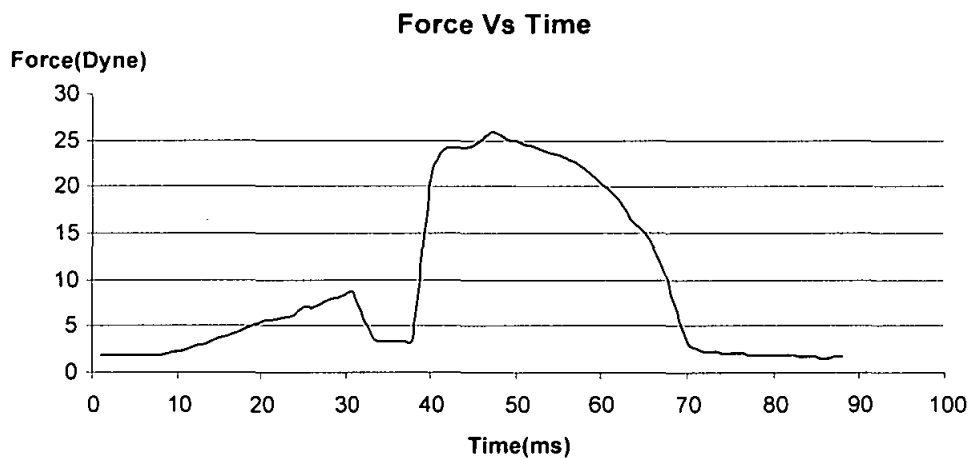


Figure 4.5 Needle reactive force vs time

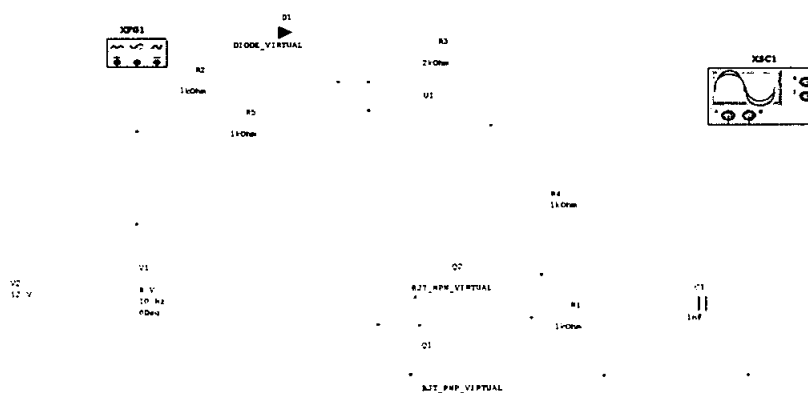


Figure 4.6 Reactive force reproductive circuit

Normalized values of the signal given as input force to the haptic feedback device is shown in Figure 4.7 and normalized values of the signal reproduced by the haptic feedback device is shown in Figure 4.8. Correlation of the input force signal and output force signal is shown in Figure 4.9. Table 4.4 is shows the correlation factor of the device.

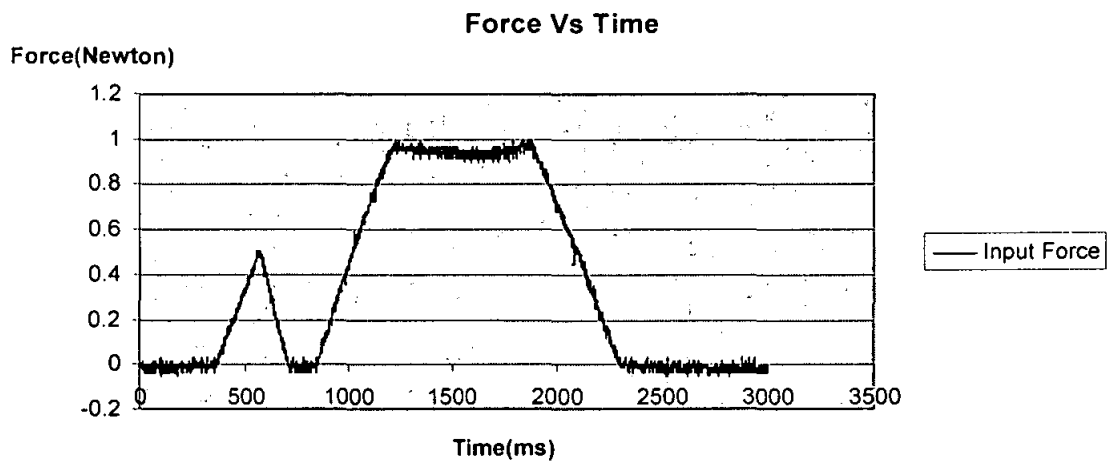


Figure 4.7 Input force signal of haptic feedback

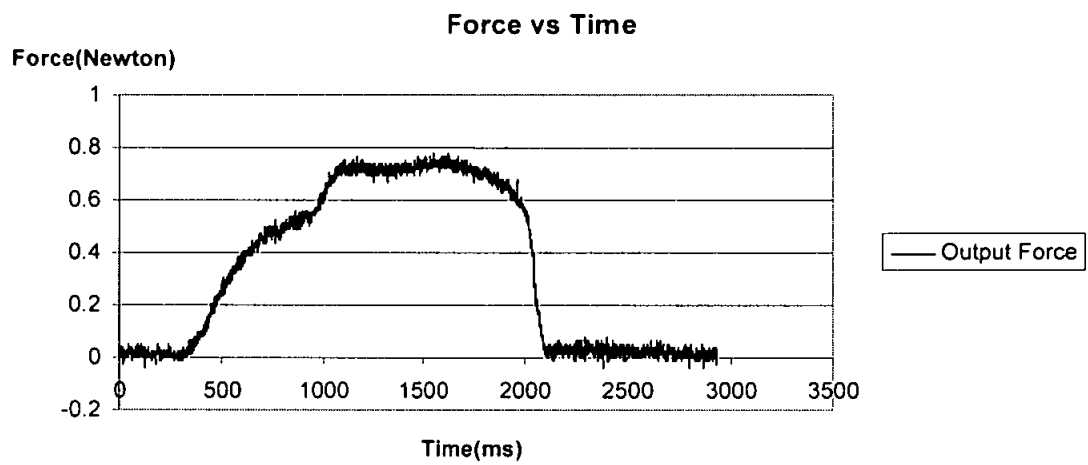


Figure 4.8 Output force of haptic feedback device

Table 4.4: Correlation factor.

Correlation Factor	Percentage	Average value	Positive Error	Negative Error	Error
0.75	75	0.696	0.186	0.124	±0.18
0.51	51				
0.82	82				
0.76	76				
0.64	64				

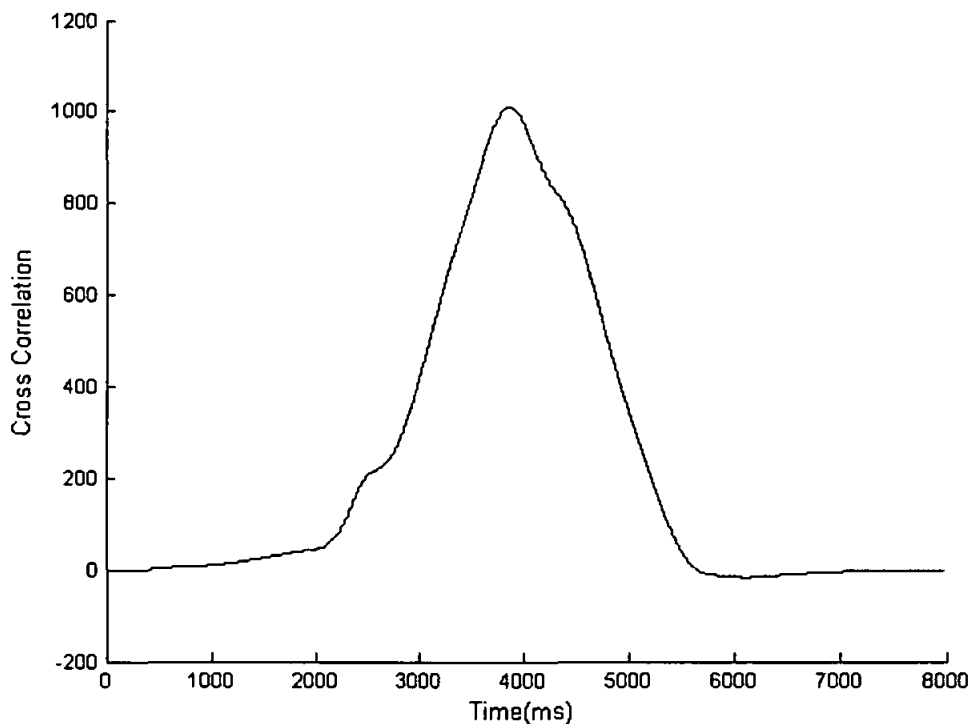


Figure 4.9 Correlation of haptic feedback device

The average correlation factor of the system is  $69.6\% \pm 18$ . The system can achieve the correlation factor of 82%. The correlation diagram is showing that the system following the input. In other words the output is of the pattern of input.

#### 4.3.5 Graphical User Interface Results

Figure 4.10 shows the graphical user interface. The processed data is shown on the screen of the computer. The graphical user interface is only for visual feedback so that a surgeon can observe the reactive force on the needle. Needle status is shown near to the start button. As the start button is pressed, the needle force is acquired by the sound card with the help of the force sensor. The needle status updates as needle force changes very abruptly. The elasticity, diameter, and depth are parameters keyed into the graphical user interface and the program calculates the model force. When the needle sensor has no data, it means that the needle is not inserted and it is moving freely. The data acquisition

card acquires noise from the sensor as the sensor is very immune to noises as shown in Figure 4.10. The graphical user interface has a feature that it can only calculate the data which is in the range of skin or tissue range. If one of the parameters is not in the range cited in the literature review, it will show an error message and it will not show the real force, as shown in Figure 4.11. The parameters key in are 23Kpa for Elasticity 0.8 millimeter for diameter of the needle and 12 millimeters for the deformation of the skin. The model force calculated by the GUI is 0.5888 Newton.

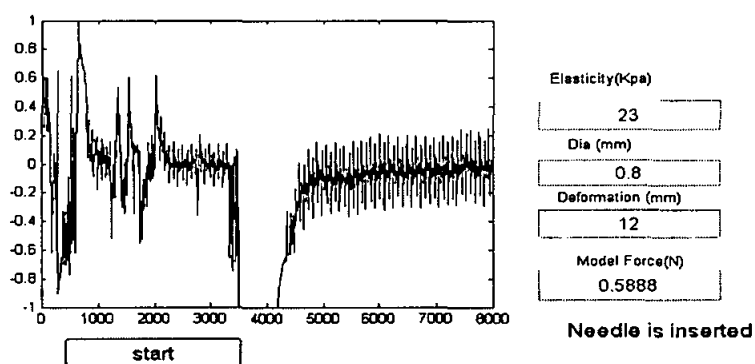


Figure 4.10 Graphical user interface of haptic feedback device with needle insertion

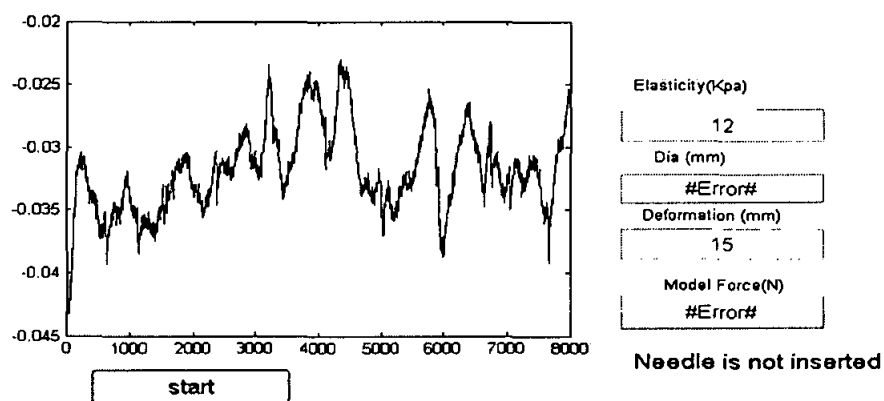


Figure 4.11 Graphical user interface of haptic feedback device with error

### 4.3.6 Sensitivity Analysis Results

The response sensitivity analysis of the device shows that system response will change with respect to mass of the stick reciprocally due to the negative sign. The mass of the stick increases by one unit the response sensitivity will decrease by one unit. The response sensitivity due to mass of the roller is also related inversely means with increase in mass of the roller the sensitivity will decrease but the decrease rate will four times as in the case of mass of the stick. While in the case of steady state error sensitivity for mass of the stick and roller is zero therefore mass of the stick and roller have no effect on steady state error.

Table 4.5: Sensitivity analysis results

Sensitivity	Sensitivity w.r.t. Mst	Sensitivity w.r.t. Mr	Sensitivity w.r.t. fr
Response	$S_{T_{st}, M_{st}} = \frac{-s^2 M_{st}}{(4M_r + M_{st})s^2 + 4F_r s + 1}$	$S_{T_{st}, M_r} = \frac{-4s^2 M_r}{(4M_r + M_{st})s^2 + 4F_r s + 1}$	$S_{T_{st}, F_r} = \frac{-4s F_r}{(4M_r + M_{st})s^2 + 4F_r s + 1}$
Steady State Error	$S_{e(\infty), M_{st}} = \frac{M_{st}}{e(\infty)} \frac{\partial e(\infty)}{\partial M_{st}} = 0$	$S_{e(\infty), M_r} = \frac{M_r}{e(\infty)} \frac{\partial e(\infty)}{\partial M_r} = 0$	$S_{e(\infty), F_r} = \frac{F_r}{e(\infty)} \frac{\partial e(\infty)}{\partial F_r} = 1$

In the case of friction force between roller and stick the response sensitivity is inversely related to it and while the steady state error sensitivity is fully depending on it. Change in the friction force between roller and stick will change steady state error. The reason is that the system is friction based i.e. it produces the opposing forces by friction forces. The device is friction based device.

## 4.4 Discussion

The needle insertion haptic feedback is one of the solutions in tele-surgery. The needle insertion force is modeled in three parts: force due to capsule stiffness, friction, and cutting. Experimental results shows that before needle pierces skin the capsule stiffness

force is acting on the needle shaft while after piercing the cutting and friction forces are acting on needle. The force due to capsule stiffness is depending on three parameters of needle, namely diameter of needle, elasticity of tissue and deformation of tissue.

Figure 4.12 shows the comparison between the experimental and the simulation results. The 23-gauge needle is deviating from the model due to its small diameter: diameter of the skin pore is 50 microns or 0.05 millimeter [45]. Hence, the needle is not piercing the skin but enlarging the skin pore. The 20- and 21-gauge needles are converging to the model and thus following the model behavior. Needles lower in diameter than the 23-gauge are deviating from the model. The model is converging for 20- and 21-gauge needles. The needle length is only affecting the friction force. The longer needle will have more friction due to more area of contact as compared to shorter needle. The friction force is only acting on needle when the needle is traveling through the tissue.

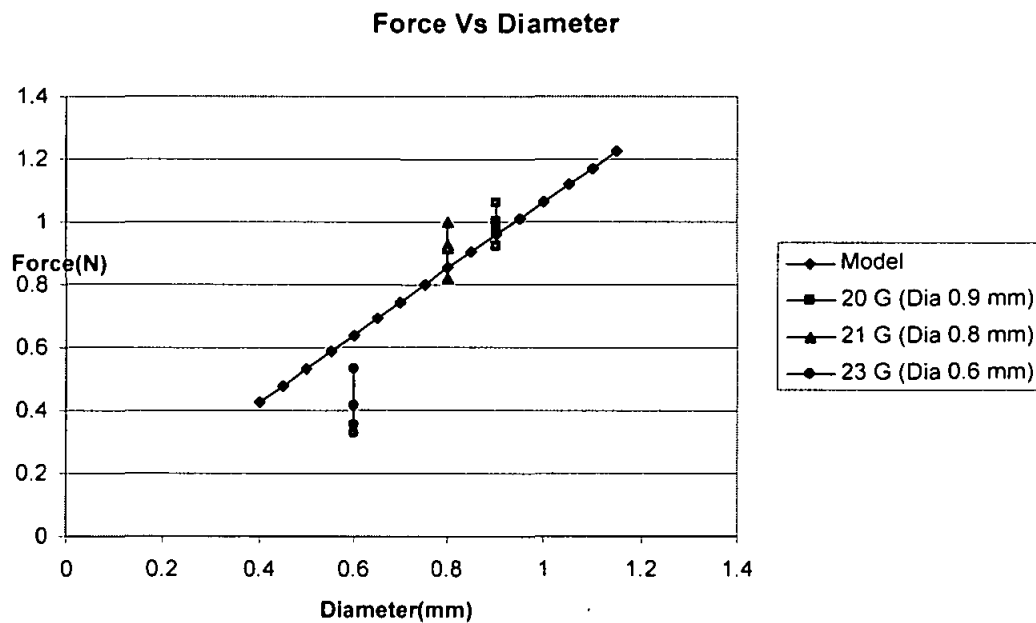


Figure 4.12: Comparison of experimental and simulation results.

Referring to Figure 4.3, the first drop is due to stiffness of the skin's first layer. When the needle is in contact with another layer the stiffness force of that layer starts to react. This layer to layer force variation takes place as the needle reaches uniform tissue or bone. Hence, the force profile as seen in the Figure 4.3 is not smooth.

The needle insertion force can be sensed and reproduced remotely with help of interface circuitry. The overshoot in the needle position occurs due to the softness of the tissue. The tissue is pressed by needle till its elastic limit and when the elastic limit of the tissue is attained the skin rupture occurs. This point the skin tends to come back to its equilibrium position and the reactive force is very low and the applied force is very high. Hence, this difference in equilibrium forces the needle position overshoot occurs.

The needle insertion performed in real time on chicken skin and the results are compared with the different models. The Table 4.6 shows the comparison between model forces and experimental forces.

Table 4.6: Experimental and model needle insertion forces

Diameter (mm)	Experimental Force(N)	Di Maio Model	Ottensmeyer Model
0.6	0.989	0.002839565	0.736
0.8	0.917	0.005048115	0.981333333
0.9	0.4095	0.006389021	1.104

The results in table show the comparison between two models. Both models are estimating the needle insertion force. The experimental results converge toward Ottensmeyer model as compared to Di Maio model.

The correlation of the input and output force is done using statistical formula. The forces are compared with help of Equation 4.1. The input force is taken as  $x$  and output force is taken as  $y$  then the cross correlation  $r$  at delay  $d$  is defined as



$$r = \frac{\sum_i [(x(i) - mx) * (y(i - d) - my)]}{\sqrt{\sum_i (x(i) - mx)^2} \sqrt{\sum_i (y(i - d) - my)^2}} \quad 4.1$$

Where  $mx$  and  $my$  are the means of the corresponding series. If the above is computed for all delays  $d=0, 1, 2...N-1$  then it results in a cross correlation series of twice the length as the original series. At best performance of the device the correlation factor is 82%. It means that output force of the haptic feedback device is 82% similar to input force.

#### 4.5 Summary

This chapter discusses haptic feedback setup results and analysis. The first section discusses the sensor calibration, which enables to find the conversion factor from sensor voltage to force. The second section discusses the needle insertion force for different diameters of needle. These forces are compared with the model simulated forces. Then the needle insertion measured forces are discussed and divided into its components. The needle insertion force is reproduced by electronic circuitry; the haptic feedback device reproduces the haptic force on the surgeon's hand. The input signal of the interface circuitry and output force of the device is correlated and correlation factor is found. The haptic feedback GUI is also discussed in the chapter. The GUI is only for visual haptic feedback, it can also calculate the model force by factors given to it. The chapter also included dynamic model of the haptic feedback system on the basis of the dynamic model. The design sensitivity analysis of the device is analyzed the steady state error sensitivity is also included in this chapter. The system response is reciprocally sensitive to mass of the stick; four times mass of the rollers and four times to the friction force between stick and rollers. System steady state error is only sensitive to the friction force between stick and rollers.

Forth coming chapter is conclusion drawn from the experimentation and analysis. The second section discusses the future recommendation for this work. Future work is based on the limitations in the system or advancement in the system.

## CHAPTER 5

### CONCLUSIONS AND SUGGESTIONS FOR FUTURE WORK

#### 5.1 Haptic Feedback Device Accuracy

The aim of this study was to design a haptic feedback device for needle insertion and study different models for needle insertion. Force from needle insertions at slave is being measured by sensor and communicated to master. At master end, the force signal is reconstructed with help of electronic circuitry. The force feedback is produced by the device on the hand of the surgeon. Previously, most of the research is based on realistic data and realistic force reproduction. Most of the studies were based to train the surgeons for tele-surgery. The goal of the work reported here was to design a device for reality-based data that results in more accurate representation of a needle insertion force feedback scenario. The device designed in this study is friction based. The device is producing the feedback force with the help of friction force. The device friction is controlled with help motors which are driven by the reproduced signal by interface circuitry.

The needle insertion model force and experimental force is compared and it is found that 0.6 millimeter is not converging to model. The 0.6 millimeter needle force profile is studied and it is found that the needle is not piercing the skin but it enlarges the pore size. Therefore its force is not dropping at skin piercing. The average skin stiffness force for 0.9 millimeter needle is 0.989 Newton, for 0.8 millimeter needle the average force is 0.91 Newton and for 0.6 millimeter needle the average force is 0.41 Newton.

The device designed is studied and checked for the needle insertion force reproduction and the device was able reproduce the prick on the operator hand. To study the accuracy and realistic production of the haptic feedback the correlation between input force and output force can give better insight. This analysis will give the percentage relation between output and input. The designed haptic feedback device correlation factor is 87%. The system correlation is only for the perpendicular needle insertion. The device is

accurate only for the perpendicular forces, if the angular needle insertion occurs than the device will only produce the vertical component of reactive force. It will be unable to produce the literal force components.

The sensitivity of the device is studied and the device response is found sensitive to mass of the stick, rollers and friction. The device steady state error is sensitive only of the friction between stick and rollers.

## **5.2 Suggestions for Future Extensions and Developments**

The haptic feedback device designed in this thesis has one degree of freedom, therefore it is not able to produce realistic force feedback for angular needle insertion. It only produces realistic haptic feedback for normal that is when needle is at 90 degrees to tissue. Therefore, in future the research is needed to be carried out to increase the degree of freedom of the device.

The graphical user interface in this study is used as visual feedback. The GUI can be made more accurate and clear as it only provide needle status in the study. The GUI can be used as simulator for the models in future research.

## REFERENCES

1. WebMD Inc, Medicine Dictionary online.[Accessed 12 February 2008], <http://www.medterms.com/script/main/art.asp?articlekey=18479>
2. Nagy I., Mayer H., and Knoll A., "The Endo[PA]R System for Minimally Invasive Robotic Surgery", *Technical Report*, Technische Universitat Munchen, TUM I2030, December 2003.
3. Engineer Partner The One Stop Outsource Inc, Visual Haptic Feedback Resource,[Accessed 12 February 2008], <http://vhbr.com/>
4. Wikipedia organization, [Accessed 10 February 2008] [www.wikipedia.org/haptic\\_feedback](http://www.wikipedia.org/haptic_feedback).
5. Goertz R. C., "Manipulator systems developed at ANL," *Proc. 12<sup>th</sup> Conf. on Remote Systems Technology*, pp 117-136, American Nuclear Society 1954.
6. Lam M. T., Boschloo H. W., Mudler M., Paassen V.M.M., and Helm D. V. F.C.T., "Effect of Haptic Feedback in a trajectory following task with an unmanned aerial vehicle," *IEEE International Conference on System, Man and Cybernetics*, IEEE, pp 2500-2506, 2004.
7. Urbano J., Terashima K., Miyoshi T. and Kitagawa H. "Impedance Control for Safety and Comfortable Navigation of an Omni-direction Mobile Wheelchair," *Proc. of International Conference on Intelligent Conference on Intelligent Robots and System*, Sendai, Japan, pp 1902-1906, Sep 2004.
8. Simone C, "*Modeling of needle insertion for precutaneous therapies*" *Master thesis*, Department of Mechanical Engineering, John Hopkins University, Baltimore, USA, 2002.

9. DiMaio, P. S. and Salcudean S. E. "Interactive simulation needle insertion models", *IEEE Transactions on Biomedical Engineering*, vol. 52, pp 1167-1179, July 2005.
- 10 Ottensmeyer M. P., "In vivo measurement of solid organ mechanical tissue properties". *Society for Experimental Mechanics Annual Meeting*, Milwaukee, WI. pp 328-333. 10-12 June 2002.
- 11 Zivanovic, A. and Davies, B.L "A robotic system for blood sampling", *IEEE Transactions on Information Technology in Biomedicine*, vol. 4, pp 8-14 Issue 1, March 2000
- 12 Saito H. and Togawa T. "Detection of puncturing vessel wall for automatic blood sampling." *BMES/EMBS Conference*, vol. 2, pg 866, Atlanta USA, Oct 1999.
- 13 Zheng Y.P. and Mak F.T., "Effective Elastic Properties for Lower Limb Soft Tissue from Manual Indentation Experiment", *IEEE Transaction on Rehabilitation Engineering*, vol. 7, no. 3, pp 257-267, September 1999.
- 14 3D-Immersive Work Station inc., [Accessed 27 January 2008], [www.sensegraphics.com/products](http://www.sensegraphics.com/products)
- 15 Nasa Robonaut, [Accessed 28 January 2008], <http://robonaut.jsc.nasa.gov/robonaut.html>
- 16 Nasa Robonaut Hand, [Accessed 28 January 2008], <http://media.nasaexplores.com>
- 17 Nintendo Inc., [Accessed 25 January 2008], [www.nintendic.com](http://www.nintendic.com)
- 18 *Virtual Environments and Tele-operation at the ARTS Lab*, ARTS Lab Technical report, Pisa, Italy, 1994.
- 19 *Force Arm Master Specification*, XOS Co. Company Brochure, Woburn MA, June 1993.

- 20 Bowler C., Caldwell D.G. and Medrano-Cerda G.A., "Pneumatic Muscle Actuator as low weight drive units in a robotic exoskeleton", *Technical Report*, University of Salford, Manchester, 1995.
- 21 Iwata H., Nakagawa T. and Nakashima T., "Force Display for Presentation of Rigidity of Virtual Objects", *Journal of Robotics and Mechatronics*, vol 24, No. 1, pp 39-42, January 1992.
- 22 Bouzit M., Richard P., & Coiffet P., "LRP dextrous hand master control system", *Technical report*, Laboratoire de Robotique de Paris, Jan 1993.
- 23 Appino A. P., Lewis B. J., Koved L., Ling T. D., Rabenhorst, A. D. and Codella F. C., "An architecture for virtual worlds", *Presence-teleoperators and Virtual Environment*, vol. 1, no. 1, MIT Press, Cambridge, MA, pp 1-17, March 1992.
- 24 Burdea G., Zhuang J., Roskos E., Silver D. and Langrana N. "A portable dextrous master with force feedback", *Presence-teleoperators and Virtual Environment*, vol. 1, no. 1, MIT Press, Cambridge, MA, pp 18-27, March 1992.
- 25 Arai T., Cleary K., Nakamura T., Adachi H. and Homma K., "Design Analysis and construction of a prototype parallel link manipulator" *IEEE international workshop on intelligent robots and systems (IROS)*, IEEE, New York, pp 205-212, July 1990.
- 26 Salcudean S.E. and Vlaar T.D. "On the Emulation of Stiff Walls and Static Friction with a Magnetically Levitated Input/Output Device." *Proceeding of ASME WAM*, DSC-vol.55-1, ASME, New York, pp.303-309, Nov. 1994.
- 27 Lindemann R. and Tesar Delbert "Construction and Demonstration of a 9-string 6 DOF force reflecting joystick for tele-robotics," *Proceeding of NASA International Conference on Space Tele-robotics*, NASA, Greenbelt, MD, vol.4, pp 55-63, 1989.

- 28 Ishii, M. and Sato, M. "A 3D interface device with force feedback: A virtual work space for pick-and-place Tasks." *IEEE Virtual Reality Annual International Symposium (VRAIS)*, IEEE, New York, pp 331-335, Sep. 1993
- 29 Universal Robotic System Inc., [Accessed 12 January 2007], <http://www.urs-ortho.de>
- 30 Integrated Surgical Systems Inc., [Accessed 12 December 2007], <http://www.robodoc.com>
- 31 Armstrong Health Care Inc., [Accessed 12 December 2007] <http://www.armstrong-healthcare.com>
- 32 Chicago Urology Deptt. [Accessed 13 December 2007], <http://www.chicagourologist.com/>
- 33 Intuitive Surgical System Inc., [Accessed 13 December 2007], [www.intuitivesurgical.com](http://www.intuitivesurgical.com)
- 34 da Vinci Surgical Console, [Accessed 20 January 2008], [www.biomed.brown.edu/Courses/BI108/BI108\\_2000\\_Groups](http://www.biomed.brown.edu/Courses/BI108/BI108_2000_Groups).
- 35 Moore G. Robert and Bishoff, T. Jay "Minimally Invasive Uro-Oncologic Surgery" Abingdon United Kingdom, Taylor & Francis, 2005.
- 36 Spaelter, U. Moix Th. Bleuler H. Ilic and Bajka M. "A 4-dof Haptic Device for Hysteroscopy Simulation," *Proc. of International Conference on Intelligent Conference on Intelligent Robots and System*, pp 3257-3263, Sep. 2004.
- 37 Franck P. V., Nicholas C., Derek A., Gouldc A. E., Healeyc, and Nigel W. J., "Developing a needle guidance virtual environment with patient specific data and force feedback." *International Congress Series*, vol. 1281, May 2005
- 38 Wang X. and Fester A., "A virtual reality based 3D real time interactive Brchytherapy simulation of needle insertion and seed implantment," *IEEE*



*International Symposium on Biomedical Imaging: Macro to Nano*, Arlington, VA, USA, pp 15 -18 April 2004

- 39 Simon P. DiMaio “Modeling Simulation and Planning of Needle Motion in Soft Tissues”. PhD Thesis, Department of Electrical and Computer Engineering. University of British Columbia, Canada, Sep. 2003.
- 40 Beer P. Ferdinand, Johnston Russell E. and DeWolf. T. John “*Mechanics of Materials*”. Mc.Graw Hill, New York, USA 1992.
- 41 Okamura, M. Allison. and Simone, Christina. “Force Modeling for Needle Insertion into Soft Tissue” *IEEE Transaction on Biomedical Engineering*, vol. 51, no. 10, pp 1707-1716 Oct. 2004.
- 42 Diller R. Kenneth “Adapting Adult Scald Safety Standards to Children” *Journal of Burn Care and Research*, vol. 27, no. 3, pp 314-322, June 2006.
- 43 Terumo Needle Inc. [ Accessed 2 December 2007], [www.terumo.com](http://www.terumo.com)
- 44 RS Malaysia Inc. [ 12 March 2008], [www.rsmalaysia.com](http://www.rsmalaysia.com)
- 45 Bruce K. R., “Human skin pore enlargement as a result of ultrasonic treatment”.
- 46 Burdea. C. G., “ *Force and Touch Feedback for Virtual Reality*”. John Willey and Sons Inc. New York, USA, 1996.
- 47 Nise S. Norman “*Control System Engineering*”. John Willey and Sons Inc., 4<sup>th</sup> Edition., New York, USA, 2004.

**APPENDICES**

## Appendix-A

## Data Sheets of Electronic Components

## Operational Amplifier LM741



August 2000

## LM741 Operational Amplifier

### General Description

The LM741 series are general purpose operational amplifiers which feature improved performance over industry standards like the LM709. They are direct, plug-in replacements for the 709C, LM201, MC1439 and 748 in most applications. The amplifiers offer many features which make their application nearly foolproof: overload protection on the input and

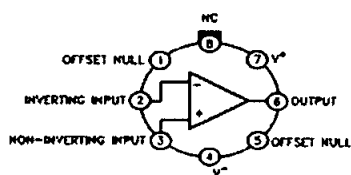
output, no latch-up when the common mode range is exceeded, as well as freedom from oscillations.

The LM741C is identical to the LM741/LM741A except that the LM741C has their performance guaranteed over a 0°C to +70°C temperature range, instead of -55°C to +125°C.

### Features

### Connection Diagrams

Metal Can Package

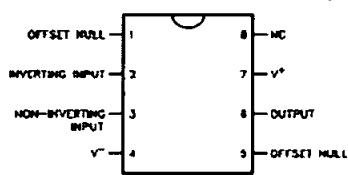


00204 K02

Note 1: LM741H is available per JM38510/10101

Order Number LM741H, LM741H/883 (Note 1),  
LM741AH/883 or LM741CH  
See NS Package Number H08C

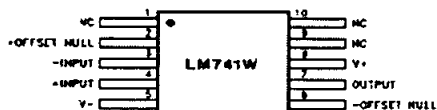
Dual-In-Line or S.O. Package



00204 K03

Order Number LM741J, LM741J/883, LM741CN  
See NS Package Number J08A, M08A or N08E

Ceramic Flatpak

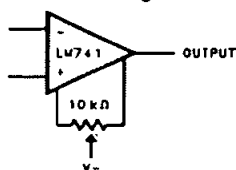


00204 K06

Order Number LM741W/883  
See NS Package Number W10A

### Typical Application

Offset Nulling Circuit



00204 K07

## Appendix-A (Continued)

**Absolute Maximum Ratings** (Note 2)

If Military/Aerospace specified devices are required, please contact the National Semiconductor Sales Office/Distributors for availability and specifications.

(Note 7)

	LM741A	LM741	LM741C
Supply Voltage	±22V	±22V	±18V
Power Dissipation (Note 3)	500 mW	500 mW	500 mW
Differential Input Voltage	±30V	±30V	±30V
Input Voltage (Note 4)	±15V	±15V	±15V
Output Short Circuit Duration	Continuous	Continuous	Continuous
Operating Temperature Range	-55°C to +125°C	-55°C to +125°C	0°C to +70°C
Storage Temperature Range	-65°C to +150°C	-65°C to +150°C	-65°C to +150°C
Junction Temperature	150°C	150°C	100°C
Soldering Information			
N-Package (10 seconds)	260°C	260°C	260°C
J- or H-Package (10 seconds)	300°C	300°C	300°C
M-Package			
Vapor Phase (60 seconds)	215°C	215°C	215°C
Infrared (15 seconds)	215°C	215°C	215°C
See AN-450 "Surface Mounting Methods and Their Effect on Product Reliability" for other methods of soldering surface mount devices.			
ESD Tolerance (Note 8)	400V	400V	400V

**Electrical Characteristics** (Note 5)

Parameter	Conditions	LM741A			LM741			LM741C			Units
		Min	Typ	Max	Min	Typ	Max	Min	Typ	Max	
Input Offset Voltage	$T_A = 25^\circ\text{C}$ $R_D \leq 10\text{ k}\Omega$ $R_G \leq 50\text{ k}\Omega$		0.8	3.0		1.0	5.0		2.0	6.0	mV
	$T_{AMIN} \leq T_A \leq T_{AMAX}$ $R_D \leq 50\text{ k}\Omega$ $R_G \leq 10\text{ k}\Omega$			4.0			6.0			7.5	mV
				15							$\mu\text{V}/^\circ\text{C}$
Average Input Offset Voltage Drift				15							$\mu\text{V}/^\circ\text{C}$
Input Offset Voltage Adjustment Range	$T_A = 25^\circ\text{C}$ , $V_D = \pm 20\text{V}$	±10				±15			±15		mV
Input Offset Current	$T_A = 25^\circ\text{C}$		3.0	30		20	200		20	200	nA
	$T_{AMIN} \leq T_A \leq T_{AMAX}$			70		85	500			300	nA
Average Input Offset Current Drift				0.5							$\text{nA}/^\circ\text{C}$
Input Bias Current	$T_A = 25^\circ\text{C}$		30	80		80	500		80	500	nA
	$T_{AMIN} \leq T_A \leq T_{AMAX}$			0.210			1.5			0.8	$\mu\text{A}$
Input Resistance	$T_A = 25^\circ\text{C}$ , $V_D = \pm 20\text{V}$	1.0	6.0		0.3	2.0		0.3	2.0		M $\Omega$
	$T_{AMIN} \leq T_A \leq T_{AMAX}$ , $V_D = \pm 20\text{V}$	0.5									M $\Omega$
Input Voltage Range	$T_A = 25^\circ\text{C}$							±12	±13		V
	$T_{AMIN} \leq T_A \leq T_{AMAX}$				±12	±13					V

## Appendix-A (Continued)

Electrical Characteristics (Note 5) (Continued)											
Parameter	Conditions	LM741A			LM741			LM741C			Units
		Min	Typ	Max	Min	Typ	Max	Min	Typ	Max	
Large Signal Voltage Gain	$T_A = 25^\circ\text{C}$ , $R_L \geq 2\text{ k}\Omega$ $V_B = \pm 20\text{V}$ , $V_O = \pm 15\text{V}$ $V_B = \pm 15\text{V}$ , $V_O = \pm 10\text{V}$	50			50	200		20	200		V/mV V/mV
	$T_{AMIN} \leq T_A \leq T_{AMAX}$ , $R_L \geq 2\text{ k}\Omega$ , $V_B = \pm 20\text{V}$ , $V_O = \pm 15\text{V}$ $V_B = \pm 15\text{V}$ , $V_O = \pm 10\text{V}$	32			25			15			V/mV V/mV V/mV
	$V_B = \pm 5\text{V}$ , $V_O = \pm 2\text{V}$	10									
Output Voltage Swing	$V_B = \pm 20\text{V}$ $R_L \geq 10\text{ k}\Omega$ $R_L \geq 2\text{ k}\Omega$	$\pm 16$									V V
	$V_B = \pm 15\text{V}$ $R_L \geq 10\text{ k}\Omega$ $R_L \geq 2\text{ k}\Omega$				$\pm 12$ $\pm 10$	$\pm 14$ $\pm 13$		$\pm 12$ $\pm 10$	$\pm 14$ $\pm 13$		V V
Output Short Circuit Current	$T_A = 25^\circ\text{C}$	10	25	35		25		25			mA mA
	$T_{AMIN} \leq T_A \leq T_{AMAX}$	10		40							
Common-Mode Rejection Ratio	$T_{AMIN} \leq T_A \leq T_{AMAX}$ $R_D \leq 10\text{ k}\Omega$ , $V_{CM} = \pm 12\text{V}$ $R_D \leq 50\Omega$ , $V_{CM} = \pm 12\text{V}$				70	90		70	90		dB dB
		80	95								
Supply Voltage Rejection Ratio	$T_{AMIN} \leq T_A \leq T_{AMAX}$ , $V_B = \pm 20\text{V}$ to $V_B = \pm 5\text{V}$ $R_D \leq 50\Omega$ $R_D \leq 10\text{ k}\Omega$	86	96		77	96		77	96		dB dB
Transient Response	$T_A = 25^\circ\text{C}$ , Unity Gain	Rise Time		0.25	0.8		0.3		0.3		$\mu\text{s}$
		Overshoot		6.0	20		5		5		%
Bandwidth (Note 6)	$T_A = 25^\circ\text{C}$	0.437	1.5								MHz
Slew Rate	$T_A = 25^\circ\text{C}$ , Unity Gain	0.3	0.7			0.5		0.5			V/ $\mu\text{s}$
Supply Current	$T_A = 25^\circ\text{C}$					1.7	2.8		1.7	2.8	mA
Power Consumption	$T_A = 25^\circ\text{C}$ $V_B = \pm 20\text{V}$ $V_B = \pm 15\text{V}$		80	150		50	85		50	85	mW mW
	$V_B = \pm 20\text{V}$ $T_A = T_{AMIN}$ $T_A = T_{AMAX}$			165							mW mW
LM741	$V_B = \pm 15\text{V}$ $T_A = T_{AMIN}$ $T_A = T_{AMAX}$					60	100				mW mW
						45	75				

Note 2: "Absolute Maximum Ratings" indicate limits beyond which damage to the device may occur. Operating Ratings indicate conditions for which the device is functional, but do not guarantee specific performance limits.

### Appendix-A (Continued)

#### Electrical Characteristics (Note 5) (Continued)

Note 2: For operation at elevated temperatures, these device must be derated based on thermal resistance, and  $T_J$  max. (listed under "Absolute Maximum Ratings").  $T_J = T_A + (\theta_{JA} P_D)$ .

Thermal Resistance	Cardip (J)	DIP (N)	HO8 (H)	SO-8 (M)
$\theta_{JA}$ (Junction to Ambient)	100°C/W	100°C/W	170°C/W	195°C/W
$\theta_{JC}$ (Junction to Case)	N/A	N/A	25°C/W	N/A

Note 4: For supply voltages less than  $\pm 15V$ , the absolute maximum input voltage is equal to the supply voltage.

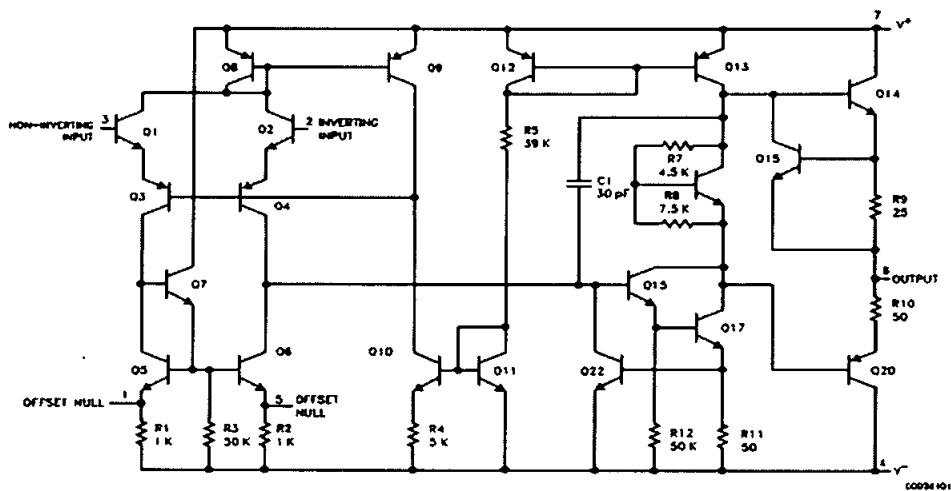
Note 5: Unless otherwise specified, these specifications apply for  $V_S = \pm 15V$ ,  $-55^\circ C \leq T_A \leq +125^\circ C$  (LM741/LM741A). For the LM741C/LM741E, these specifications are limited to  $0^\circ C \leq T_A \leq +70^\circ C$ .

Note 6: Calculated value from:  $BW$  (MHz) =  $0.95/\text{Rise Time}(\mu s)$ .

Note 7: For military specifications see RETS741K for LM741 and RETS741AX for LM741A.

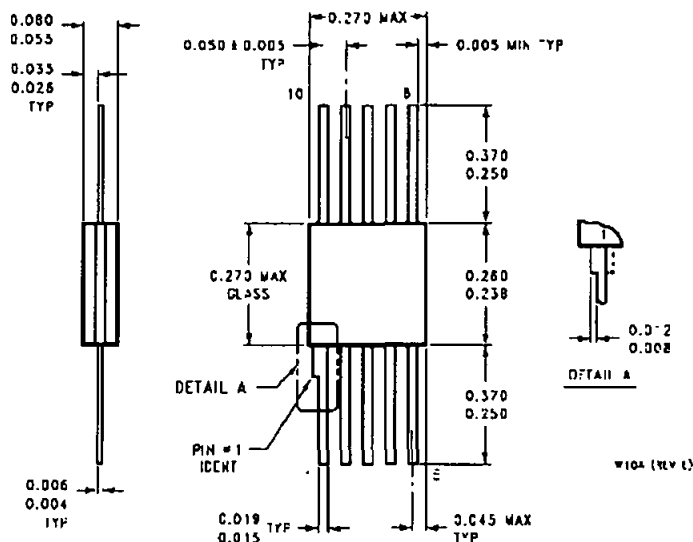
Note 8: Human body model, 1.5 k $\Omega$  in series with 100 pF.

#### Schematic Diagram



00294 101

## Appendix-A (Continued)

**Physical Dimensions** inches (millimeters) unless otherwise noted (Continued)

10-Lead Ceramic Flatpak (W)  
 Order Number LM741W/883, LM741WG-MPR or LM741WG/883  
 NS Package Number W10A

National does not assume any responsibility for use of any circuitry described, no circuit patent licenses are implied and National reserves the right at any time without notice to change said circuitry and specifications.

For the most current product information visit us at [www.national.com](http://www.national.com).

**LIFE SUPPORT POLICY**

NATIONAL'S PRODUCTS ARE NOT AUTHORIZED FOR USE AS CRITICAL COMPONENTS IN LIFE SUPPORT DEVICES OR SYSTEMS WITHOUT THE EXPRESS WRITTEN APPROVAL OF THE PRESIDENT AND GENERAL COUNSEL OF NATIONAL SEMICONDUCTOR CORPORATION. As used herein:

1. Life support devices or systems are devices or systems which: (a) are intended for surgical implant into the body, or (b) support or sustain life, and whose failure to perform when properly used in accordance with instructions for use provided in the labeling, can be reasonably expected to result in a significant injury to the user.
2. A critical component is any component of a life support device or system whose failure to perform can be reasonably expected to cause the failure of the life support device or system, or to affect its safety or effectiveness.

**BANNED SUBSTANCE COMPLIANCE**

National Semiconductor certifies that the products and packing materials meet the provisions of the Customer Products Stewardship Specification (CSP-9-111C2) and the Banned Substances and Materials of Interest Specification (CSP-9-111S2) and contain no "Banned Substances" as defined in CSP-9-111S2.



National Semiconductor  
 Americas Customer  
 Support Center  
 Email: [nas.leadback@nsc.com](mailto:nas.leadback@nsc.com)  
 Tel: 1-800-272-6969

[www.national.com](http://www.national.com)

National Semiconductor  
 Europe Customer Support Center  
 Fax: +49 (0) 180-530-85 86  
 Email: [eurqa.support@nsc.com](mailto:eurqa.support@nsc.com)  
 Deutsch Tel: +49 (0) 69 9526 6208  
 English Tel: +44 (0) 870 24 0 217 1  
 Français Tel: +33 (0) 1 41 91 8760

National Semiconductor  
 Asia Pacific Customer  
 Support Center  
 Email: [ap.support@nsc.com](mailto:ap.support@nsc.com)

National Semiconductor  
 Japan Customer Support Center  
 Fax: 81-3-5639-7507  
 Email: [jpn.leadback@nsc.com](mailto:jpn.leadback@nsc.com)  
 Tel: 81-3-5639-7550

## Appendix-A (Continued)

## Power MOSFET MTP2955

**MTP2955V**

Preferred Device

**Power MOSFET  
12 Amps, 60 Volts  
P-Channel TO-220**

This Power MOSFET is designed to withstand high energy in the avalanche and commutation modes. Designed for low voltage, high speed switching applications in power supplies, converters and power motor controls, these devices are particularly well suited for bridge circuits where diode speed and commutating safe operating areas are critical and offer additional safety margin against unexpected voltage transients.

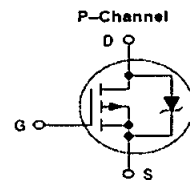
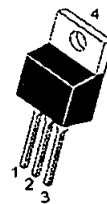
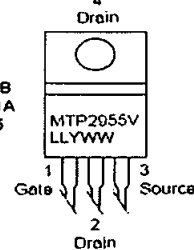
- Avalanche Energy Specified
- $IDSS$  and  $V_{DS(on)}$  Specified at Elevated Temperature

**MAXIMUM RATINGS** ( $T_C = 25^\circ\text{C}$  unless otherwise noted)

Rating	Symbol	Value	Unit
Drain-to-Source Voltage	$V_{DS}$	60	Vdc
Drain-to-Gate Voltage ( $R_{GS} = 1.0\text{ M}\Omega$ )	$V_{DGR}$	60	Vdc
Gate-to-Source Voltage	$V_{GS}$	$\pm 15$	Vdc
- Continuous	$V_{GSM}$	$\pm 25$	Vpk
- Non-Repetitive ( $t_p \leq 10\text{ ms}$ )			
Drain Current - Continuous	$I_D$	12	Adc
- Continuous @ $100^\circ\text{C}$	$I_{D100}$	8.0	
- Single Pulse ( $t_p \leq 10\ \mu\text{s}$ )	$I_{DM}$	42	Apk
Total Power Dissipation	$P_D$	60	Watts
Derate above $25^\circ\text{C}$		0.40	$\text{W}/^\circ\text{C}$
Operating and Storage Temperature Range	$T_J, T_{stg}$	$-55$ to $175$	$^\circ\text{C}$
Single Pulse Drain-to-Source Avalanche Energy - Starting $T_J = 25^\circ\text{C}$ ( $V_{DD} = 25\text{ Vdc}$ , $V_{GS} = 10\text{ Vdc}$ , Peak $I_L = 12\text{ Apk}$ , $L = 3.0\text{ mH}$ , $R_G = 25\ \Omega$ )	$E_{AS}$	218	mJ
Thermal Resistance			$^\circ\text{C}/\text{W}$
- Junction to Case	$R_{\theta JC}$	2.5	
- Junction to Ambient	$R_{\theta JA}$	62.5	
Maximum Lead Temperature for Soldering Purposes, $1/8"$ from case for 10 seconds	$T_L$	260	$^\circ\text{C}$



ON Semiconductor™

<http://onsemi.com>**12 AMPERES  
60 VOLTS** **$R_{DS(on)} = 230\text{ m}\Omega$** **MARKING DIAGRAM  
& PIN ASSIGNMENT**TO-220AB  
CASE 221A  
STYLE 5

MTP2955V = Device Code  
LL = Location Code  
Y = Year  
WW = Work Week

**ORDERING INFORMATION**

Device	Package	Shipping
MTP2955V	TO-220AB	50 Units/Rail

Preferred devices are recommended choices for future use and best overall value.



## Appendix-A (Continued)

ELECTRICAL CHARACTERISTICS (T<sub>J</sub> = 25°C unless otherwise noted)

Characteristic	Symbol	Min	Typ	Max	Unit				
<b>OFF CHARACTERISTICS</b>									
Drain-to-Source Breakdown Voltage (V <sub>GS</sub> = 0 Vdc, I <sub>D</sub> = 0.25 mAdc) Temperature Coefficient (Positive)	V <sub>(BR)DSS</sub>	60 -	- 58	- -	Vdc mV/°C				
Zero Gate Voltage Drain Current (V <sub>DS</sub> = 80 Vdc, V <sub>GS</sub> = 0 Vdc) (V <sub>DS</sub> = 60 Vdc, V <sub>GS</sub> = 0 Vdc, T <sub>J</sub> = 150°C)	I <sub>DSS</sub>	- -	- -	10 100	μAdc				
Gate-Body Leakage Current (V <sub>GS</sub> = ± 15 Vdc, V <sub>DS</sub> = 0 Vdc)	I <sub>GSS</sub>	-	-	100	nAdc				
<b>ON CHARACTERISTICS (Note 1.)</b>									
Gate Threshold Voltage (V <sub>DS</sub> = V <sub>GS</sub> , I <sub>D</sub> = 250 μAdc) Threshold Temperature Coefficient (Negative)	V <sub>GS(th)</sub>	2.0 -	2.8 5.0	4.0 -	Vdc mV/°C				
Static Drain-to-Source On-Resistance (V <sub>GS</sub> = 10 Vdc, I <sub>D</sub> = 6.0 Adc)	R <sub>DS(on)</sub>	-	0.185	0.230	Ohm				
Drain-to-Source On-Voltage (V <sub>GS</sub> = 10 Vdc, I <sub>D</sub> = 12 Adc) (V <sub>GS</sub> = 10 Vdc, I <sub>D</sub> = 6.0 Adc, T <sub>J</sub> = 150°C)	V <sub>DS(on)</sub>	- -	- -	2.9 2.5	Vdc				
Forward Transconductance (V <sub>DS</sub> = 10 Vdc, I <sub>D</sub> = 6.0 Adc)	g <sub>FS</sub>	3.0	5.0	-	mhos				
<b>DYNAMIC CHARACTERISTICS</b>									
Input Capacitance	C <sub>iss</sub>	-	550	700	pF				
Output Capacitance						C <sub>oss</sub>	-	200	280
Reverse Transfer Capacitance						C <sub>rss</sub>	-	50	100
<b>SWITCHING CHARACTERISTICS (Note 2.)</b>									
Turn-On Delay Time	V <sub>DD</sub> = 30 Vdc, I <sub>D</sub> = 12 Adc, V <sub>GS</sub> = 10 Vdc, R <sub>G</sub> = 9.1 Ω	t <sub>d(on)</sub>	-	15	30	ns			
Rise Time		t <sub>r</sub>	-	50	100				
Turn-Off Delay Time		t <sub>d(off)</sub>	-	24	50				
Fall Time		t <sub>f</sub>	-	39	80				
Gate Charge	V <sub>DS</sub> = 48 Vdc, I <sub>D</sub> = 12 Adc, V <sub>GS</sub> = 10 Vdc	Q <sub>T</sub>	-	19	30	nC			
		Q <sub>1</sub>	-	4.0	-				
		Q <sub>2</sub>	-	9.0	-				
		Q <sub>3</sub>	-	7.0	-				
<b>SOURCE-DRAIN DIODE CHARACTERISTICS</b>									
Forward On-Voltage (Note 1.)	(I <sub>S</sub> = 12 Adc, V <sub>GS</sub> = 0 Vdc) (I <sub>S</sub> = 12 Adc, V <sub>GS</sub> = 0 Vdc, T <sub>J</sub> = 150°C)	V <sub>SD</sub>	- -	1.8 1.5	3.0 -	Vdc			
Reverse Recovery Time	(I <sub>S</sub> = 12 Adc, V <sub>GS</sub> = 0 Vdc, di <sub>S</sub> /dt = 100 A/μs)	t <sub>rr</sub>	-	115	-	ns			
		t <sub>a</sub>	-	90	-				
		t <sub>b</sub>	-	25	-				
Reverse Recovery Stored Charge		Q <sub>RR</sub>	-	0.53	-	μC			
<b>INTERNAL PACKAGE INDUCTANCE</b>									
Internal Drain Inductance (Measured from the drain lead 0.25" from package to center of die)	L <sub>D</sub>	-	4.5	-	nH				
Internal Source Inductance (Measured from the source lead 0.25" from package to source bond pad)	L <sub>S</sub>	-	7.5	-	nH				

- Pulse Test: Pulse Width ≤ 300 μs, Duty Cycle ≤ 2%.
- Switching characteristics are independent of operating junction temperature.
- Reflects typical values.  $C_{pk} = \left| \frac{\text{Max limit} - \text{Typ}}{3 \times \text{SIGMA}} \right|$

Appendix-A (Continued)

TYPICAL ELECTRICAL CHARACTERISTICS

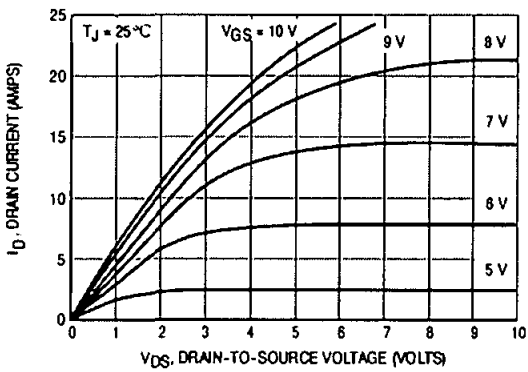


Figure 1. On-Region Characteristics

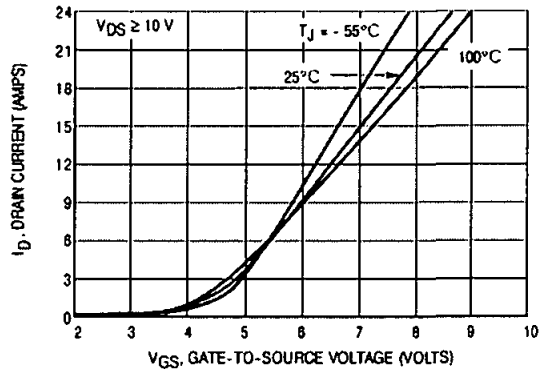


Figure 2. Transfer Characteristics

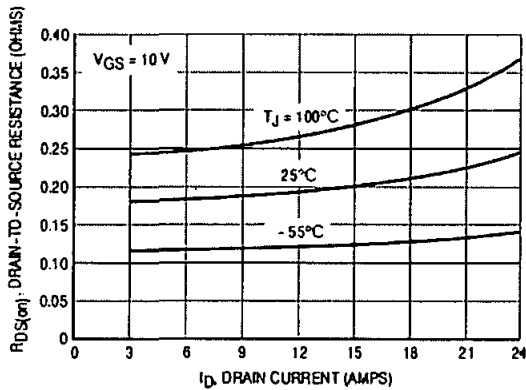


Figure 3. On-Resistance versus Drain Current and Temperature

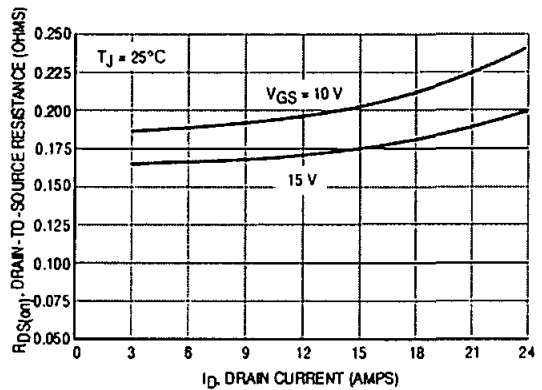


Figure 4. On-Resistance versus Drain Current and Gate Voltage

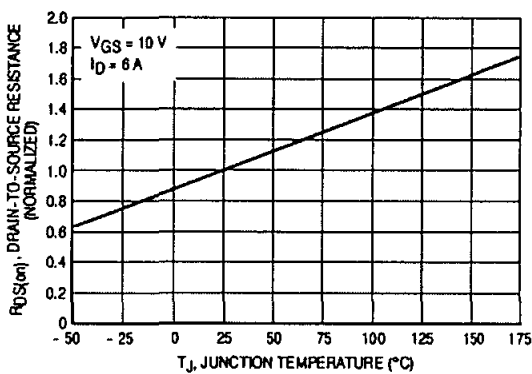


Figure 5. On-Resistance Variation with Temperature

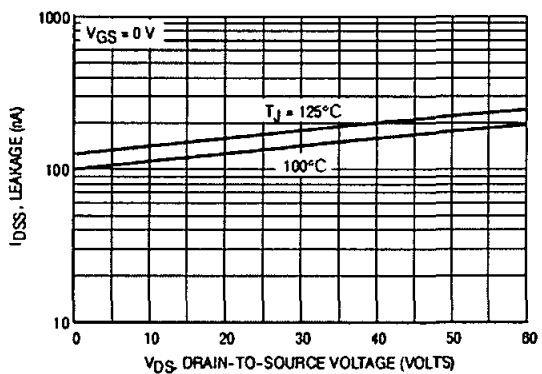


Figure 6. Drain-to-Source Leakage Current versus Voltage

## Appendix-A (Continued)

## POWER MOSFET SWITCHING

Switching behavior is most easily modeled and predicted by recognizing that the power MOSFET is charge controlled. The lengths of various switching intervals ( $\Delta t$ ) are determined by how fast the FET input capacitance can be charged by current from the generator.

The published capacitance data is difficult to use for calculating rise and fall because drain-gate capacitance varies greatly with applied voltage. Accordingly, gate charge data is used. In most cases, a satisfactory estimate of average input current ( $I_{G(AV)}$ ) can be made from a rudimentary analysis of the drive circuit so that

$$t = Q/I_{G(AV)}$$

During the rise and fall time interval when switching a resistive load,  $V_{GS}$  remains virtually constant at a level known as the plateau voltage,  $V_{GSP}$ . Therefore, rise and fall times may be approximated by the following:

$$t_r = Q_2 \times R_G / (V_{GG} - V_{GSP})$$

$$t_f = Q_2 \times R_G / V_{GSP}$$

where

$V_{GG}$  = the gate drive voltage, which varies from zero to  $V_{GG}$

$R_G$  = the gate drive resistance

and  $Q_2$  and  $V_{GSP}$  are read from the gate charge curve.

During the turn-on and turn-off delay times, gate current is not constant. The simplest calculation uses appropriate values from the capacitance curves in a standard equation for voltage change in an RC network. The equations are:

$$t_{d(on)} = R_G C_{iss} \ln [V_{GG}/(V_{GG} - V_{GSP})]$$

$$t_{d(off)} = R_G C_{iss} \ln (V_{GG}/V_{GSP})$$

The capacitance ( $C_{iss}$ ) is read from the capacitance curve at a voltage corresponding to the off-state condition when calculating  $t_{d(on)}$  and is read at a voltage corresponding to the on-state when calculating  $t_{d(off)}$ .

At high switching speeds, parasitic circuit elements complicate the analysis. The inductance of the MOSFET source lead, inside the package and in the circuit wiring which is common to both the drain and gate current paths, produces a voltage at the source which reduces the gate drive current. The voltage is determined by  $L di/dt$ , but since  $di/dt$  is a function of drain current, the mathematical solution is complex. The MOSFET output capacitance also complicates the mathematics. And finally, MOSFETs have finite internal gate resistance which effectively adds to the resistance of the driving source, but the internal resistance is difficult to measure and, consequently, is not specified.

The resistive switching time variation versus gate resistance (Figure 9) shows how typical switching performance is affected by the parasitic circuit elements. If the parasitics were not present, the slope of the curves would maintain a value of unity regardless of the switching speed. The circuit used to obtain the data is constructed to minimize common inductance in the drain and gate circuit loops and is believed readily achievable with board mounted components. Most power electronic loads are inductive; the data in the figure is taken with a resistive load, which approximates an optimally snubbed inductive load. Power MOSFETs may be safely operated into an inductive load; however, snubbing reduces switching losses.

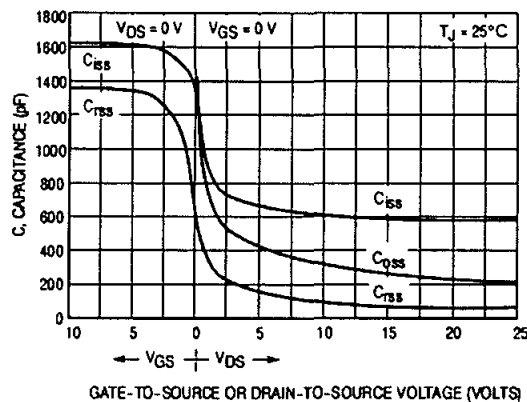


Figure 7. Capacitance Variation

Appendix-A (Continued)

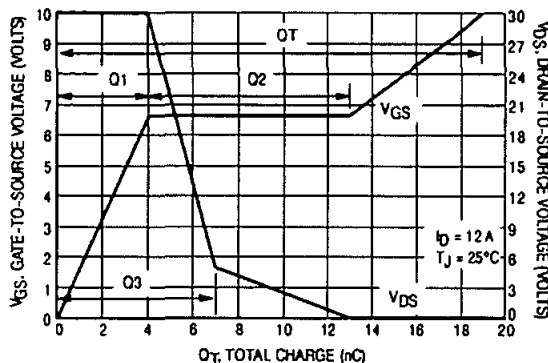


Figure 8. Gate-To-Source and Drain-To-Source Voltage versus Total Charge

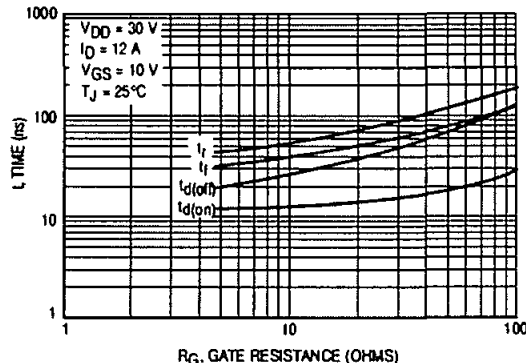


Figure 9. Resistive Switching Time Variation versus Gate Resistance

DRAIN-TO-SOURCE DIODE CHARACTERISTICS

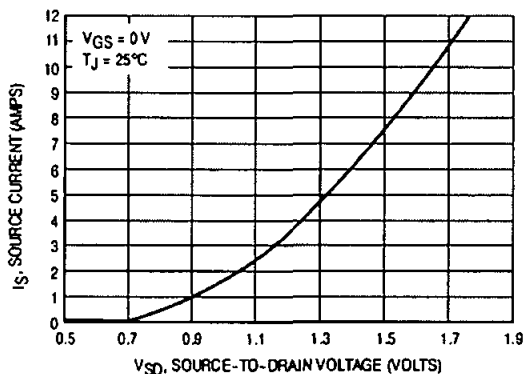


Figure 10. Diode Forward Voltage versus Current

SAFE OPERATING AREA

The Forward Biased Safe Operating Area curves define the maximum simultaneous drain-to-source voltage and drain current that a transistor can handle safely when it is forward biased. Curves are based upon maximum peak junction temperature and a case temperature ( $T_C$ ) of 25°C. Peak repetitive pulsed power limits are determined by using the thermal response data in conjunction with the procedures discussed in AN569, "Transient Thermal Resistance—General Data and Its Use."

Switching between the off-state and the on-state may traverse any load line provided neither rated peak current ( $I_{DM}$ ) nor rated voltage ( $V_{DSS}$ ) is exceeded and the transition time ( $t_r, t_f$ ) do not exceed 10  $\mu s$ . In addition the total power averaged over a complete switching cycle must not exceed  $(T_{J(MAX)} - T_C)/(R_{\theta JC})$ .

A Power MOSFET designated E-FET can be safely used in switching circuits with unclamped inductive loads. For

reliable operation, the stored energy from circuit inductance dissipated in the transistor while in avalanche must be less than the rated limit and adjusted for operating conditions differing from those specified. Although industry practice is to rate in terms of energy, avalanche energy capability is not a constant. The energy rating decreases non-linearly with an increase of peak current in avalanche and peak junction temperature.

Although many E-FETs can withstand the stress of drain-to-source avalanche at currents up to rated pulsed current ( $I_{DM}$ ), the energy rating is specified at rated continuous current ( $I_D$ ), in accordance with industry custom. The energy rating must be derated for temperature as shown in the accompanying graph (Figure 13). Maximum energy at currents below rated continuous  $I_D$  can safely be assumed to equal the values indicated.

Appendix-A (Continued)

SAFE OPERATING AREA

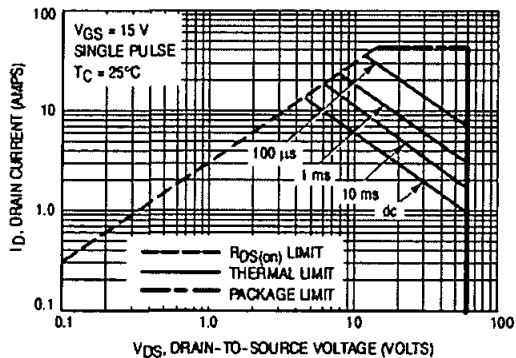


Figure 11. Maximum Rated Forward Biased Safe Operating Area

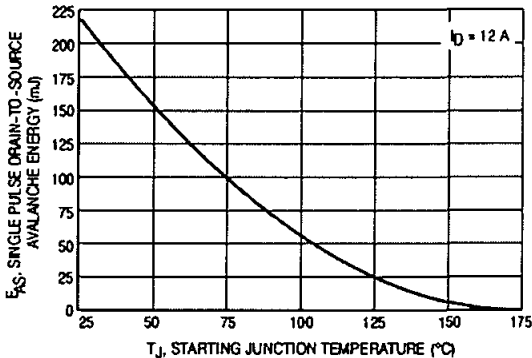


Figure 12. Maximum Avalanche Energy versus Starting Junction Temperature

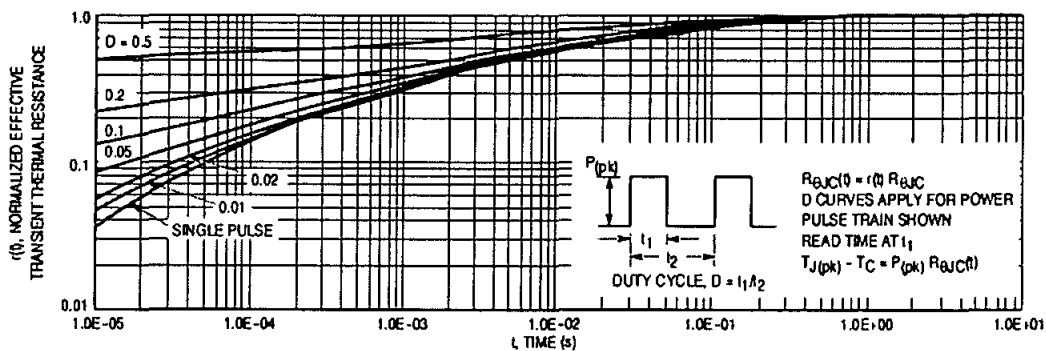


Figure 13. Thermal Response

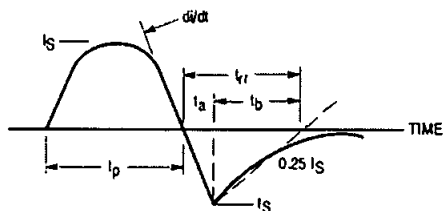
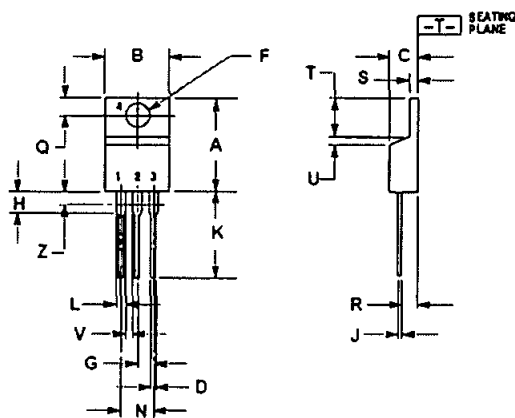


Figure 14. Diode Reverse Recovery Waveform

## Appendix-A (Continued)

## PACKAGE DIMENSIONS

TO-220 THREE-LEAD  
TO-220AB  
CASE 221A-09  
ISSUE AA




- NOTES:
1. DIMENSIONING AND TOLERANCING PER ANSI Y14.5M, 1982.
  2. CONTROLLING DIMENSION: INCH.
  3. DIMENSION Z DEFINES A ZONE WHERE ALL BODY AND LEAD IRREGULARITIES ARE ALLOWED.

DIM	INCHES		MILLIMETERS	
	MIN	MAX	MIN	MAX
A	0.570	0.620	14.48	15.75
B	0.200	0.405	5.08	10.28
C	0.180	0.190	4.67	4.82
D	0.025	0.035	0.64	0.88
E	0.142	0.147	3.61	3.73
F	0.095	0.105	2.42	2.68
H	0.110	0.155	2.80	3.93
J	0.018	0.025	0.46	0.64
K	0.500	0.562	12.70	14.27
L	0.045	0.090	1.15	2.29
M	0.190	0.210	4.83	5.33
O	0.100	0.120	2.54	3.04
R	0.030	0.110	0.76	2.79
S	0.045	0.065	1.15	1.65
T	0.235	0.255	5.97	6.47
U	0.060	0.060	0.00	1.27
V	0.045	---	1.15	---
Z	---	0.090	---	2.04

STYLE 5:

1. DATE
2. DRAWN
3. SOURCE
4. DRAWN

ON Semiconductor and  are trademarks of Semiconductor Components Industries, LLC (SCILLC). SCILLC reserves the right to make changes without further notice to any products herein. SCILLC makes no warranty, representation or guarantee regarding the suitability of its products for any particular purpose, nor does SCILLC assume any liability arising out of the application or use of any product or circuit, and specifically disclaims any and all liability, including without limitation special, consequential or incidental damages. "Typical" parameters which may be provided in SCILLC data sheets and/or specifications can and do vary in different applications and actual performance may vary over time. All operating parameters, including "Typicals" must be validated for each customer application by customer's technical experts. SCILLC does not convey any license under its patent rights nor the rights of others. SCILLC products are not designed, intended, or authorized for use as components in systems intended for surgical implant into the body, or other applications intended to support or sustain life, or for any other application in which the failure of the SCILLC product could create a situation where personal injury or death may occur. Should Buyer purchase or use SCILLC products for any such unintended or unauthorized application, Buyer shall indemnify and hold SCILLC and its officers, employees, subsidiaries, affiliates, and distributors harmless against all claims, costs, damages, and expenses, and reasonable attorney fees arising out of, directly or indirectly, any claim of personal injury or death associated with such unintended or unauthorized use, even if such claim alleges that SCILLC was negligent regarding the design or manufacture of the part. SCILLC is an Equal Opportunity/Affirmative Action Employer.

## PUBLICATION ORDERING INFORMATION

## NORTH AMERICA Literature Fulfillment:

Literature Distribution Center for ON Semiconductor  
P.O. Box 5163, Denver, Colorado 80217 USA  
Phone: 303-675-2175 or 800-344-3860 Toll Free USA/Canada  
Fax: 303-675-2176 or 800-344-3867 Toll Free USA/Canada  
Email: ONlit@hibbertco.com  
Fax Response Line: 303-675-2157 or 800-344-3810 Toll Free USA/Canada

## N. American Technical Support: 800-282-9855 Toll Free USA/Canada

## EUROPE: LDC for ON Semiconductor - European Support

German Phone: (+1) 303-308-7140 (Mon-Fri 2:30pm to 7:00pm CET)  
Email: ONlit-german@hibbertco.com  
French Phone: (+1) 303-308-7141 (Mon-Fri 2:00pm to 7:00pm CET)  
Email: ONlit-french@hibbertco.com  
English Phone: (+1) 303-308-7142 (Mon-Fri 12:00pm to 5:00pm GMT)  
Email: ONlit@hibbertco.com

## EUROPEAN TOLL-FREE ACCESS: 00-800-4422-3781

\*Available from Germany, France, Italy, UK, Ireland

## CENTRAL/SOUTH AMERICA:

Spanish Phone: 303-308-7143 (Mon-Fri 8:00am to 5:00pm MST)  
Email: ONlit-spanish@hibbertco.com  
Toll-Free from Mexico: Dial 01-800-288-2872 for Access -  
then Dial 866-297-9322

## ASIA/PACIFIC: LDC for ON Semiconductor - Asia Support

Phone: 303-675-2121 (Tue-Fri 9:00am to 1:00pm, Hong Kong Time)  
Toll Free from Hong Kong & Singapore:  
001-800-4422-3781  
Email: ONlit-asia@hibbertco.com

## JAPAN: ON Semiconductor, Japan Customer Focus Center

4-32-1 Nishi-Gotanda, Shinagawa-ku, Tokyo, Japan 141-0031  
Phone: 81-3-5740-2700  
Email: r14525@onsemi.com

ON Semiconductor Website: <http://onsemi.com>

For additional information, please contact your local Sales Representative.

## Appendix-A (Continued)

## Power MOSFET MTP 3055

**MTP3055V**

Preferred Device

**Power MOSFET  
12 Amps, 60 Volts  
N-Channel TO-220**

This Power MOSFET is designed to withstand high energy in the avalanche and commutation modes. Designed for low voltage, high speed switching applications in power supplies, converters and power motor controls, these devices are particularly well suited for bridge circuits where diode speed and commutating safe operating areas are critical and offer additional safety margin against unexpected voltage transients.

- On-resistance  $R_{DS(on)}$  about One-half that of Standard MOSFETs with New Low Voltage, Low  $R_{DS(on)}$  Technology
- Faster Switching than E-FET Predecessors
- Avalanche Energy Specified
- $I_{DSS}$  and  $V_{DS(on)}$  Specified at Elevated Temperature
- Static Parameters are the Same for both TMOS V and TMOS E-FET

**MAXIMUM RATINGS** ( $T_C = 25^\circ\text{C}$  unless otherwise noted)

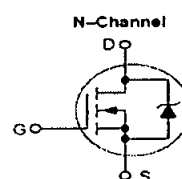
Rating	Symbol	Value	Unit
Drain-Source Voltage	$V_{DS}$	60	Vdc
Drain-Gate Voltage ( $R_{GS} = 1.0\text{ M}\Omega$ )	$V_{DGR}$	60	Vdc
Gate-Source Voltage	$V_{GS}$	$\pm 20$	Vdc
	$V_{GSM}$	$\pm 25$	Vpk
Drain Current - Continuous @ 25°C	$I_D$	12	Adc
	$I_D$	7.3	Adc
	$I_{DM}$	37	Apk
Total Power Dissipation @ 25°C Derate above 25°C	$P_D$	48	Watts
		0.32	W/°C
Operating and Storage Temperature Range	$T_J, T_{stg}$	-55 to 175	°C
Single Pulse Drain-to-Source Avalanche Energy - Starting $T_J = 25^\circ\text{C}$ ( $V_{DD} = 25\text{ Vdc}$ , $V_{GS} = 10\text{ Vdc}$ , $I_L = 12\text{ Apk}$ , $L = 1.0\text{ mH}$ , $R_G = 25\ \Omega$ )	$E_{AS}$	72	mJ
Thermal Resistance - Junction to Case - Junction to Ambient	$R_{\theta JC}$	3.13	°C/W
	$R_{\theta JA}$	62.5	°C/W
Maximum Lead Temperature for Soldering Purposes, 1/8" from case for 10 seconds	$T_L$	260	°C



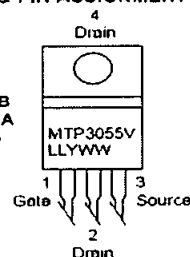
ON Semiconductor™

<http://onsemi.com>

**12 AMPERES  
50 VOLTS  
 $R_{DS(on)} = 150\text{ m}\Omega$**

**MARKING DIAGRAM  
& PIN ASSIGNMENT**

TO-220AB  
CASE 221A  
STYLE 5



MTP3055V = Device Code  
LL = Location Code  
Y = Year  
WW = Work Week

**ORDERING INFORMATION**

Device	Package	Shipping
MTP3055V	TO-220AB	50 Units/Rail

Preferred devices are recommended choices for future use and best overall value.

## Appendix-A (Continued)

ELECTRICAL CHARACTERISTICS ( $T_J = 25^\circ\text{C}$  unless otherwise noted)

Characteristic	Symbol	Min	Typ	Max	Unit	
<b>OFF CHARACTERISTICS</b>						
Drain-Source Breakdown Voltage ( $V_{GS} = 0\text{ Vdc}$ , $I_D = 250\ \mu\text{Adc}$ ) Temperature Coefficient (Positive)	$V_{(BR)DSS}$	60 -	- 65	- -	Vdc mV/ $^\circ\text{C}$	
Zero Gate Voltage Drain Current ( $V_{DS} = 60\text{ Vdc}$ , $V_{GS} = 0\text{ Vdc}$ ) ( $V_{DS} = 60\text{ Vdc}$ , $V_{GS} = 0\text{ Vdc}$ , $T_J = 150^\circ\text{C}$ )	$I_{DSS}$	- -	- -	10 100	$\mu\text{Adc}$	
Gate-Body Leakage Current ( $V_{GS} = \pm 20\text{ Vdc}$ , $V_{DS} = 0$ )	$I_{GSS}$	-	-	100	nAdc	
<b>ON CHARACTERISTICS (Note 1.)</b>						
Gate Threshold Voltage ( $V_{DS} = V_{GS}$ , $I_D = 250\ \mu\text{Adc}$ ) Temperature Coefficient (Negative)	$V_{GS(th)}$	2.0 -	2.7 5.4	4.0 -	Vdc mV/ $^\circ\text{C}$	
Static Drain-Source On-Resistance ( $V_{GS} = 10\text{ Vdc}$ , $I_D = 6.0\text{ Adc}$ )	$R_{DS(on)}$	-	0.10	0.15	Ohm	
Drain-Source On-Voltage ( $V_{GS} = 10\text{ Vdc}$ ) ( $I_D = 12\text{ Adc}$ ) ( $I_D = 6.0\text{ Adc}$ , $T_J = 150^\circ\text{C}$ )	$V_{DS(on)}$	- -	1.3 -	2.2 1.9	Vdc	
Forward Transconductance ( $V_{DS} = 7.0\text{ Vdc}$ , $I_D = 6.0\text{ Adc}$ )	$g_{FS}$	4.0	5.0	-	mhos	
<b>DYNAMIC CHARACTERISTICS</b>						
Input Capacitance	$(V_{DS} = 25\text{ Vdc}$ , $V_{GS} = 0\text{ Vdc}$ , $f = 1.0\text{ MHz}$ )	$C_{iss}$	-	410	500	pF
Output Capacitance		$C_{oss}$	-	130	180	
Reverse Transfer Capacitance		$C_{rss}$	-	25	50	
<b>SWITCHING CHARACTERISTICS (Note 2.)</b>						
Turn-On Delay Time	$(V_{DD} = 30\text{ Vdc}$ , $I_D = 12\text{ Adc}$ , $V_{GS} = 10\text{ Vdc}$ , $R_G = 9.1\ \Omega$ )	$t_{d(on)}$	-	7.0	10	ns
Rise Time		$t_r$	-	34	60	
Turn-Off Delay Time		$t_{d(off)}$	-	17	30	
Fall Time		$t_f$	-	18	50	
Gate Charge (See Figure 8)	$(V_{DS} = 48\text{ Vdc}$ , $I_D = 12\text{ Adc}$ , $V_{GS} = 10\text{ Vdc}$ )	$Q_T$	-	12.2	17	nC
		$Q_1$	-	3.2	-	
		$Q_2$	-	5.2	-	
		$Q_3$	-	5.5	-	
<b>SOURCE-DRAIN DIODE CHARACTERISTICS</b>						
Forward On-Voltage (Note 1.)	$(I_S = 12\text{ Adc}$ , $V_{GS} = 0\text{ Vdc}$ ) $(I_S = 12\text{ Adc}$ , $V_{GS} = 0\text{ Vdc}$ , $T_J = 150^\circ\text{C}$ )	$V_{SD}$	- -	1.0 0.91	1.6 -	Vdc
Reverse Recovery Time (See Figure 15)	$(I_S = 12\text{ Adc}$ , $V_{GS} = 0\text{ Vdc}$ , $di_S/dt = 100\text{ A}/\mu\text{s}$ )	$t_{rr}$	-	56	-	ns
		$t_a$	-	40	-	
		$t_b$	-	16	-	
Reverse Recovery Stored Charge		$Q_{RR}$	-	0.128	-	$\mu\text{C}$
<b>INTERNAL PACKAGE INDUCTANCE</b>						
Internal Drain Inductance (Measured from contact screw on tab to center of die) (Measured from the drain lead 0.25" from package to center of die)	$L_D$	-	3.5 4.5	-	nH	
Internal Source Inductance (Measured from the source lead 0.25" from package to source bond pad)	$L_S$	-	7.5	-	nH	

1. Pulse Test: Pulse Width  $\leq 300\ \mu\text{s}$ , Duty Cycle  $\leq 2\%$ .

2. Switching characteristics are independent of operating junction temperature.



## Appendix-A (Continued)

### TYPICAL ELECTRICAL CHARACTERISTICS

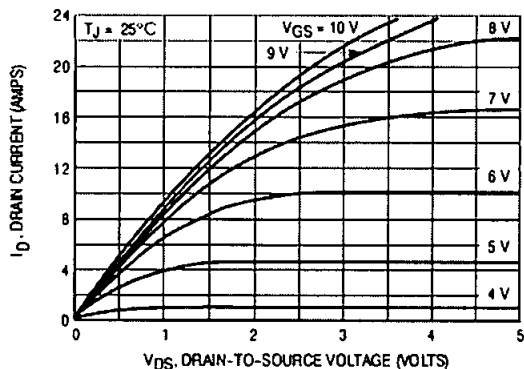


Figure 1. On-Region Characteristics

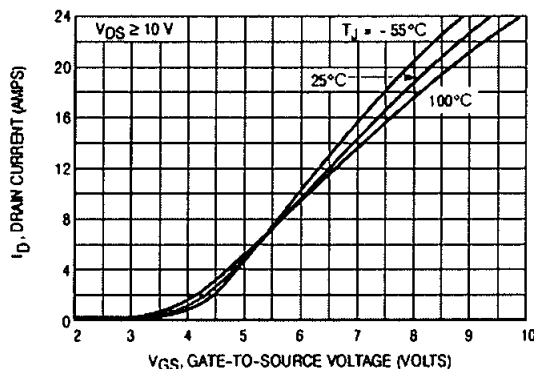


Figure 2. Transfer Characteristics

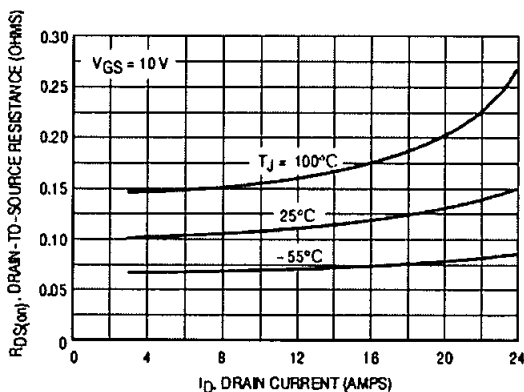


Figure 3. On-Resistance versus Drain Current and Temperature

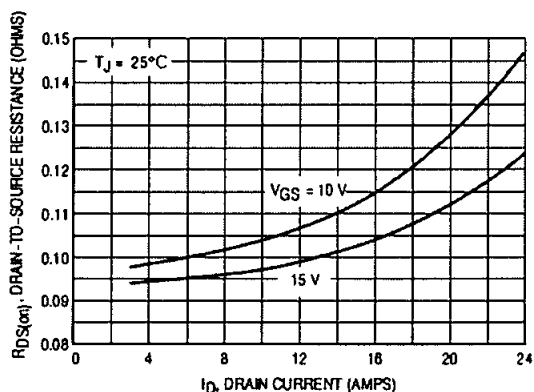


Figure 4. On-Resistance versus Drain Current and Gate Voltage

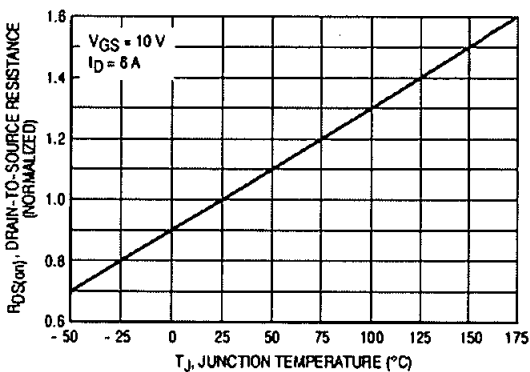


Figure 5. On-Resistance Variation with Temperature

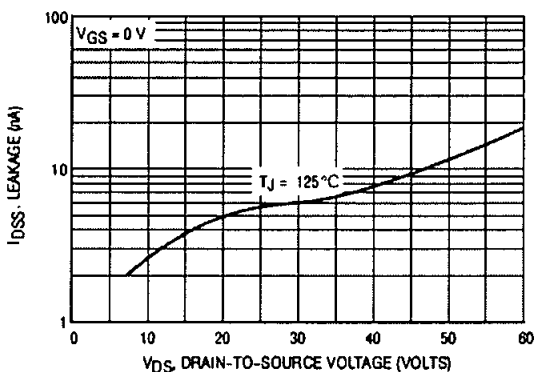


Figure 6. Drain-To-Source Leakage Current versus Voltage

## Appendix-A (Continued)

### POWER MOSFET SWITCHING

Switching behavior is most easily modeled and predicted by recognizing that the power MOSFET is charge controlled. The lengths of various switching intervals ( $\Delta t$ ) are determined by how fast the FET input capacitance can be charged by current from the generator.

The published capacitance data is difficult to use for calculating rise and fall because drain-gate capacitance varies greatly with applied voltage. Accordingly, gate charge data is used. In most cases, a satisfactory estimate of average input current ( $I_{G(AV)}$ ) can be made from a rudimentary analysis of the drive circuit so that

$$t = Q/I_{G(AV)}$$

During the rise and fall time interval when switching a resistive load,  $V_{GS}$  remains virtually constant at a level known as the plateau voltage,  $V_{GSP}$ . Therefore, rise and fall times may be approximated by the following:

$$t_r = Q_2 \times R_G / (V_{GG} - V_{GSP})$$

$$t_f = Q_2 \times R_G / V_{GSP}$$

where

$V_{GG}$  = the gate drive voltage, which varies from zero to  $V_{GG}$

$R_G$  = the gate drive resistance

and  $Q_2$  and  $V_{GSP}$  are read from the gate charge curve.

During the turn-on and turn-off delay times, gate current is not constant. The simplest calculation uses appropriate values from the capacitance curves in a standard equation for voltage change in an RC network. The equations are:

$$t_{d(on)} = R_G C_{iss} \ln [V_{GG}/(V_{GG} - V_{GSP})]$$

$$t_{d(off)} = R_G C_{iss} \ln (V_{GG}/V_{GSP})$$

The capacitance ( $C_{iss}$ ) is read from the capacitance curve at a voltage corresponding to the off-state condition when calculating  $t_{d(on)}$  and is read at a voltage corresponding to the on-state when calculating  $t_{d(off)}$ .

At high switching speeds, parasitic circuit elements complicate the analysis. The inductance of the MOSFET source lead, inside the package and in the circuit wiring which is common to both the drain and gate current paths, produces a voltage at the source which reduces the gate drive current. The voltage is determined by  $L di/dt$ , but since  $di/dt$  is a function of drain current, the mathematical solution is complex. The MOSFET output capacitance also complicates the mathematics. And finally, MOSFETs have finite internal gate resistance which effectively adds to the resistance of the driving source, but the internal resistance is difficult to measure and, consequently, is not specified.

The resistive switching time variation versus gate resistance (Figure 9) shows how typical switching performance is affected by the parasitic circuit elements. If the parasitics were not present, the slope of the curves would maintain a value of unity regardless of the switching speed. The circuit used to obtain the data is constructed to minimize common inductance in the drain and gate circuit loops and is believed readily achievable with board mounted components. Most power electronic loads are inductive; the data in the figure is taken with a resistive load, which approximates an optimally snubbed inductive load. Power MOSFETs may be safely operated into an inductive load; however, snubbing reduces switching losses.

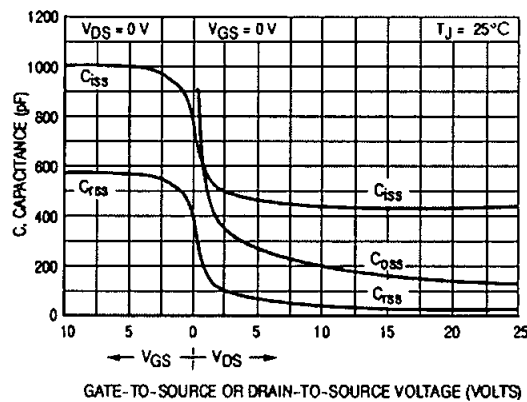


Figure 7. Capacitance Variation

### Appendix-A (Continued)

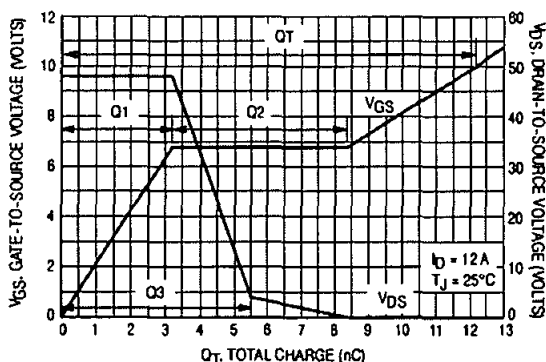


Figure 8. Gate-To-Source and Drain-To-Source Voltage versus Total Charge

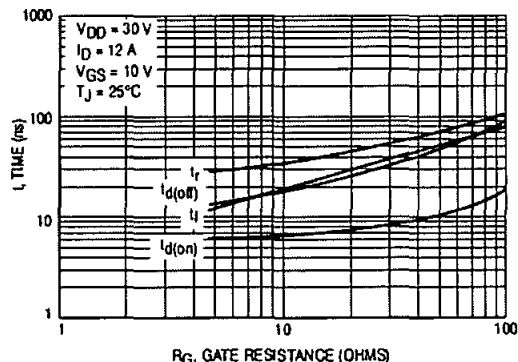


Figure 9. Resistive Switching Time Variation versus Gate Resistance

#### DRAIN-TO-SOURCE DIODE CHARACTERISTICS

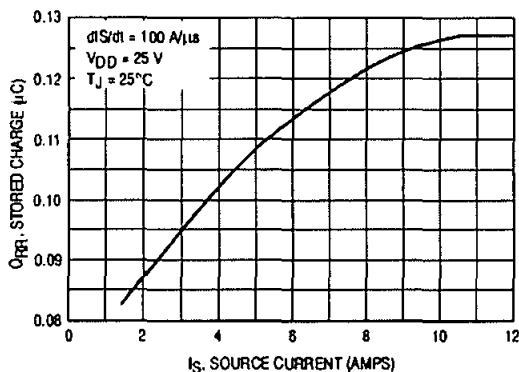


Figure 10. Stored Charge

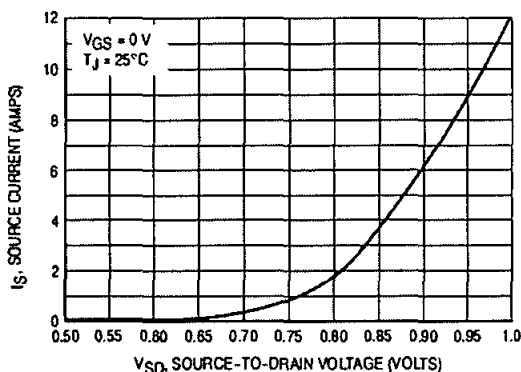


Figure 11. Diode Forward Voltage versus Current

#### SAFE OPERATING AREA

The Forward Biased Safe Operating Area curves define the maximum simultaneous drain-to-source voltage and drain current that a transistor can handle safely when it is forward biased. Curves are based upon maximum peak junction temperature and a case temperature ( $T_C$ ) of 25°C. Peak repetitive pulsed power limits are determined by using the thermal response data in conjunction with the procedures discussed in AN569, "Transient Thermal Resistance—General Data and Its Use."

Switching between the off-state and the on-state may traverse any load line provided neither rated peak current ( $I_{DM}$ ) nor rated voltage ( $V_{DSS}$ ) is exceeded and the transition time ( $t_r, t_f$ ) do not exceed 10  $\mu$ s. In addition the total power averaged over a complete switching cycle must not exceed  $(T_J(MAX) - T_C)/(R_{\theta JC})$ .

A Power MOSFET designated E-FET can be safely used in switching circuits with unclamped inductive loads. For

reliable operation, the stored energy from circuit inductance dissipated in the transistor while in avalanche must be less than the rated limit and adjusted for operating conditions differing from those specified. Although industry practice is to rate in terms of energy, avalanche energy capability is not a constant. The energy rating decreases non-linearly with an increase of peak current in avalanche and peak junction temperature.

Although many E-FETs can withstand the stress of drain-to-source avalanche at currents up to rated pulsed current ( $I_{DM}$ ), the energy rating is specified at rated continuous current ( $I_D$ ), in accordance with industry custom. The energy rating must be derated for temperature as shown in the accompanying graph (Figure 13). Maximum energy at currents below rated continuous  $I_D$  can safely be assumed to equal the values indicated.

### Appendix-A (Continued)

#### SAFE OPERATING AREA

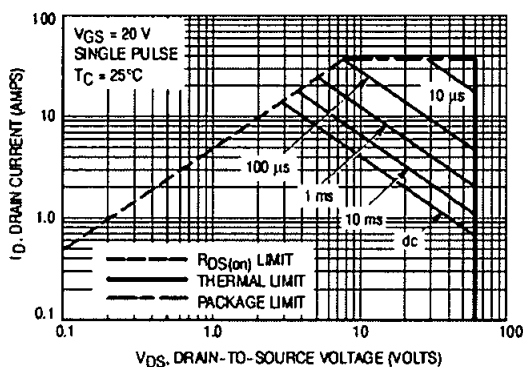


Figure 12. Maximum Rated Forward Biased Safe Operating Area

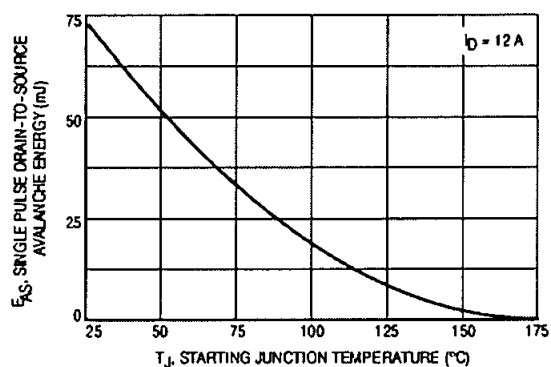


Figure 13. Maximum Avalanche Energy versus Starting Junction Temperature

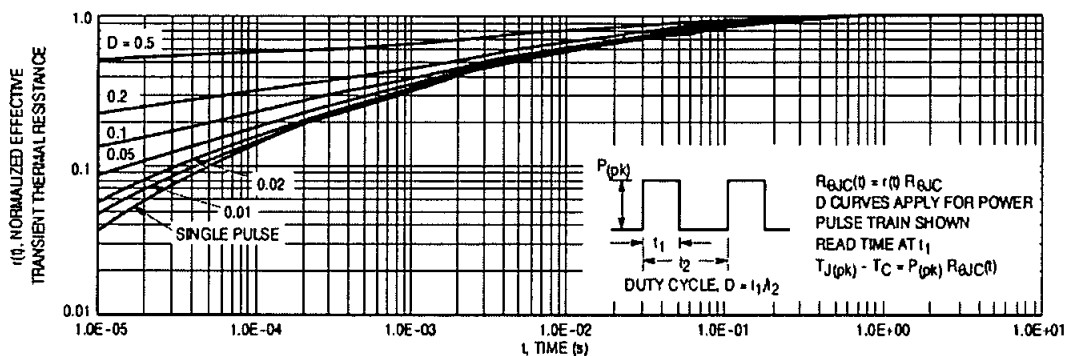


Figure 14. Thermal Response

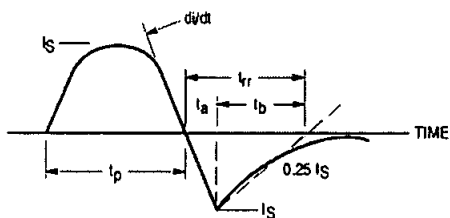
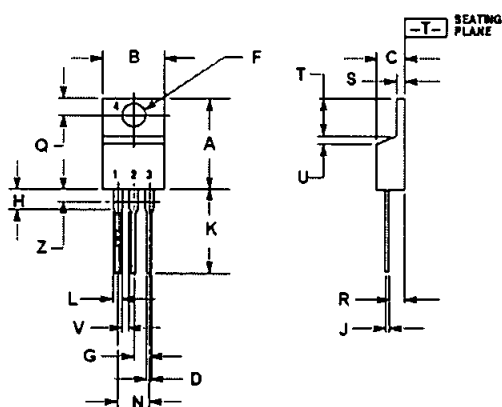


Figure 15. Diode Reverse Recovery Waveform

## Appendix-A (Continued)

## PACKAGE DIMENSIONS


TO-220 THREE-LEAD  
TO-220AB  
CASE 221A-09  
ISSUE AA



- NOTES:
1. DIMENSIONING AND TOLERANCING PER ANSI Y14.5M, 1982.
  2. CONTROLLING DIMENSION: INCH.
  3. DIMENSION Z DEFINES A ZONE WHERE ALL BODY AND LEAD IRREGULARITIES ARE ALLOWED.

DIM	INCHES		MILLIMETERS	
	MIN	MAX	MIN	MAX
A	0.570	0.620	14.48	15.75
B	0.380	0.425	9.65	10.78
C	0.180	0.190	4.67	4.82
D	0.025	0.025	0.64	0.64
F	0.142	0.147	3.61	3.73
G	0.025	0.105	2.42	2.68
H	0.110	0.155	2.80	3.93
J	0.018	0.025	0.46	0.64
K	0.500	0.252	12.70	14.27
L	0.045	0.060	1.15	1.52
M	0.190	0.210	4.83	5.33
O	0.100	0.120	2.54	3.04
R	0.080	0.110	2.04	2.79
S	0.245	0.265	6.19	6.73
T	0.225	0.255	5.71	6.47
U	0.060	0.050	1.52	1.27
V	0.245	---	6.19	---
Z	---	0.080	---	2.04

- STYLE 5:  
PIN 1: GATE  
2: DRAIN  
3: SOURCE  
4: DRAIN

ON Semiconductor and  are trademarks of Semiconductor Components Industries, LLC (SCILLC). SCILLC reserves the right to make changes without further notice to any products herein. SCILLC makes no warranty, representation or guarantee regarding the suitability of its products for any particular purpose, nor does SCILLC assume any liability arising out of the application or use of any product or circuit, and specifically disclaims any and all liability, including without limitation special, consequential or incidental damages. Typical parameters which may be provided in SCILLC data sheets and/or specifications can and do vary in different applications and actual performance may vary over time. All operating parameters, including "Typicals" must be validated for each customer application by customer's technical experts. SCILLC does not convey any license under its patent rights nor the rights of others. SCILLC products are not designed, intended, or authorized for use as components in systems intended for surgical implant into the body, or other applications intended to support or sustain life, or for any other application in which the failure of the SCILLC product could create a situation where personal injury or death may occur. Should Buyer purchase or use SCILLC products for any such unintended or unauthorized application, Buyer shall indemnify and hold SCILLC and its officers, employees, subsidiaries, affiliates, and distributors harmless against all claims, costs, damages, and expenses, and reasonable attorney fees arising out of, directly or indirectly, any claim of personal injury or death associated with such unintended or unauthorized use, even if such claim alleges that SCILLC was negligent regarding the design or manufacture of the part. SCILLC is an Equal Opportunity/Affirmative Action Employer.

## PUBLICATION ORDERING INFORMATION

**NORTH AMERICA Literature Fulfillment:**  
Literature Distribution Center for ON Semiconductor  
P.O. Box 5163, Denver, Colorado 80217 USA  
Phone: 303-675-2175 or 800-344-3860 Toll Free USA/Canada  
Fax: 303-675-2176 or 800-344-3867 Toll Free USA/Canada  
Email: ONlit@nibberco.com  
Fax Response Line: 303-675-2167 or 800-344-3810 Toll Free USA/Canada

**N. American Technical Support:** 800-282-9855 Toll Free USA/Canada

**EUROPE:** LDC for ON Semiconductor – European Support  
German Phone: (+1) 303-308-7140 (Mon-Fri 2:30pm to 7:00pm CET)  
Email: ONlit-german@nibberco.com  
French Phone: (+1) 303-308-7141 (Mon-Fri 2:00pm to 7:00pm CET)  
Email: ONlit-french@nibberco.com  
English Phone: (+1) 303-308-7142 (Mon-Fri 12:00pm to 5:00pm GMT)  
Email: ONlit@nibberco.com

**EUROPEAN TOLL-FREE ACCESS:** 00-800-4422-3781  
\*Available from Germany, France, Italy, UK, Ireland

**CENTRAL/SOUTH AMERICA:**  
Spanish Phone: 303-308-7143 (Mon-Fri 8:00am to 5:00pm MST)  
Email: ONlit-spanish@nibberco.com  
Toll-Free from Mexico: Dial 01-800-288-2872 for Access –  
then Dial 866-297-9322

**ASIA/PACIFIC:** LDC for ON Semiconductor – Asia Support  
Phone: 303-675-2121 (Tue-Fri 9:00am to 1:00pm, Hong Kong Time)  
Toll Free from Hong Kong & Singapore:  
001-800-4422-3781  
Email: ONlit-asia@nibberco.com

**JAPAN:** ON Semiconductor, Japan Customer Focus Center  
4-32-1 Nishi-Gotanda, Shinagawa-ku, Tokyo, Japan 141-0031  
Phone: 81-3-5740-2700  
Email: r14525@onsemi.com

**ON Semiconductor Website:** <http://onsemi.com>

For additional information, please contact your local Sales Representative.

## Appendix-A (Continued)

## Permanent Magnet Brush Less D.C. Motor

**Airpax Series 9904 120 52..****DC Geared Motors**

39mm square flange - plastic geared DC motor

RS 336-343 : 9904 120 52402

RS 336-321 : 9904 120 52602

RS 336-337 : 9904 120 52405

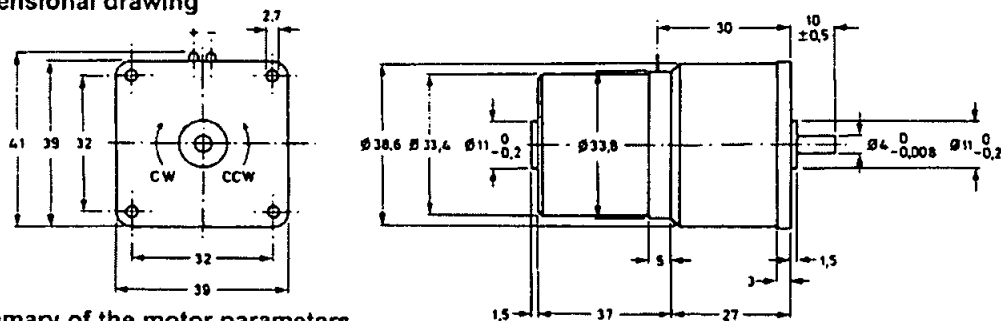
RS 336-315 : 9904 120 52605

This range of small d.c. motors with integrated gear train is designed for applications requiring quality design and long life drive units. The motor has been designed with a permanent magnet stator system. The reduction gearbox has gearwheels of polyacetal resin. Spark suppression is obtained by a sandwich mounted disc-VDR between commutator and rotor coils. The grey injected plastic housing is highly resistant to chemicals and corrosion. Mounting of the motor is provided for with four M2.5 clearance holes on the flange.

Application examples include:

- \* vending & coffee machines
- \* air valve control
- \* ticket dispensers
- \* office automation
- \* printing machines
- \* entertainment products, scale models

## Dimensional drawing



## Summary of the motor parameters

Rated working point:

3.5mNm @ 3000rpm (1 Watt, continuous, motor typical life approx. 2500 hours)

Not relevant for all gear ratios - Max. gearbox torque to be considered

Part Number	Rated Voltage (V)	Rotor Resist. (Ohm)	No Load Speed (rpm)	Stall Torque (mNm)	Torque Constant (mNm/A)
9904 120 52 4xx	6	4.7	3900	15	11
9904 120 52 6xx	12	14.5	3900	15	21

Brushes : Carbon

Commutator : flat copper  
3 segments

Connections : Solder tags

Thermal res. : 30°K/W  
(winding/ambient)

Product designed and manufactured in the EEC to ISO 9001 standards

## Appendix-A (Continued)

Operating temperature Range	-20 to +60°C
Storage temperature Range	-40 to +70°C
Bearings	Sleeve Bronze, Self Lubricating
Maximum axial play	0.5mm
Housing material	Polycetal Resin - Grey
Gear material	Polycetal Resin
Mass	125g approx.

The values given below apply to an ambient temperature of  $22 \pm 5^\circ\text{C}$ , an atmospheric pressure of 86 to 106kPA and a relative humidity of 45 to 75%.

catalogue number 9904 120 62..	402	602	405	605	
reduction ratio	9 : 1		60 : 1		
Nominal values					
voltage (d.c.)	6	12	6	12	V
torque	25		125		mNm
speed at nom. load at no load	330 415		60 78		rev/ min
current at nom. load at no load	360 80	185 45	360 80	185 45	mA mA
input power	2.1	2.2	2.1	2.2	W
direction of rotation *	CW		CW + CCW		
max. radial force on the bearings	2		6		N
max. axial force	2		6		N
Limiting conditions					
max voltage (d.c.)	9	18	9	18	V
max. perm. load	37.5		150		mNm

\* Viewed from the shaft end

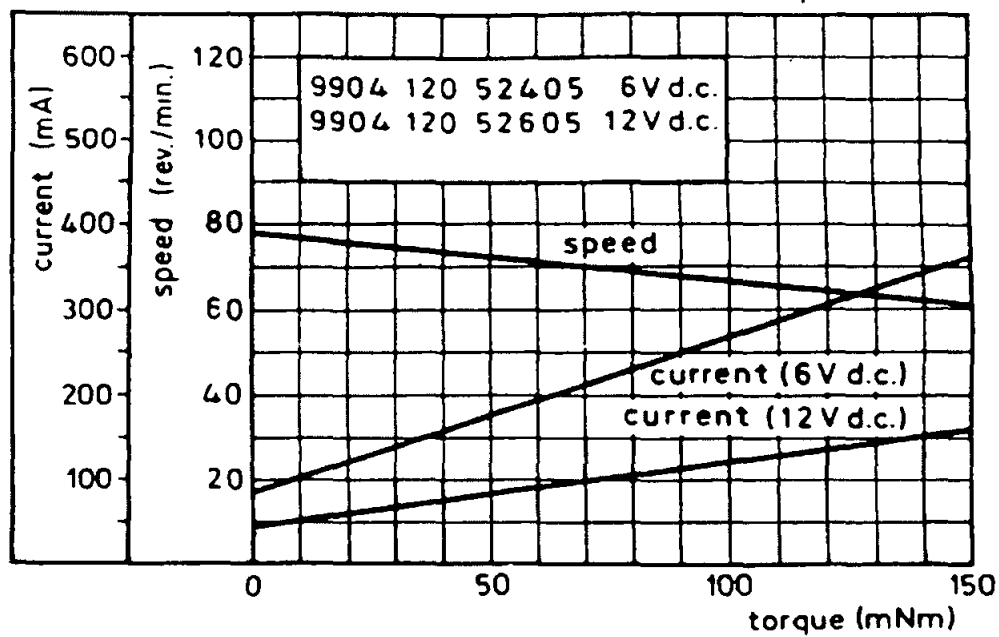
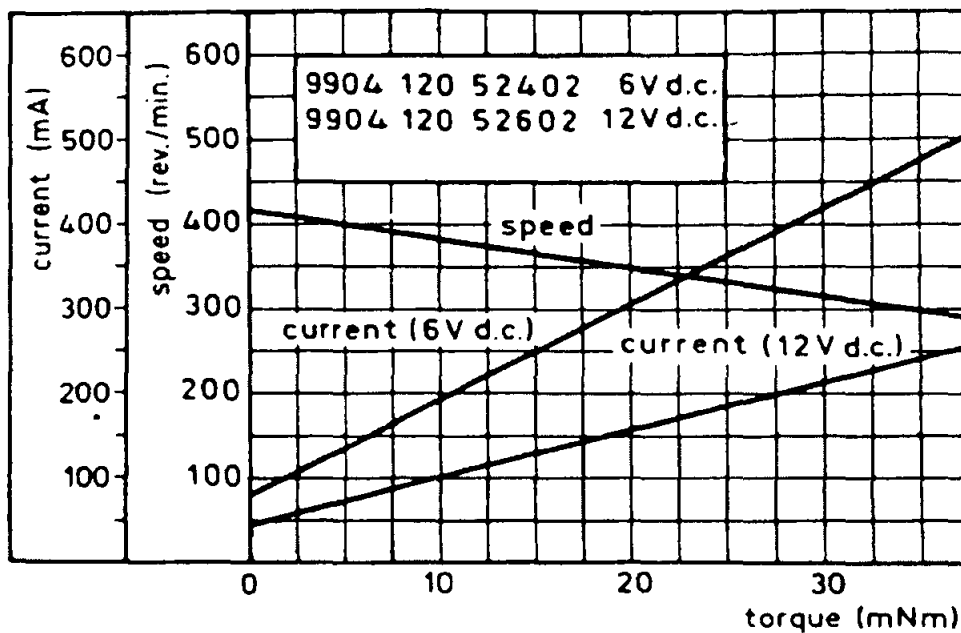
Notes: - The specified rated current values should not be exceeded.

- The gearbox should be externally protected (eg. torque limiter or current control) in systems where torque peaks (or stall) can be expected.

- Indicated no-load-currents are maximum values, to be considered as worst case over the whole motor life. In practice, new motors will show significantly lower values.

Appendix-A (Continued)

Typical Performance curves at 6 and 12V,  $T_{amb} = 22\text{ }^{\circ}\text{C}$





## Appendix-A (Continued)

## Force Sensor Data Sheet

**MICRO SWITCH Force Sensors**

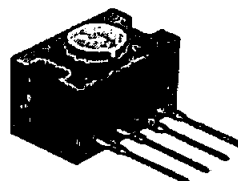
## Force Sensor

*FS Series***FEATURES**

- Robust performance characteristics
- Precision force sensing
- Adaptable product design
- Highly reliable
- Signal conditioning available
- Electrically ratiometric output
- Extremely low deflection (30 microns typical @ Full Scale)
- Low repeatability errors ( $\pm 0.2\%$  Span)
- Low linearity errors ( $\pm 0.5\%$  Span)
- Low off-center loading errors
- Resolution to 1.0 gram force
- Fast response time
- Low power consumption
- High ESD resistance - 10 KV

**TYPICAL APPLICATIONS**

- Medical infusion pumps
- Kidney dialysis machines
- Robotic end-effectors
- Variable tension control
- Load and compression sensing
- Contact sensing



The FS Series Force Sensor provides precise, reliable force sensing performance in a compact commercial grade package. The sensor features a proven sensing technology that utilizes a specialized piezoresistive micro-machined silicon sensing element. The low power, unamplified, non-compensated Wheatstone bridge circuit design provides inherently stable mV outputs over the 1,500 gram force range.

The force sensor operates on the principle that the resistance of silicon implanted piezoresistors will increase when the resistors flex under an applied force. The sensor concentrates force from the application through the stainless steel plunger directly to the silicon sensing element. The amount of resistance changes in proportion to the amount of force being applied. This change in circuit resistance results in a corresponding mV output level.

The sensor package design incorporates a patented modular construction. The use of innovative elastomeric technology and engineered molded plastics results in load capacities of 5.5 Kg over-force. The stainless steel plunger provides excellent mechanical stability and is adaptable to a variety of applications. Various electrical interconnects can accept pre-wired connectors, printed circuit board mounting, and surface mounting. The unique sensor design also provides a variety of mounting options including mounting brackets, as well as application-specific mounting requirements.

## Appendix-A (Continued)

**MICRO SWITCH Force Sensors**

## Force Sensor

*FS Series***PERFORMANCE CHARACTERISTICS @  $10 \pm 0.01$  VDC, 25°C**

Preliminary, based on limited test data

Parameter	Min.	Typ.	Max.	Units
Excitation*	—	10	12	VDC
Null shift, 25 to 0°, 25 to 50°C	—	$\pm 0.5$	—	mV
Null offset	-30	0	+30	mV
Linearity (BFSL)	—	$\pm 0.5$	—	% Span
Sensitivity	—	0.24	—	mV/grf
Sensitivity shift 25 to 0°, 25 to 50°C	—	$\pm 5.0$	—	% Span
Repeatability	—	$\pm 0.2$	—	% Span
Response time	—	—	1.0	msec
Input resistance	—	5.0 K	—	ohms
Output resistance	—	5.0 K	—	ohms
Plunger deflection	—	30	—	microns
Weight	—	2.0	—	grams
ESD (direct contact - terminals and plunger)	10	—	—	kVolts

\* Non-compensated force sensors, excited by constant current (1.5 mA) instead of voltage, exhibit partial temperature compensation of Span.

**ENVIRONMENTAL SPECIFICATIONS**

Operating temperature	-40 to +85°C (-40 to +185°F)
Storage temperature	-55 to +105°C (-67 to +221°F)
Shock	Qualification tested to 150 g
Vibration	Qualification tested to 0 to 2 kHz, 20 g sine

Note: All force related specifications are established using dead weight or compliant force.

**ORDER GUIDE**

Catalog Listing	Force Range (grams)	Span, mV			Overforce grams Max.
		Min.	Typ.	Max.	
FSG-15N1A	1,500	290	360	430	5,500

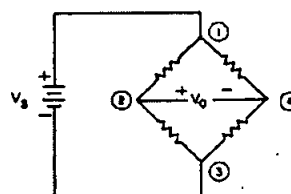
**MOUNTING**

The sensor output characteristics do not change with respect to mounting orientation. Care should be taken not to obstruct the vent hole in the bottom of the sensor housing. Improper venting may result in unstable output.

Mounting bracket mounting torque: 2-5 in. lb. (.21-.56 Nm).

**APPLYING FORCE**

Evaluation of the sensor is to be performed using dead-weight or compliant force. Application of a rigid, immobile force will result in output drift (decrease) as elastomeric seals relax. Off-center plunger loading has minimal effect on sensor performance and maintains operation within design specifications.

**EXCITATION SCHEMATIC****FS SERIES CIRCUIT**

1. Circled numbers refer to sensor terminals (pins). Pin 1 is designated with a notch. Pin 1 = Supply  $V_s$  (+)  
Pin 2 = Output, (+)  
Pin 3 = Ground, (-)  
Pin 4 = Output, (-)
2. The force sensor may be powered by voltage or current. Maximum supply voltage is not to exceed 12 volts. Maximum supply current is not to exceed 1.6 mA. Power is applied across Pin 1 and Pin 3.
3. The sensor output should be measured as a differential voltage across Pin 2 and Pin 4 ( $V_o = V_2 - V_4$ ). The output is ratiometric to the supply voltage. Shifts in supply voltage will cause shifts in output. Neither Pin 2 nor Pin 4 should be tied to ground or voltage supply.

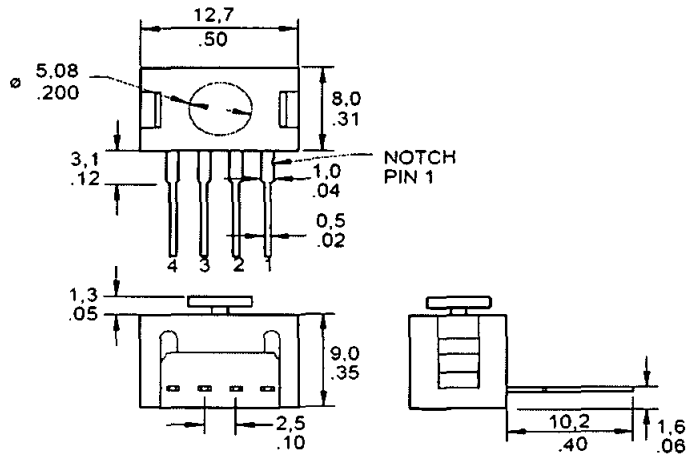
Appendix-A (Continued)

**MICRO SWITCH Force Sensors**

Force Sensor

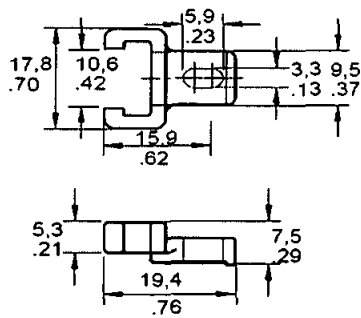
*FS Series*

MOUNTING DIMENSIONS (for reference only)



**ACCESSORY**

Catalog Listing	Description
PC15132	Plastic mounting bracket



## Appendix-A (Continued)

**MICRO SWITCH Force Sensors**

Force Sensor

*FS Series***SALES AND SERVICE**

Honeywell's MICRO SWITCH Division serves its customers through a worldwide network of sales offices and distributors. For application assistance, current specifications, pricing or name of the nearest Authorized Distributor, contact a nearby sales office. Or call:

1-800-537-6945 USA  
1-416-293-8111 Canada  
1-815-235-6847 International

**INTERNET**

<http://www.sensing.honeywell.com>  
[info@micro.honeywell.com](mailto:info@micro.honeywell.com)

Specifications may change without notice. The information we supply is believed to be accurate and reliable as of this printing. However, we assume no responsibility for its use.

While we provide application assistance, personally and through our literature, it is up to the customer to determine the suitability of the product in the application.

**Honeywell**

Sensing & Control  
Honeywell Inc.  
11 West Spring Street  
Freeport, Illinois 61032



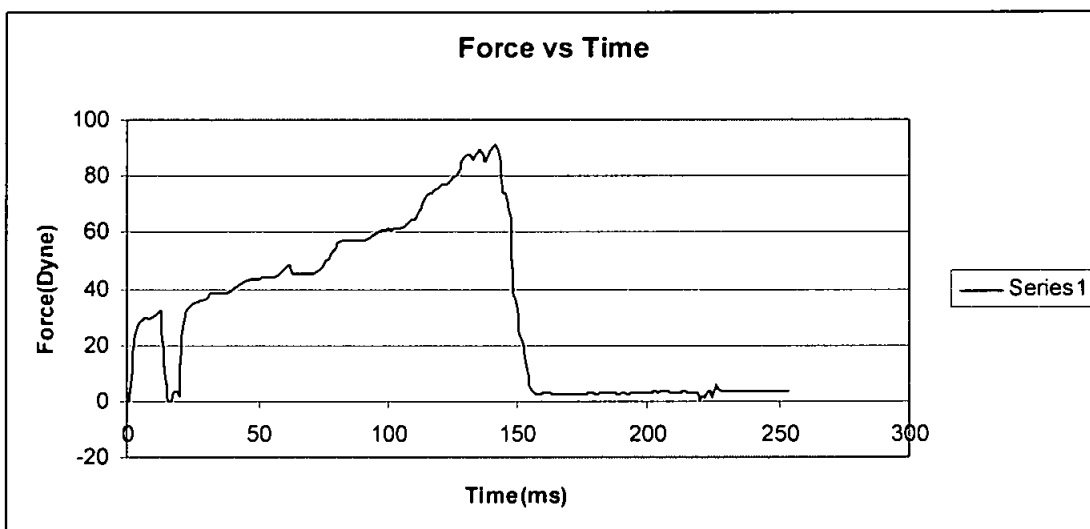
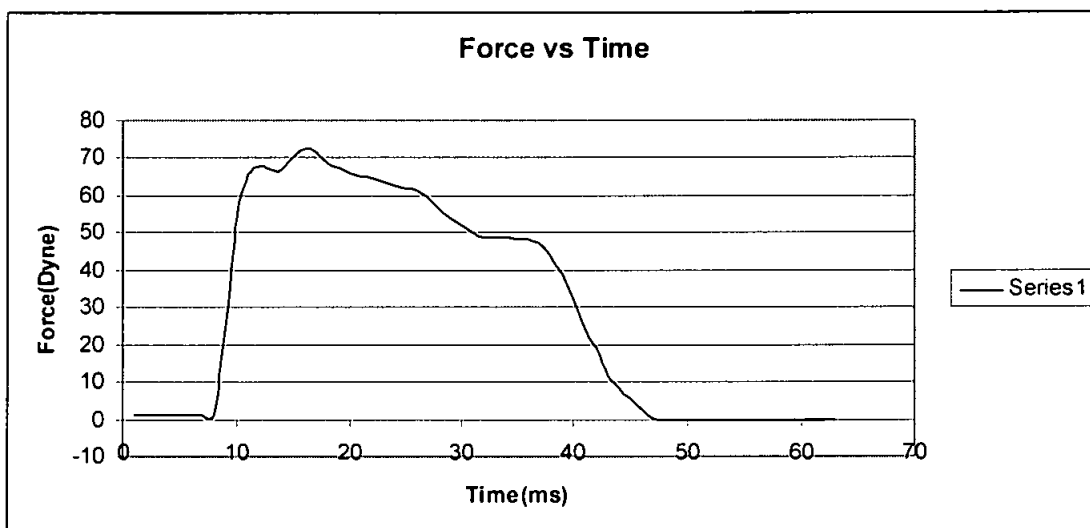
Printed with 50% or more Recycled Paper  
84-0822A-0 704 Printed in USA

*Helping You Control Your World*

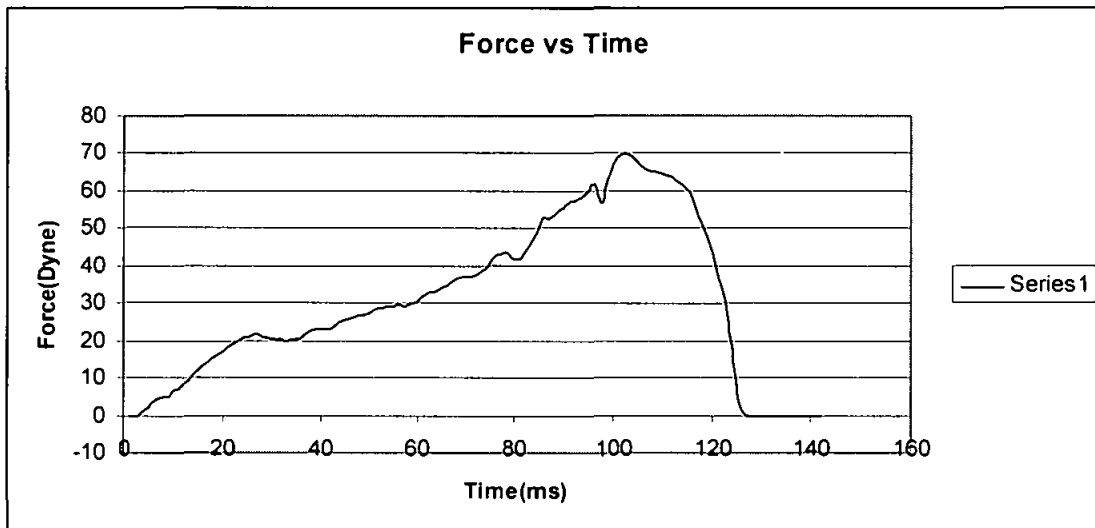
## Appendix-B

## Needle Insertion Force by XRF 440M Pocket Data Logger

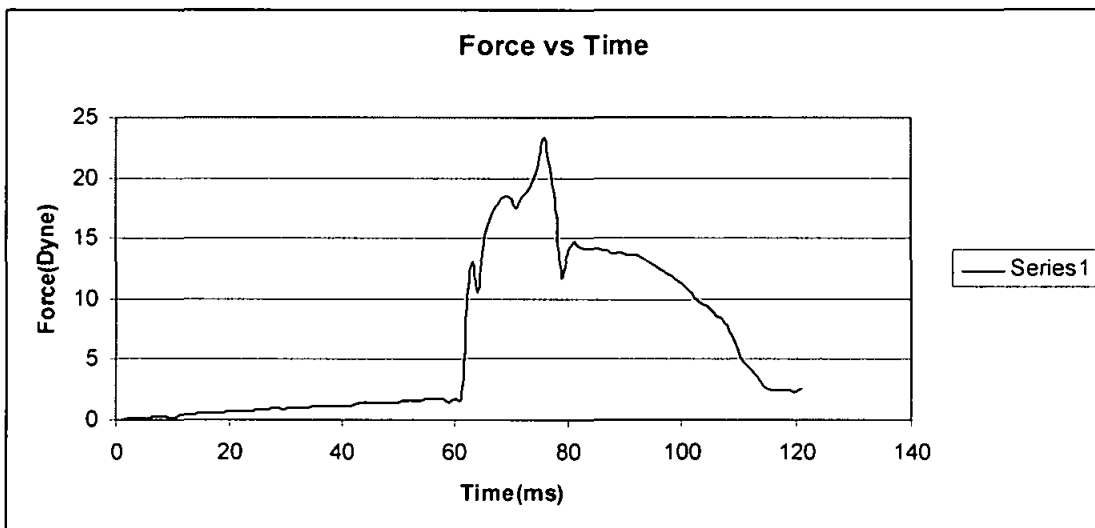
## 21 Gauge/0.9 millimeter Diameter Needle insertion Force



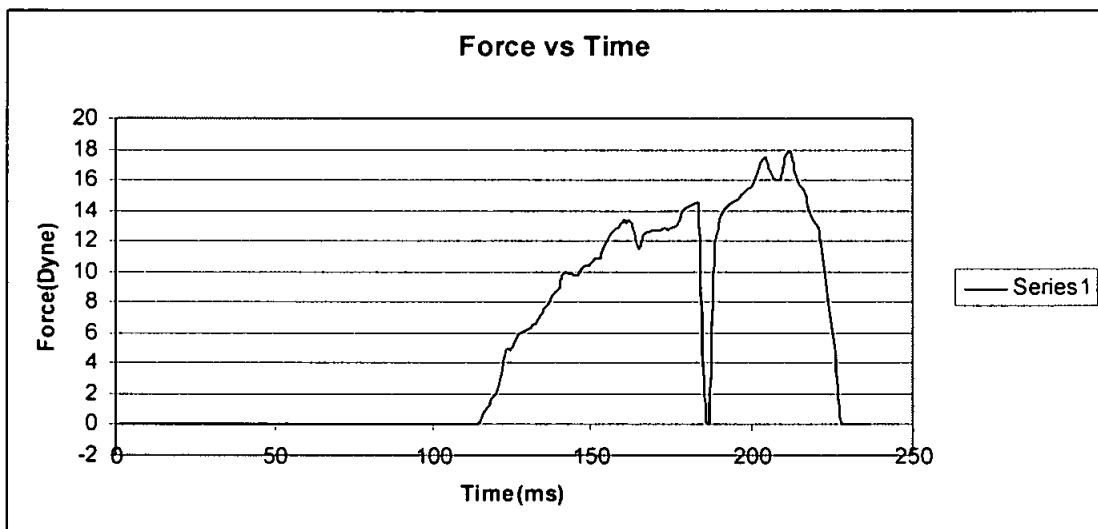
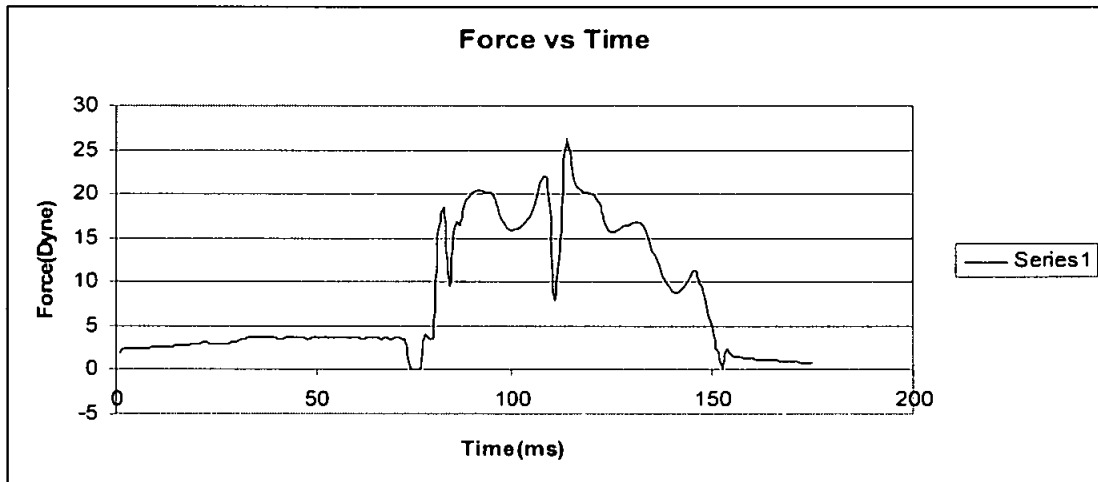
## Appendix-B (Continued)



20 Gauge/0.8 millimeter Diameter Needle Insertion Force

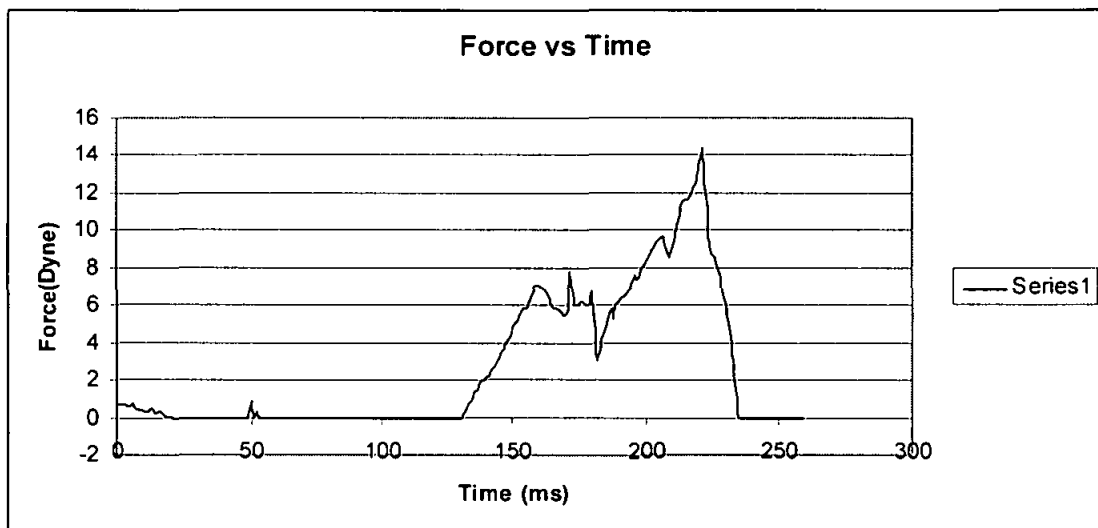
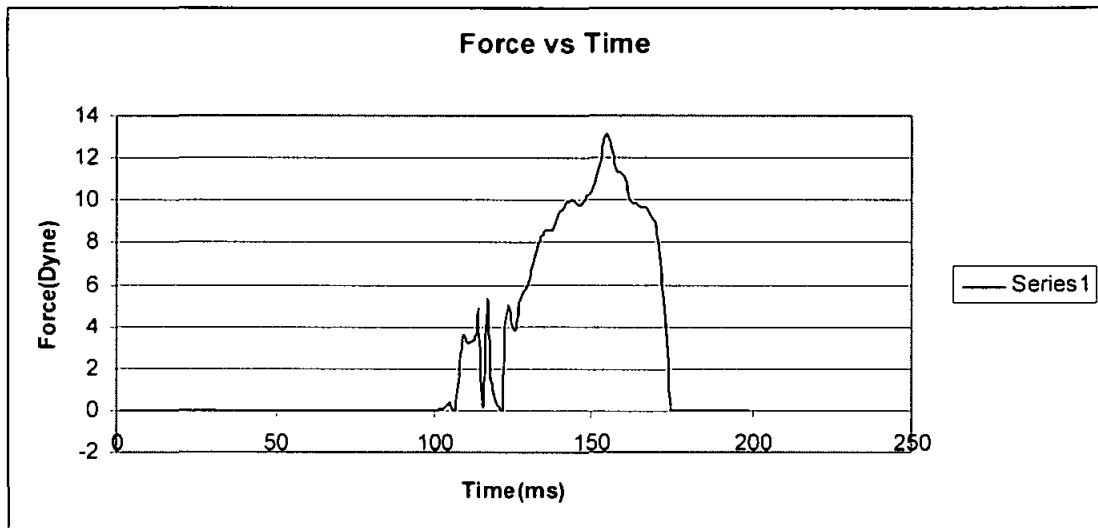


## Appendix-B (Continued)



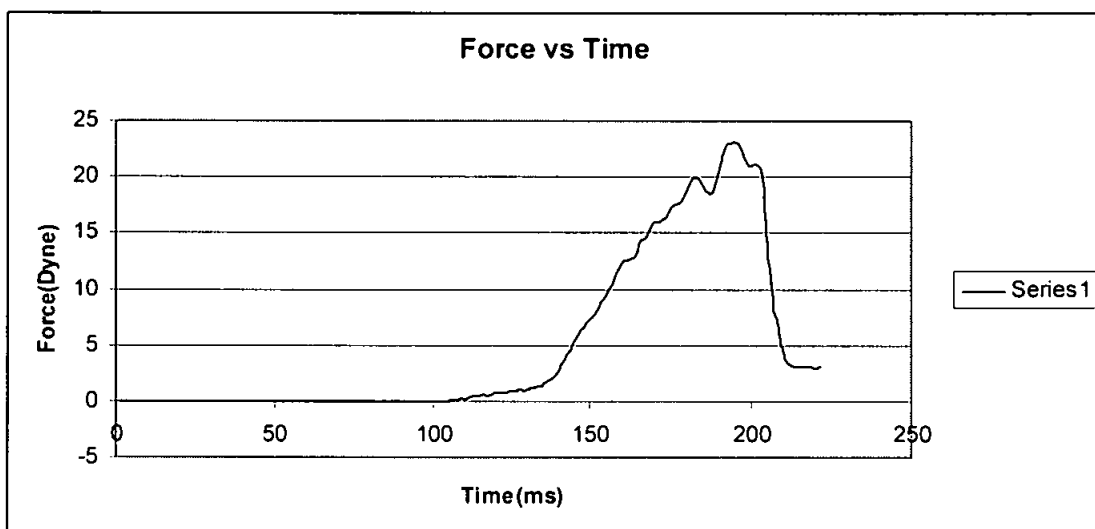
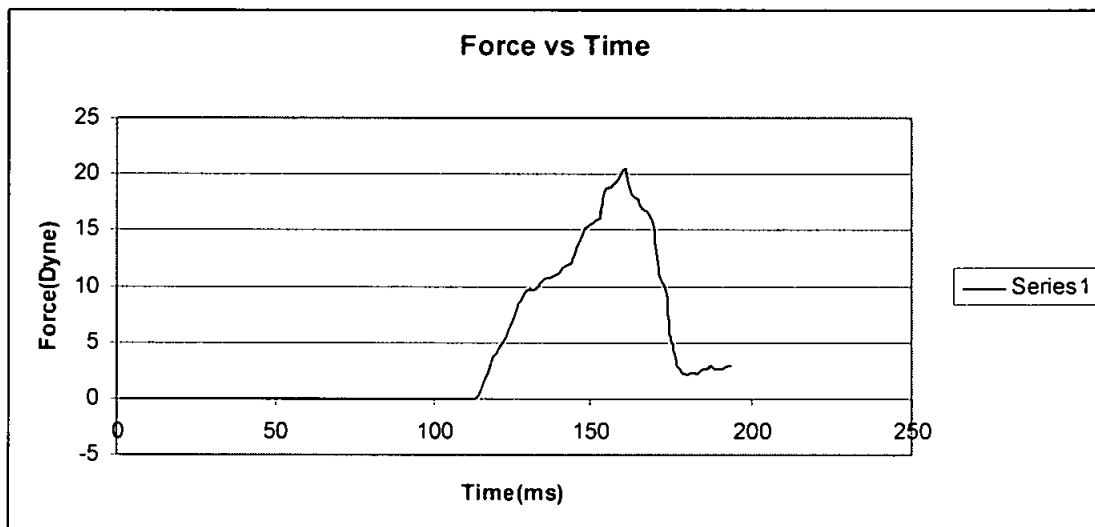
## Appendix-B (Continued)

## 23 Gauge/0.6 millimeter Diameter Needle Insertion Force

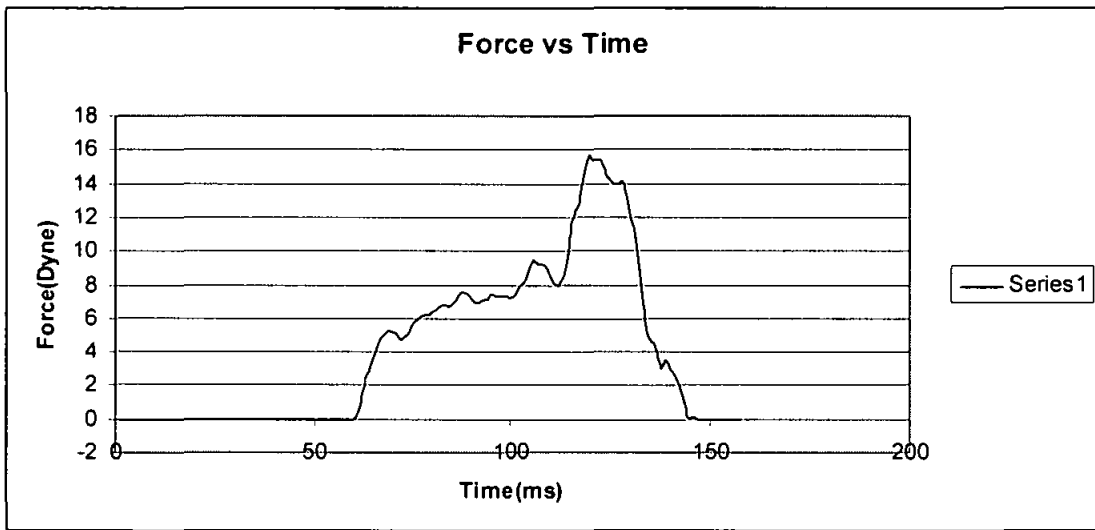




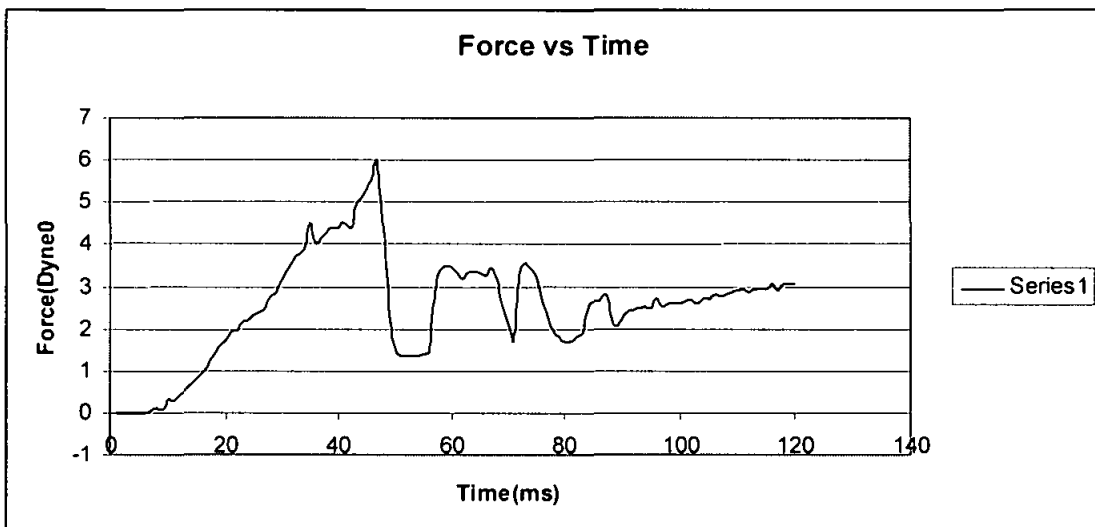
## Appendix-B (Continued)



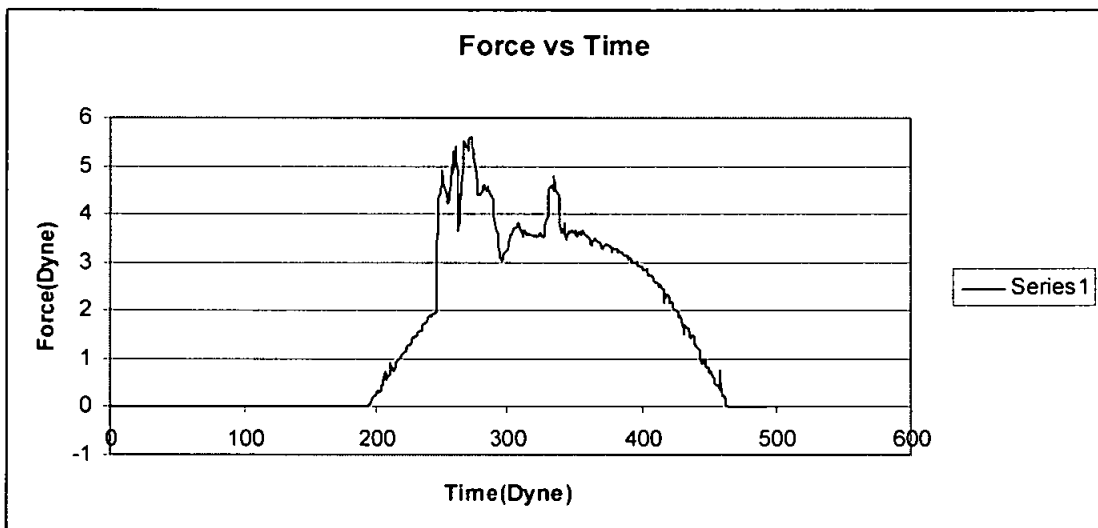
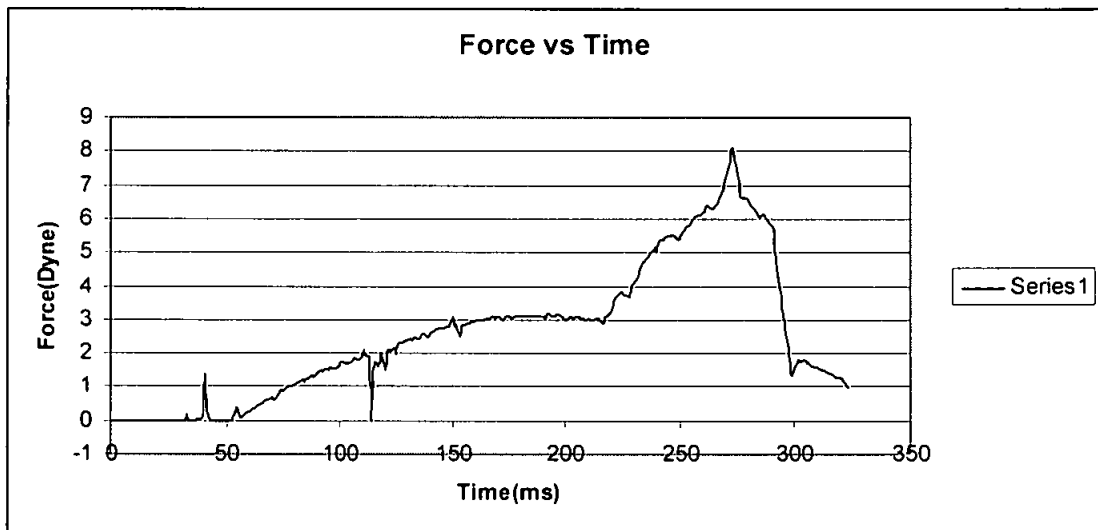
## Appendix-B (Continued)



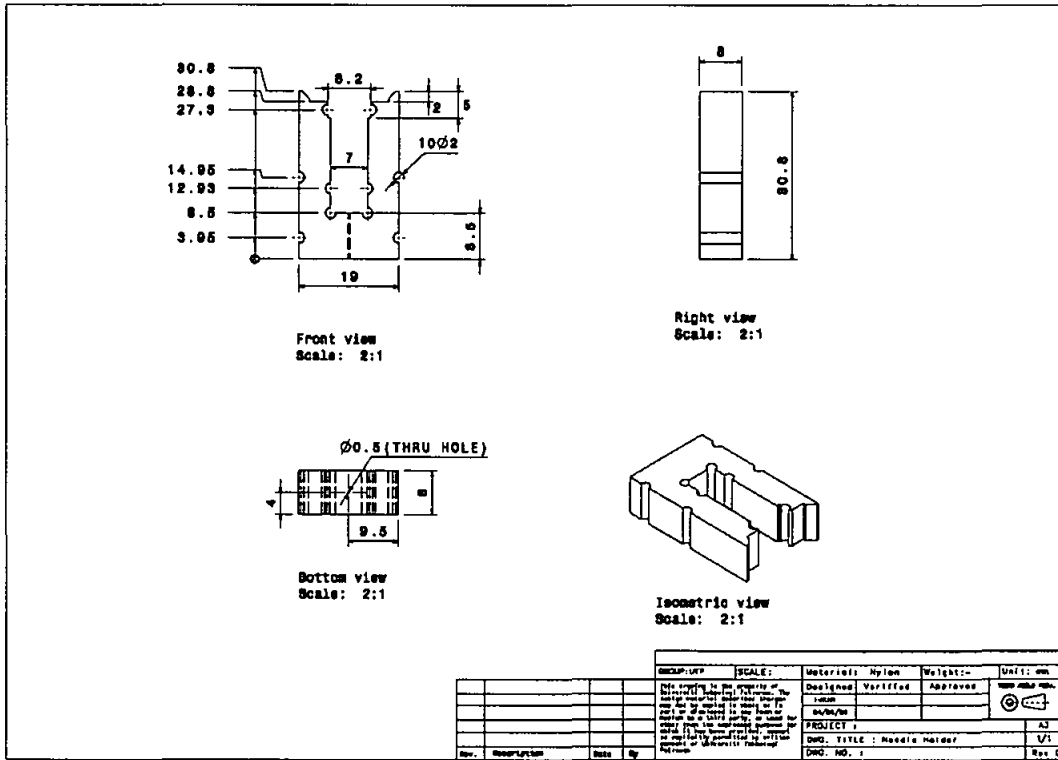
25 Gauge/0.5 millimeters Diameter Needle Insertion Force



## Appendix-B (Continued)





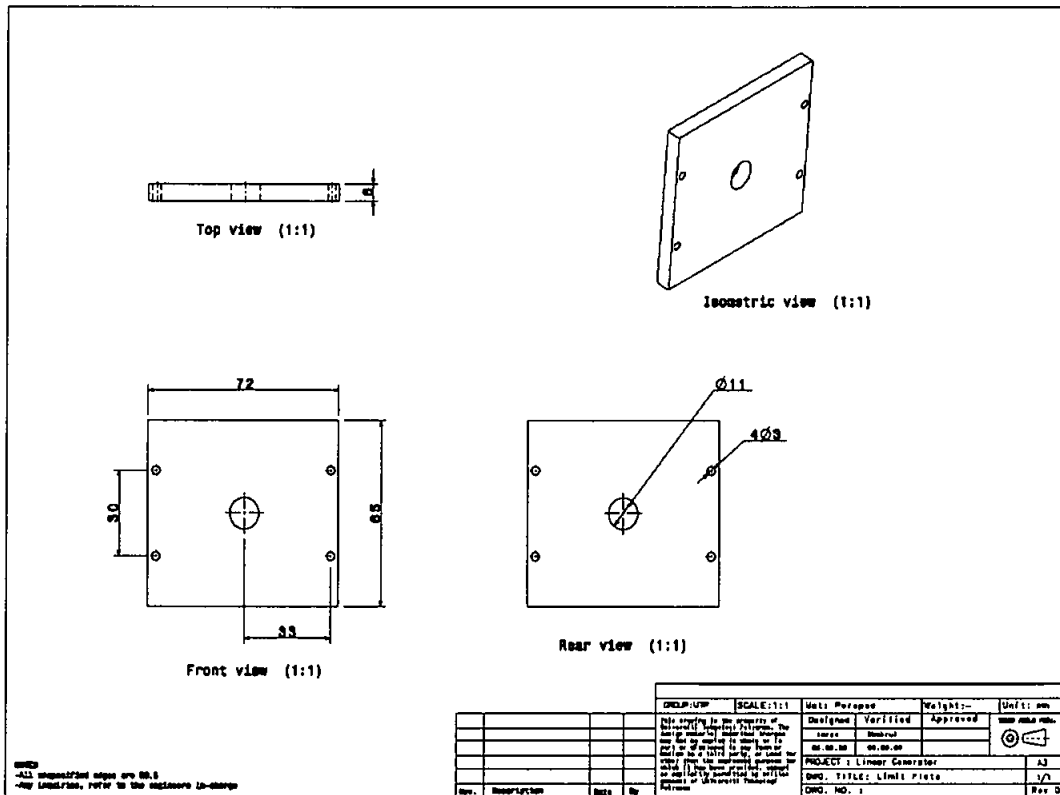


GROUP/APP	SCALE	Material	Nylon	Weight	Unit: mm
		Designed	Verified	Approved	
		PROJECT :			AJ
		DWG. TITLE : Needle holder			V1
		DWG. NO. :			Rev. 0



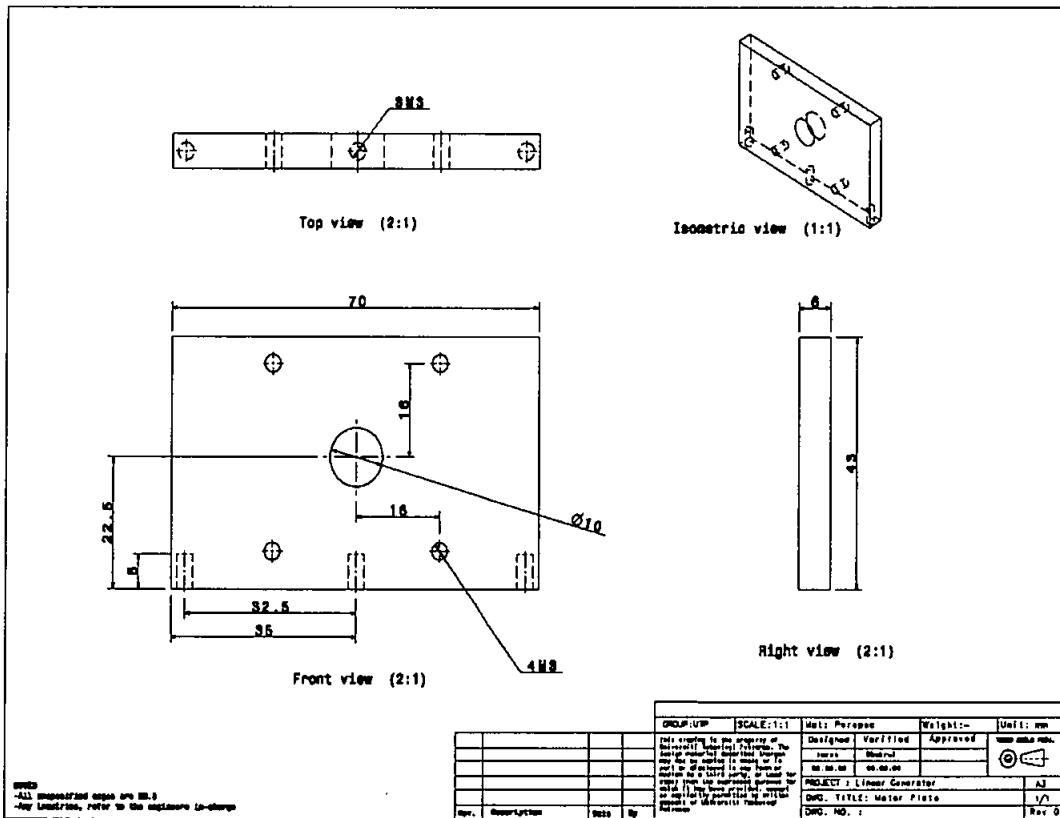
Appendix-C (Continued)

Limit Switch Plate



Appendix-C (Continued)

Motor Plate











## Appendix-D

## M-file of Graphical user interface

```

function varargout = Ngui2(varargin)
% Ngui2 M-file for Ngui2.fig
%   Ngui2, by itself, creates a new Ngui2 or raises the existing
%   singleton*.
%
%   H = Ngui2 returns the handle to a new Ngui2 or the handle to
%   the existing singleton*.
%
%   Ngui2('CALLBACK',hObject,eventData,handles,...) calls the local
%   function named CALLBACK in Ngui2.M with the given input arguments.
%
%   Ngui2('Property','Value',...) creates a new Ngui2 or raises the
%   existing singleton*. Starting from the left, property value pairs are
%   applied to the GUI before Ngui2_OpeningFunction gets called. An
%   unrecognized property name or invalid value makes property application
%   stop. All inputs are passed to Ngui2_OpeningFcn via varargin.
%
%   *See GUI Options on GUIDE's Tools menu. Choose "GUI allows only one
%   instance to run (singleton)".
%
% See also: GUIDE, GUIDATA, GUIHANDLES

% Copyright 2002-2003 The MathWorks, Inc.

% Edit the above text to modify the response to help Ngui2

% Last Modified by GUIDE v2.5 06-Apr-2008 00:34:48

% Begin initialization code - DO NOT EDIT
gui_Singleton = 1;
gui_State = struct('gui_Name',    mfilename, ...
                  'gui_Singleton', gui_Singleton, ...
                  'gui_OpeningFcn', @Ngui2_OpeningFcn, ...
                  'gui_OutputFcn', @Ngui2_OutputFcn, ...
                  'gui_LayoutFcn', [], ...
                  'gui_Callback', []);
if nargin && ischar(varargin{1})
    gui_State.gui_Callback = str2func(varargin{1});

```

## Appendix-D (Continued)

```

end

if nargin
    [varargout{1:nargout}] = gui_mainfcn(gui_State, varargin{:});
else
    gui_mainfcn(gui_State, varargin{:});
end
% End initialization code - DO NOT EDIT

% --- Executes just before Ngui2 is made visible.
function Ngui2_OpeningFcn(hObject, eventdata, handles, varargin)
% This function has no output args, see OutputFcn.
% hObject    handle to figure
% eventdata  reserved - to be defined in a future version of MATLAB
% handles    structure with handles and user data (see GUIDATA)
% varargin   command line arguments to Ngui2 (see VARARGIN)

% Choose default command line output for Ngui2
handles.output = hObject;

% Update handles structure
guidata(hObject, handles);

% UIWAIT makes Ngui2 wait for user response (see UIRESUME)
% uiwait(handles.figure1);

% --- Outputs from this function are returned to the command line.
function varargout = Ngui2_OutputFcn(hObject, eventdata, handles)
% varargout  cell array for returning output args (see VARARGOUT);
% hObject    handle to figure
% eventdata  reserved - to be defined in a future version of MATLAB
% handles    structure with handles and user data (see GUIDATA)

% Get default command line output from handles structure
varargout{1} = handles.output;

% --- Executes on button press in start.
function start_Callback(hObject, eventdata, handles)
% hObject    handle to start (see GCBO)
% eventdata  reserved - to be defined in a future version of MATLAB

```

## Appendix-D (Continued)

```

% handles structure with handles and user data (see GUIDATA)
AI=analoginput('winsound');
chan=addchannel(AI,1);
duration=1;
set(AI,'SampleRate',8000);
start(AI);

d1=getdata(AI);
%downsample (d1,50);
E=str2num(get(handles.Elasticity,'String'));

a=str2num(get(handles.Dia,'String'));

d=str2num(get(handles.Depth,'String'));

f=((8*E*1e3*a*1e-3*d*1e-3)/3);

F=num2str(f);

set(handles.force,'String',F);

if (E-100>=0)

    set(handles.Elasticity,'String','#Error#');

    set(handles.force,'String','#Error#');
else

    e=num2str(E);

    set(handles.Elasticity,'String',e);
end

if (a-0.9>=0)

    set(handles.Dia,'String','#Error#');

    set(handles.force,'String','#Error#');

else

    A=num2str(a);

```

## Appendix-D (Continued)

```

    set(handles.Dia,'String',A);

end

if (d-20>=0)

    set(handles.Depth,'String','#Error#');
    set(handles.force,'String','#Error#');
else

    D=num2str(d);
    set(handles.Depth,'String',D);
end

plot(d1);

if (d1-f<=0);

    set(handles.text1,'String','Needle is not inserted');

else

    set(handles.text1,'String','Needle is inserted');
end

function Elasticity_Callback(hObject, eventdata, handles)
% hObject    handle to Elasticity (see GCBO)
% eventdata  reserved - to be defined in a future version of MATLAB
% handles    structure with handles and user data (see GUIDATA)

% Hints: get(hObject,'String') returns contents of Elasticity as text
%        str2double(get(hObject,'String')) returns contents of Elasticity as a double

% --- Executes during object creation, after setting all properties.
function Elasticity_CreateFcn(hObject, eventdata, handles)
% hObject    handle to Elasticity (see GCBO)
% eventdata  reserved - to be defined in a future version of MATLAB
% handles    empty - handles not created until after all CreateFcns called

```

## Appendix-D (Continued)

```
% Hint: edit controls usually have a white background on Windows.
%   See ISPC and COMPUTER.
if ispc
    set(hObject,'BackgroundColor','white');
else
    set(hObject,'BackgroundColor',get(0,'defaultUicontrolBackgroundColor'));
end
```

```
function Dia_Callback(hObject, eventdata, handles)
% hObject   handle to Dia (see GCBO)
% eventdata reserved - to be defined in a future version of MATLAB
% handles   structure with handles and user data (see GUIDATA)

% Hints: get(hObject,'String') returns contents of Dia as text
%   str2double(get(hObject,'String')) returns contents of Dia as a double
```

```
% --- Executes during object creation, after setting all properties.
function Dia_CreateFcn(hObject, eventdata, handles)
% hObject   handle to Dia (see GCBO)
% eventdata reserved - to be defined in a future version of MATLAB
% handles   empty - handles not created until after all CreateFcns called
```

```
% Hint: edit controls usually have a white background on Windows.
%   See ISPC and COMPUTER.
if ispc
    set(hObject,'BackgroundColor','white');
else
    set(hObject,'BackgroundColor',get(0,'defaultUicontrolBackgroundColor'));
end
```

```
function Depth_Callback(hObject, eventdata, handles)
% hObject   handle to Depth (see GCBO)
% eventdata reserved - to be defined in a future version of MATLAB
% handles   structure with handles and user data (see GUIDATA)

% Hints: get(hObject,'String') returns contents of Depth as text
%   str2double(get(hObject,'String')) returns contents of Depth as a double
```



## Appendix-D (Continued)

```

% --- Executes during object creation, after setting all properties.
function Depth_CreateFcn(hObject, eventdata, handles)
% hObject    handle to Depth (see GCBO)
% eventdata  reserved - to be defined in a future version of MATLAB
% handles    empty - handles not created until after all CreateFcns called

% Hint: edit controls usually have a white background on Windows.
%       See ISPC and COMPUTER.
if ispc
    set(hObject,'BackgroundColor','white');
else
    set(hObject,'BackgroundColor',get(0,'defaultUicontrolBackgroundColor'));
end

function force_Callback(hObject, eventdata, handles)
% hObject    handle to force (see GCBO)
% eventdata  reserved - to be defined in a future version of MATLAB
% handles    structure with handles and user data (see GUIDATA)

% Hints: get(hObject,'String') returns contents of force as text
%       str2double(get(hObject,'String')) returns contents of force as a double

% --- Executes during object creation, after setting all properties.
function force_CreateFcn(hObject, eventdata, handles)
% hObject    handle to force (see GCBO)
% eventdata  reserved - to be defined in a future version of MATLAB
% handles    empty - handles not created until after all CreateFcns called

% Hint: edit controls usually have a white background on Windows.
%       See ISPC and COMPUTER.
if ispc
    set(hObject,'BackgroundColor','white');
else
    set(hObject,'BackgroundColor',get(0,'defaultUicontrolBackgroundColor'));
end

```